Bergische Universität Wuppertal

Fachbereich D – Sicherheitstechnik

Lehrstuhl für Baustofftechnologie und Brandschutz

MASTER'S THESIS

THE DEVELOPMENT OF TECHNIQUES TO IMPROVE FIRE DYNAMICS INFORMED LOSS ESTIMATION FOR CLEANROOMS IN THE SEMICONDUCTOR INDUSTRY

Name:	Steffen Kahrmann
Anschrift:	Dr. Kurt Schumacherstr. 16
	67256 Weisenheim am Sand
Matrikelnummer:	843772
Studienrichtung:	Brandschutz
Hochschullehrer:	Univ.-Prof. Dr.-Ing. Wolfram Klingsch
Betreuer:	Dr. David Lange

DECLARATION

This thesis and the work described within have been completed solely by Steffen Kahrmann at the Bergische University of Wuppertal, under the supervision of Univ.-Prof. Dr.-Ing. Wolfram Klingsch and Dr. David Lange from the University of Edinburgh. Where others have contributed or other sources are quoted, references are given.

Edinburgh, 14/09/2010

_____

Steffen Kahrmann

ACKNOWLEDGEMENTS

First and foremost, I would like to thank my supervisors, Univ.-Prof. Dr.-Ing. Wolfram Klingsch for offering help and support whenever needed, and Dr. David Lange for sharing his cleanroom expertise, the truely countless amount of time spent on discussions and generously programming the required MATLAB scripts.

I would also like to thank Prof. José Torero from the University of Edinburgh and Alastair Brown from Rushbrook Consultants without whose engagement and sponsoring this thesis would not have been possible in the first place.

Last but not least thanks also go out to Dr. Guillermo Rein, Dimitrios Toris, Wolfram, Nicolas, Francesco, Pedro, Thomas, Hubert and Adam for giving valuable insight into the field of CFD, to everyone else (too numerous to name) of the Edinburgh Fire Group for being great companions for the last five months and of course to my family for their consistent support.

ABSTRACT

Our understanding of the behaviour of fire and smoke under common conditions as they occur e.g. in compartment fires has evolved in the last decades. This also took place due to progress made in computing capacity and Computational Fluid Dynamics (CFD) which is now also usable in the field of Fire Safety Engineering. However, this did not apply to cleanrooms where the unique pattern of recirculation airflow led to an incomparable spread of smoke. It is only recently that this technology can be applied to conduct fire research in these environments where real scale fire tests are too expensive and complex to carry out.

The purpose of this thesis is to study cleanroom smoke spread by utilizing CFD and link these findings to loss estimations in the semiconductor industry. This approach would allow to improve the accuracy of these estimations and could also lead to the development of innovative smoke management strategies.

A numerical 3D model was tested and rated beneficial in supporting smoke extraction by using cleanroom ventilation systems. Instead of studying the efficiency of "separate" extraction systems, this approach focuses on the already installed clean air systems which usually facilitate the characteristic airflow.

In the course of this thesis a novel method of smoke management was developed which is referred to as "buoyancy control". Other than smoke exhaust venting equipment in common buildings which utilise smoke's buoyancy for extraction, this new cleanroom strategy works reversely by deliberately decreasing buoyancy.

ABBREVIATIONS

B&S	Building and Structure
C/R	Cleanroom
CFD	Computational Fluid Dynamics
CMOS	Complementary Metal-Oxide Semiconductor
Fab	Fabrication Area
FDS	Fire Dynamics Simulator
FFU	Fan Filter Unit
HEPA	High Efficiency Particulate Air
HRR	Heat Release Rate [kW]
HRRPUA	Heat Release Rate Per Unit Area [kW]
IC	Integrated Circuits
ISO	International Organization for Standardization
LCD	Liquid Crystal Display
LES	Large Eddy Simulation
M&E	Machinery and Equipment
MATLAB	Programming Language
NASA	National Aeronautics and Space Administration
OpenFOAM	Open Field Operation and Manipulation
S	Sprinklered
Subfab	Sub Fabrication Area
ULPA	Ultra Low Penetration Air
ULSI	Ultra Large Scale Integration
VLF	Vertical Laminar Flow
VLSI	Very Large Scale Integration
WIP	Work in Progress

CONTENTS

1 Introduction

1.1 Necessity

Associated with a steadily increasing demand for microchips the semiconductor industry is one of the fastest growing, most expensive and complex industries in the world. Producing in some of the most technologically advanced production cleanrooms purpose built to meet the requirements of the latest product. The limited number of this type of plants possibly leads, in cases of business interruption e.g. caused by fire and smoke, to product and supply shortage around the world. Being dependent on semiconductor products nowadays, it is vital to develop emergency strategies that are capable of decreasing losses and minimizing disruptions. To this day a priori loss estimation still is a guesstimate due to missing standardised and general approaches. This frequently results in financial underestimation of insurers exposure and therefore, is of particular interest to this high-risk industry.

1.2 Margin of Topic

The characteristic airflow pattern in cleanrooms is used to realise clean environments with as less airborne contamination as possible. In addition to the approach of this thesis, to utilise this effect in terms of smoke control, there are other strategies that could be evaluated by CFD modelling. Fire curtains and separate exhaust hoods for potentially dangerous machinery and equipment can also have positive effects on fire and smoke control, but are not considered due to time and resource limitations. Particularly changes in air velocity and fan filter unit arrangement are expected to reveal recent knowledge but have not been taken into account yet because of an associated rise of computing time. For these reasons this thesis shall universally study and show the behaviour of smoke in cleanrooms and use means already available in order to be generally and instantly applicable.

1.3 Objective

When talking about fire safety in cleanrooms, understanding of smoke spread is of special interest. Within this work this is achieved by the usage of numerical models to

study smoke flow and identify other critical parameters. In terms of cleanroom risk engineering improvements in loss estimation are necessary. The thesis second part attempts to link these improvements to the numerical models developed and to come up with an innovative contamination based method to optimise loss estimation accuracy.

2 Cleanroom Environments

More than 100 years ago, in the early days of cleanrooms, they were used within hospitals to reduce patients risk of catching and spreading bacteria infections. Many various techniques to achieve cleanroom conditions were launched, but it was only after the introduction of the so called positive ventilation, which added filtered air to the environment, that contamination control was revolutionised. The Second World War marks a breakthrough in clean environment use in England and the USA, where tanks, guns and aeroplane parts were produced under clean conditions to increase quality and reliability and diminish the number of rejected products. Further milestones were the development of HEPA [1] filters for even cleaner air supply and the introduction of laminar, unidirectional airflow via filters mounted in ceiling or walls [2].

Manufacturing processes in the high-end electronics industry for semiconductors, hard-disk drives, flat panel LCD [3] - screens and aerospace systems require essential control of airborne contamination [4]. Semiconductor devices are particularly endangered by the exposure to particles like dust and smoke due to the very small feature sizes and the thickness of deposited layers on the wafer surface (micron range [µm]) (see also chapter 3).

2.1 Cleanroom Classes

Cleanrooms are defined in the ISO Standard Series >209< as follows: *"A room in which the number concentration of airborne particles is controlled, and which is constructed and used in a manner to minimize the introduction, generation and retention of particles inside the room and in which other relevant parameters, e.g. temperature, humidity and pressure are controlled if necessary" [5].*

Cleanroom classes are characterised by the diameter and density of particles in air. Class numbers are given in *Federal Standard 209E - Airborne Particulate Cleanliness Classes in Cleanrooms and Clean Zones* and defines the number of

[1] High Efficiency Particulate Air
[2] Ramstorp, Matts, 2000
[3] Liquid Crystal Display
[4] Sze, M.S.,2002
[5] ISO 14644, 1999

particles 0.5 µm or larger in a cubic foot of air [6]. Table 1 links class number and maximum particle size to equivalent environment conditions.

Class Number	Particle Size	Environment
0.01	<<0.1	Projected-256 Mbit
0.1	<0.1	Mini environment
1	0.1	ULSI [7] - C/R [8]
10	0.3	VLSI [9] - C/R
100	0.5	VLF [10] station
1000 - 10,000	0.5	Assembly area
100,000		House room
≤ 5 000 000		Outdoors

Table 1: Specific class numbers for various environments (US Fed. Standard 209) [11].

Standard 209E is mentioned here although expired and superseded by the *ISO/TC 209 Series*. However, it is still in common use to describe cleanroom classes. ISO/TC 209 is a series of documents of the ISO 14644 and 14698 and no longer just an US standard [12]. The actual ISO 14644 classifies slightly different classes of cleanliness as shown in table 2.

Cleanrooms (also called fabs [13]) for semiconductor manufacturing purposes are located within large multi-storey structures with a surface area of up to 20,000 – 40,000 m^2 per storey.

6 Ramstorp, Matts, 2000

7 Ultra Large Scale Integration

8 Cleanroom

9 Very Large Scale Integration

10 Vertical Laminar Flow

11 Van Zant, Peter, 1997

12 ISO 14644, 1999

13 Fabrication areas

ISO class number (N)	Maximum concentration limits (particles/m^3 air) for particles equal to and larger than the considered sizes shown below.					
	0.1 µm	0.2 µm	0.3 µm	0.5 µm	1 µm	5 µm
ISO Class 1	10	2				
ISO Class 2	100	24	10	4		
ISO Class 3	1 000	237	102	35	8	
ISO Class 4	10 000	2 370	1 020	352	83	
ISO Class 5	100 000	23 700	10 200	3 520	832	29
ISO Class 6	1 000 000	237 000	102 000	35 200	8 320	293
ISO Class 7				352 000	83 200	2 930
ISO Class 8				3 520 000	832 000	29 300
ISO Class 9				35 200 000	8 320 000	293 000

Table 2: Cleanliness classes for cleanrooms and clean zones (ISO 14644) [14].

In order to operate a cleanroom, several other facilities are needed to ensure proper supply and maintainance of the environment. Factors like airflow, particle loading, humidity and temperature have to be monitored.

2.2 Basic Cleanroom Design

The main building components are as shown in figure 1.

1. The cleanroom itself contains the semiconductor production lines and is separated into different manufacturing areas. It also includes so called mini- or microenvironments that can be considered as additional internal high - class cleanrooms of usually smaller size. Ceiling mounted FFU's [15] generate laminar downward airflow that leaves the room through a perforated floor.
2. The so called subfab [16] is the storey located underneath the cleanroom. The air entering through the perforated ceiling is lead to both sides of the building and passes cooling coils which maintain a stable air temperature.

[14] ISO 14644, 1999

[15] Fan Filter Units

[16] sub fabrication area

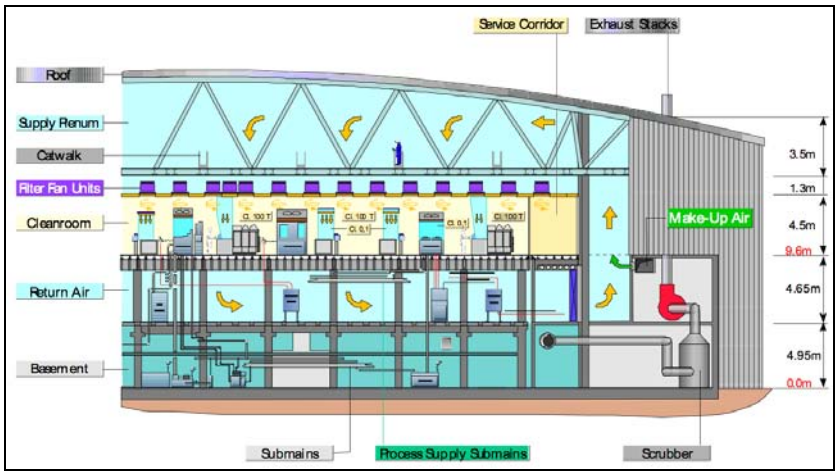

Figure 1: Cross section of a fab with recirculation air system [17].

3. In return air paths the cooled air is led upwards into the plenum. Prefiltered and fresh make-up air is added to ensure a steady exchange of stagnant air.
4. After returning to the plenum, the air is again injected into the fab.

2.3 Cleanroom Airflow

In unidirectional airflow cleanrooms, filtered air is uniformly distributed by filters mounted to the ceiling, flowing at constant velocities across the room and extracted through the floor.

Process equipment and personnel generate particles in submicron range. In order to avoid damages caused by these contaminats, laminar airflow is used. Experimentation revealed the correlation between air velocity and the level of particle contamination. Air velocities below 0.34 ms^{-1} diffuse contamination, whereas velocities above 0,56 ms^{-1} contribute little to contamination removal and may generate turbulences on obstructions, being considered to cause high contamination concentrations [18].

However, these results must not be applied to cases in which fire is the major source of airborne contamination. The airflow next to the fire is no longer unidirectional and laminar due to turbulent flow of hot plume gases which mix up with ambient air. After a certain distance travelled, causing a decrease in temperature and velocity, it is

17 Naughton, Phil, 2006

18 Cheng, M., 1998

possible to remove smoke particles through the perforated floor (see chapter 5.1 & 5.5).

2.4 Sources of Contamination

Under cleanroom conditions, literally everything that comes into contact with the product during manufacturing processes is a potential hazard to it and its performance. Major sources are (a.o.):

- Air
- Production Facility
- Cleanroom personnel

2.4.1 Air

Ordinary air is charged with airborne particulates (also called aerosols) which float and remain in the air for a certain time and must be filtered out before entering the cleanroom. Cleanliness levels in these rooms are defined by the aerosol diameters and their density in the air (see chapter 2.1).

2.4.1.1 Clean Air Strategies

In cleanroom design it is crutial to produce wafers free of contamination. Therefore particularly the process areas are of major interest in the overall design. Four different cleanroom design strategies are in use nowadays.

- Clean Work Stations
- Tunnel Design
- Total Cleanroom Strategy
- Micro- / Minienvironments

Cleanroom Work Stations:

First developed by NASA [19], the semiconductor industry adopted clean assembly rooms containing ceiling and wall filters.

However, the levels of cleanliness achieved in these relatively small rooms could not be transferred to large fabs with a larger number of employees. In order to solve this problem, the industry switched to another concept, focussing on single work stations. The transportation of wafers outside of these stations is performed in air-sealed boxes.

The fab itself is constructed of a single room including the working stations (also called hoods or VLF stations) that are arranged in a row to transport the wafer from station to station without exposure to ambient air. Basically there are two methods of keeping wafers clean. First, the inside air passes filters, and second, positive pressure prevents airborne particles from entering the machine through the housing. The most common filters are of the HEPA type (see chapter 2.5) which are also used in other cleanroom sections.

Tunnel Design:

With increasing contamination control requirements, the VLF hood technology revealed a number of disadvantages, especially those generated by personnel working within the room. The solution was found in separating the clean area in discrete tunnels / bays where filters are no longer located in VLF hoods but mounted into the ceiling. This causes less personnel generated contamination. Wafers are better separated from the employees and less people stay within the wafers vicinity.

Total Cleanroom Strategy:

Progress in filter- and cleanroom design allowed to return to the open fab strategy in which the clean air is filtered by ceiling-mounted HEPA units. Nowadays open fabs achieve classes up to 10 or 1 (see table 1).

Since the advent of CMOS [20] IC's [21], more and more fabrication-steps and -stations had to be included and led to larger rooms, tunnels and numbers of workers. This

---

[19] National Aeronautics and Space Administration

[20] Complementary Metal-Oxide Semiconductor

[21] Integrated Circuits

increase in potential contamination sources raised costs of a single cleanroom into the US$ 1oo million level.

Micro- and Minienvironments:

Due to losses in effectiveness by increasing cleanroom costs in the mid-1980's, so called microenvironments were introduced. The aim was to produce and transport wafers in as small environments as possible in a way such that the wafer is never exposed to ambient air.

Figure 2: Sealed and pressurised wafer run boxes (orange coloured) [22].

Later on commonly used run boxes were replaced by air or nitrogen pressurised wafer enclosures (microenvironments) which are hermetically sealed off from outside air. Figure 2 shows a so called minienvironment system, consisting of the isolated microenvironments, the tool and the docking station for loading and extraction of wafers. This strategy allows higher aisle [23] air cleanliness and consequently decreases construction and operation costs.

Another advantage is a smaller loss caused by contamination [[24]]. Recent strategies generally tend towards lower cleanliness levels in the overall cleanroom and specific areas within these rooms where higher demands are realised in smaller compartments (clean zones) [[25]].

---

[22] Brown, Al, 20

[23] Automated wafer transport route

[24] Van Zant, Peter, 1997

[25] Ramstorp, Matts, 2000

2.5 HEPA & ULPA - Filters

HEPA (see figure 3), ULPA[26] and Super-ULPA are replaceable fibros filters of different efficiency classes representing an assembly of randomly arranged and to mats compressed fibres which vary in diameter and length. Although the efficiency of HEPA filters is relatively high (> 99,97 % at 0.3 µm particle size), they are not able to protect the cleanroom entirely from contamination of ambient environments [27].

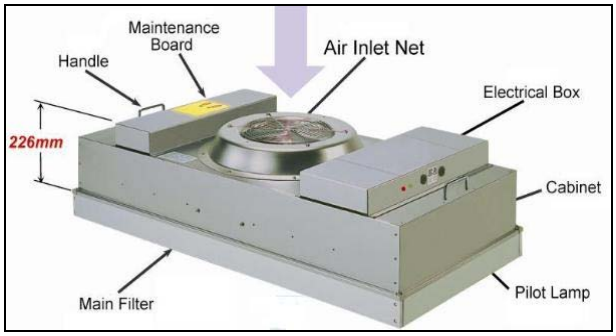

Figure 3: HEPA FFU [28].

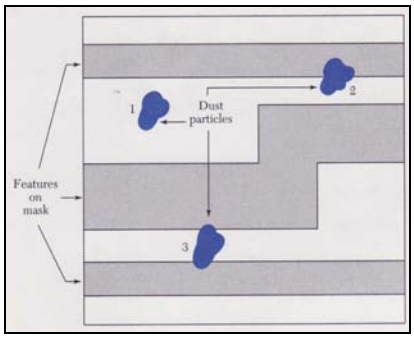

Figure 4: Ways of interference between particles and photomask patterns [29].

Typical airflows of 0.45 to 0.50 ms^{-1} exit velocity are provided depending on the filter design. High density of tiny holes and the large area filter medium allow large flow rates to pass at relatively low velocities. This also contributes to the level of cleanliness (no air currents) and operators comfort [30].

2.6 Impact of Smoke on Semiconductor Wafer Production

Particularly in photolithography [31] areas, particles can cause severe damage to wafers once settled onto them (resp. on lithographic photomasks) causing circuit failure. Behaving as opaque patterns, they are transferred to the wafer surface along with the mask's circuit patterns. Figure 4 shows dust (particles of smoke) on a photomask and different ways of interference with circuits. Particle 1 results in a harmless pinhole

---

26 Ultra Low Penetration Air
27 Tolliver, Donald L., 1988
28 UCT, 2010
29 Sze, M.S., 2002
30 Van Zant, Peter, 1997
31 Pattern definition method which uses UV radiation

formation on the underlying layer. Particle 2 is settled near the pattern edge and may cause a “bottleneck“ of current flow in the metal runner. Particle 3 may result in a short circuit between two conductive areas leading to microchip destruction [32].

32 Sze, M.S.,2002

3 Semiconductors

3.1 Stages of Manufacturing

Manufacturing solid state devices basically requires four separate phases. These are material preparation, crystal growth and wafer preparation, wafer fabrication and packaging. Wafer production takes up to two months and includes up to two dozen steps.

Stage 1:

Step one includes mining and purification of the raw semiconducting materials to meet semiconductor standards (silicon, sand).

Stage 2:

During crystal growth and wafer preparation the semiconducting material is formed into thin disks, called wafers.

Stage 3:

In phase three, IC's or devices are formed on resp. in the wafer's surface. Several thousands of devices (e.g. microchips) can possibly be placed on each wafer slice. So called chips or dies are areas on the wafer staffed with discrete devices or IC's [33]. The development of p-n junctions serves an important role in modern electronic applications as well as in understanding other semiconductor devices. Exposed to light or given biasing conditions, p-n junctions also function as either photonic device or microwave.

Nowadays particularly the planar technology, including process steps like oxidation, lithography, ion implanation and metallization, is used to fabricate IC's. Figure 5 shows a bare silicon wafer (5a) which gets oxidised (5b) in order to develop high-quality silicon dioxide (SiO_2). This functions as an insulator in several device structures, as well as a barrier to diffusion or implanation during device fabrication.

In p-n junction fabrication, the SiO_2 film defines the junction area. The wafer gets coated with an UV-light-sensitive layer called photoresist (figure 5c) which is baked onto the wafer for improved adhesion. Figure 5d shows the following wafer exposure to UV-light through a patterned mask. A chemical reaction proceeds in the exposed

33 Van Zant, Peter, 1997

region and polymerizes the resist for making it difficult to remove. In future processes the unexposed area dissolves and is washed away (figure 6a). The unprotected SiO_2 surface is etched off using buffered hydrofluoric acid (figure 6c).

Figure 6d shows the uncoated SiO_2 layer that is exposed to a high concentration of opposite type impurity that moves into the semiconductor crystal.

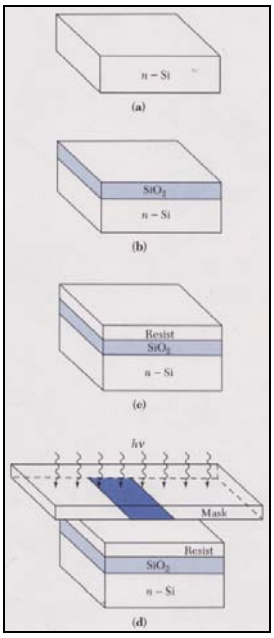

Figure 5: Steps of IC-Fabrication [34].

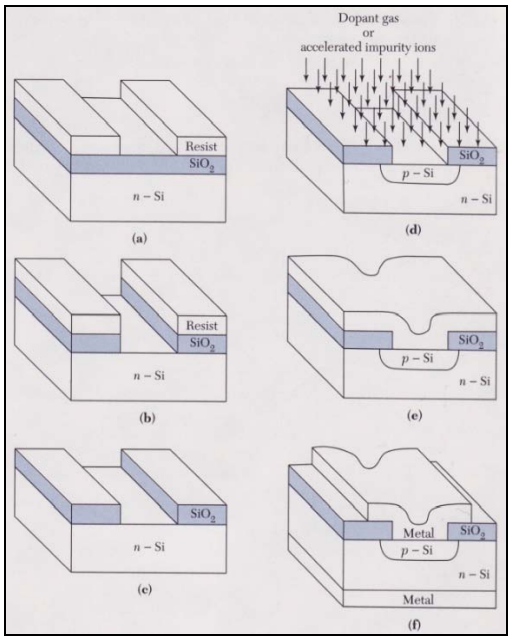

Figure 6: Steps of IC-Fabrication [35].

Figure 6d shows the uncoated SiO_2 layer that is exposed to a high concentration of opposite type impurity that moves into the semiconductor crystal. Metallization is used to form contacts and interconnections (figure 6e). Lithography is again applied to form front contacts (figure 6f) [36].

Stage 4:

Completed but still untested, the wafer's microchips undergo an electrical test (wafer sort) to guarantee correct manufacturing and customer specifications in the fourth and last phase. Afterwards the wafers get separated into single dies and is placed in packages [37].

---

34 Sze, M.S., 2002

35 Sze, M.S.,2002

36 Sze, M.S.,2002

37 Van Zant, Peter, 1997

4 Computational Fluid Dynamics

As mentioned later on in chapter 5, real fire or hot smoke tests to study smoke spread in cleanrooms are not runable. Therefore CFD modelling was used to conduct research to this issue. In general CFD is a numerical technique for the simulation of fluid flow that solves equations for energy and mass transfer between cells in a numerical domain. Within the range of industrial and non-industrial applications are:

- Vehicles and Aircraft Aerodynamics
- Hydrodynamics for Ships
- Fire Modelling
- Combustion Processes in Combustion Engines and Gas Turbines

Initially CFD was utilised by the aerospace industry in the 1960's to design and manufacture aircraft and jet engines. Nowadays drag forces of motor vehicles and flows in car environments are predicted using CFD. Due to the increasing availability of high-end computer hardware, this engineering tool is recently in wider use than ever.

Another advantage is the relatively cost-effective realisation compared to real scale experiments. Especially in the field of Fire Safety Engineering, where large experimental setups can often only be tested once, CFD can be applied to run complex and expensive tests serveral times without a need of rebuilding. Moreover, an almost unlimited number of data points, hence results, can be included into the test cases without actually increasing expenses. In real experiments, facility hire and person/hour costs are proportional to the number of data points and configurations.

Mentioning that increasing computing performance is generally able to solve more complex jobs, it is absolutely viable that this step-up has to go along with better skilled and qualified CFD users [38]. Particularly programmes integrating the spread of fire and smoke into their calculations are still under a continous improvement

38 Versteeg, 2007

process. As stated in the FDS 5 [39] user's guide, users should have experience in the fields of fluid dynamics, thermodynamics, combustion and heat transfer. Evaluation and judgement of the results should be conducted by informed users only [40]. For further information on CFD and the governing methods and equations, see e.g. [41].

4.1 The Fire Dynamics Simulator

FDS 5 is a CFD model that is able to calculate fire-driven fluid flow solving numerically a form of Navier-Stokes equations appropriate for low speed, thermally-driven flow with focus on smoke and heat transport from fires. To visualise the output data in images and animations it uses its companion programme *Smokeview.* Following phenomenas can generally be modelled by using FDS 5:

- Low speed heat and combustion products transport from fire
- Heat transfer (radiation and convection) between gas and solid surface
- Activation of sprinklers, heat and smoke detectors

4.1.1 Advantages

The fact that FDS 5 is a no-cost open source CFD code led to its wide use in research and industry which offers room and a community for discussions to a variety of issues. It's internal software structure also requires less computing capacity than competitive programmes, respectively calculation time is shortened. Furthermore, it already contains important tools like fire sprinklers and smoke detectors which come in handy when modelling fire. With *Smokeview* it is possible to track dynamic smoke flow and design complex structure- and room geometries.

---

39 Fire Dynamics Simulator

40 McGrattan, Kevin, 2009

41 Versteeg, 2007

4.1.2 Disadvantages

As with every other CFD code, operators of FDS 5 need to have the appropriate background in thermodynamics, fluid mechanics as well as in fire dynamics. Problems often arise from a lack of user's unterstanding in these fields and, when results are not compared to approved methods in engineering. Further disadvantages are:

- high programming effort in large simulations
- underventilated fires not applicable
- structure geometries limited to mesh properties
- pressure solver fails at parallel computing or when multiple meshes are used
- questionalble interpretation of Large Eddy Simulations (LES)

4.1.3 Software

Despite of FDS 5 there are several other commercial and non-commercial CFD codes available which are adapted to the field of fire engineering and are capable of modelling fire and smoke spread. Some of them are:

FireFOAM is an open source LES solver written in C++ and based on the OpenFOAM [42] platform. It is a variable density, low Mach number flow solver that is able to treat buoyancy driven turbulent flow. A mixture fraction based approach is used to model turbulent non- premixed combustions.

KOBRA-3D was initially developed to study enclosure hydrocarbon pool fires offshore. This 3D CFD model bases on the solution of three-dimensional time-dependent local hydrodynamic conservation laws, including various sub-models for e.g. turbulence modelling (LES), heat transfer analysis, flame modelling, detector response, fire sprinkler interaction. It is also programmed in C++.

SOFIE (Simulation of Fires in Enclosures) is a field model written in Fortran / C. It bases on the solution of Reynolds averaged Navier-Stokes equations using a finite volume approach and an underlying general non-orthogonal coordinate system with momentum smoothing and a pressure correction algorithm. Combustions processes

[42] Open Field Operation and Manipulation

can be simulated by either an eddy breakup model or a prescribed pdf laminar flamelet model.

JASMINE (Analysis of Smoke Movement In Enclosures) is written in FORTRAN 77/90 and simulates processes of convection, diffusion and entrainment by Navier-Stokes equations. It is finite-volume code using a Cartesian grid and is based on the SIMPLEST pressure-correction procedure. The processes of convection, diffusion and entrainment are simulated by the Navier-Strokes equations. It describes heat and mass transfer processes associated with the dispersion of combustion products from a fire. A variety of different physical sub-models are included for combustion and radiation processes, gas phase properties and solid boundary heat transfer.

SOLVENT is a Computational Fluid Dynamics model for the simulation of fluid flow, heat transfer and smoke transport in tunnels and is written in Fortran/C++. It is designed to model longitudinal and transverse ventilation systems. It bases on the standard finite-volume method and uses a staggered arrangement of the grid. The pressure field is also calculated by the SIMPLER algorithm [43].

43 CS&E, 2008

5 Fire Modelling in Cleanrooms

Contrary to other fields of fire safety engineering, where results determined by fire modelling can be compared to real fire tests, it is nearly impossible to conduct real tests under cleanroom conditions. The main reason for this are enormous costs to reproduce similar testing facilities in such a way that physical circumstances (humidity, temperature, cleanliness of the environment) match with existing up to date fabs. In terms of studying smoke spread within cleanrooms it is also not feasible to carry out hot smoke tests. This would result in severe contaminations by Propylenglycol and anhydrous oils and a clean up of weeks or months with losses in production (see chapter 6). To date, computer modelling is the only way to simulate time- and costeffective smoke spread in cleanroom fabrication areas.

One aim to this thesis is to understand the behaviour of smoke under conditions of down flow air streaming from the ceiling across the room to the perforated floor. Although there have been former approaches in modelling this issue (see [44,45,46,47]), rapid evolutions in the field of CFD necessitates a remake of cleanroom modelling.

5.1 Influence of unidirectional Air Velocity on Smoke Spread

The main factor of influence on smoke behaviour in cleanrooms is clean air velocity. According to [48], todays cleanrooms operate in the range of 0.13 ms^{-1} (average fab) and 0.4 ms^{-1} (photolithography area). Reduced-scale tests have shown that the distribution of combustion products was strongly affected by down flow air although there were no visually observed effects on the fire source's behaviour and flame height. The overall spread of smoke formed an umbrella-shaped cloud starting from the fire source [49].

44 Ferreira, Michael, 1999
45 Nam, Soonil, 2000
46 Heskestad, Gunnar, 2004
47 I, Yet-Pole, 2009
48 Ferreira, Michael, 1999
49 Heskestad, Gunnar, 2004

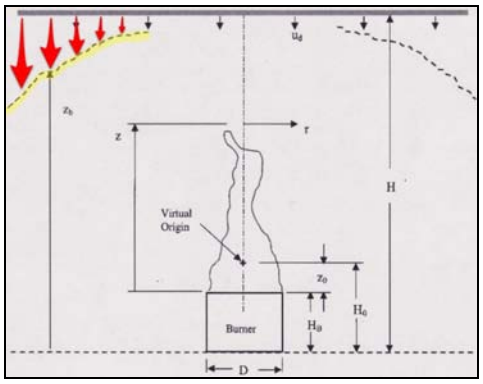

Figure 7: Umbrella-shaped smoke cloud affected by downdraft air [50].

Figure 7 illustrates this phenomenon. Unidirectional downdraft air [u_d] is provided across the ceiling and forms the typical shape. The injection of cold air into the layer of hot combustion gases is responsible for the loss of buoyancy (increasing with travelling distance away from the fire source).

According to [51], down flow air is not rated to be sufficient in smoke control. The assumption is that the clean air shall force the total amount of combustion gases through the perforated floor, where they could be removed by exhaust points before entering the plenum again. This is generally true due to the fact that upward velocities of fire plumes are higher than usually existing FFU velocities within cleanrooms. Assuming an average velocity of 0.4 ms^{-1} in the photolithography area, even very small fire sizes easily exceed the countering forces (see table 3).

Based on fire properties in the developed CFD models, a calculation shall clarify.

Equation 1 gives z_v, the vitual plume origin above a reference location based on HRR [52] ($\dot{Q}$) and the diameter (D_{eff}) of the fuel bed.

$$z_v = 0.083\dot{Q}^{\frac{2}{5}} - 1.02D_{eff} \qquad (1)\ [53]$$

The HRRPUA [54] in the FDS input file was set to 2222 kW, which results in a total HRR of 9999 kW (see also chapter 5.2.1), assuming a fire source of 4.5 m^2 surface area. D_{eff} is the circle diameter featuring the same plan area as the actual array (2.39 m) and is calculated using equation 2.

---

50 Heskestad, Gunnar, 2004

51 Ferreira, Michael, 1999

52 Heat Release Rate

53 SFPE, 2008

54 Heat release rate per unit area

$$D_{eff} = 2\left(\sqrt{\frac{A}{\pi}}\right) \quad (2)$$

Applying these values to equation 1, the virtual origin z_v equals 0.87 m (positive direction). Since the burner's surface area is elevated in the actual simulation by one metre in order to reproduce wet bench properties (burner), the value for z_v had to be corrected to 1,87 m. Equation 3 gives U_m, the velocity along the plume centerline, whereas z is the height of the ceiling (5 m). Inserting the corresponding values, U_m equals 15.30 ms^{-1}.

$$U_m = 1.04\frac{\dot{Q}^{\frac{1}{3}}}{(z - z_v)^{\frac{1}{3}}} \quad (3)\,[55]$$

Ceiling Height [m]	Fire Size [kW]	Virtual Origin [m]	Velocity [ms^{-1}]
5	1	-1.36	0.56
	5	-1.28	0.96
	50	-1.04	2.10
	100	-0.91	2.67
	1000	-0.12	6.03
	5000	1.07	11.27
	9999 (ca 10 MW)	1.87	15.32

Table 3: Plume velocities at 5 m ceiling height.

Assuming a fire of approximately 10 MW the average flame height is based on equation 4 expected to be 6.92 m. Again, elevated by 1 m the fire is now 7.92 m high. Since room height is 5 m, the ceiling will be affectect by fire within the proximity of the fire source.

$$L = -1.02D + 0.235\dot{Q}^{\frac{2}{5}} \quad (4)\,[56]$$

Depending on the materials used, burning through HEPA filters or even solid parts of the ceiling (if not fire proof) can be expected. This can possibly destroy filter material

[55] Ferreira, Michael, 1999

[56] SFPE, 2008

and the FFU's affected by fire. Smoke spread into the plenum can no longer be prevented. Once smoke reaches this part of the complex, it could possibly return into other, still unaffected areas of the cleanroom through surrounding and still operating FFU's.

Although unidirectional downward airflow is not sufficient in terms of total smoke control, the effects of air velocity on the umbrella-shaped smoke cloud has to be investigated. Therefore research using various FDS simulations has been conducted (see chapter 5.4).

5.2 The virtual Cleanroom Model

Up-to-date cleanroom fabrication generally consist of several areas. The term covers a variety of supply and support environments which allow the room itself to operate and maintain the required conditions. Therefore the developed cleanroom model contains all basic facilities like real factories do.

In order to achieve a reduction in the overall number of cells [57], a first attempt in scaling the main domain (outer volume representing the whole building complex) to a surface area of 22000 m^2 was abolished and corrected to 6000 m^2 (rectangle shaped, 60 x 100 m). This cutback had no effect on simulation results. The cleanroom is still large enough to analyse the travelling behaviour of smoke but quarters the number of cells and consequently the time of computation.

Figure 8 illustrates an overview of the complex in which the inner rectangular box represents the cleanroom containing the fabrication area (100 x 50 x 5 m). Two raspberry-coloured meshes on top embody over 5000 single FFU's mounted to the ceiling. They enable the characteristic recirculation airflow throughout the entire system.

[57] Cells in FDS simulations

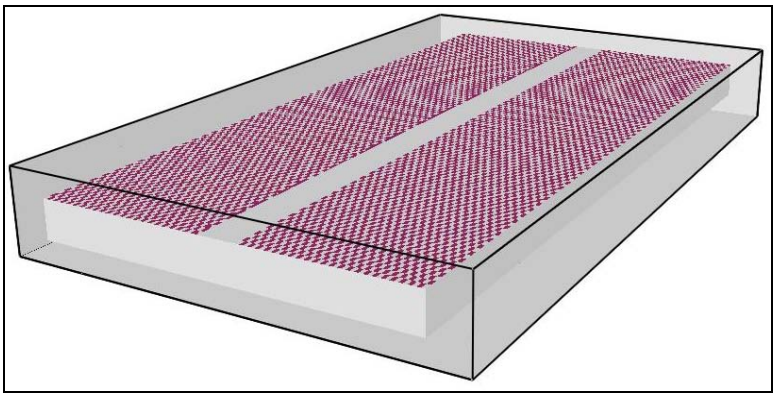

Figure 8: FDS cleanroom model.

The subfab is represented by open space below the cleanroom (height 3 m) and is connected to the cleanroom via a perforated ceiling (resp. floor). The space above the cleanroom stands for the plenum (height 3 m). The return air paths are located on both sides of the cleanroom (width 5 m) and connect subfab and plenum. Along the aisle, which is a FFU un-equipped strip in the cleanroom, wafer transporting robots operate.

A simplified demonstration of the recirculation airflow in the actual model is shown in figure 9 (main obstructions have been left out deliberately).

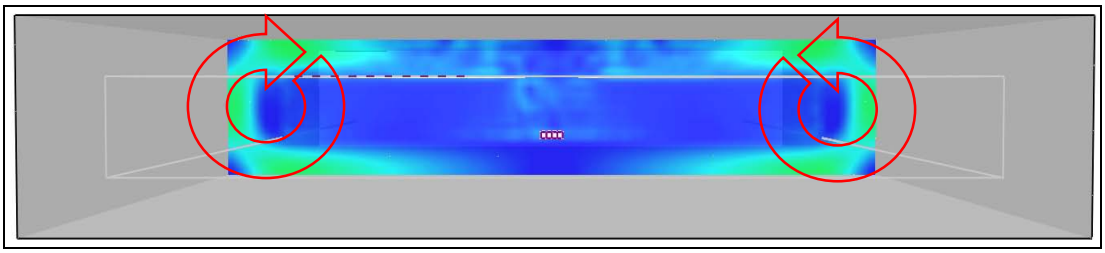

Figure 9: Slice file plot of recirculation air path.

The green coloured zones in the plot show higher velocities relative to the inside of the cleanroom. A roughly constant and laminar distribution of air velocities can be seen. Figure 10 shows the actual developed cleanroom design. The fire source was assumed to be in room seven and is visualised as a red square (see also chapter 5.2.1). The arrangement is as follows:

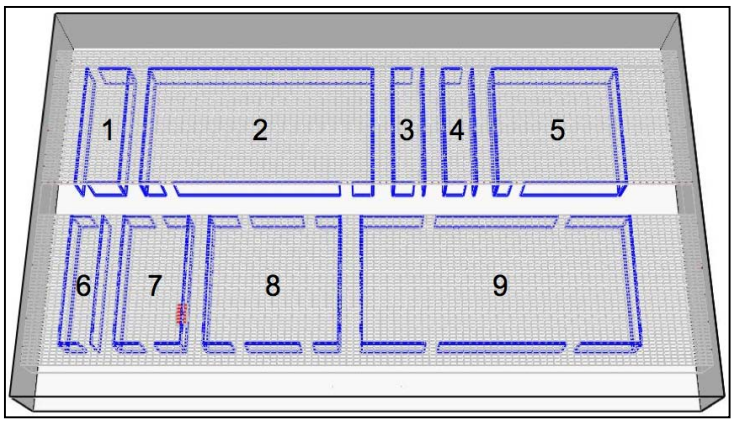

R1: Furnace & Reactor
R2: Alcohol Vapor Dryer
R3: Stepper / Scanner
R4: Stepper / Scanner
R5: Ion Implanter & CMP
R6: Storage
R7: Wet Benches
R7: Fire Source (red)
R8: SRD
R9: Dry Etcher

Figure 10: Typical cleanroom design applied to FDS model.

Compartment walls are 0.25 m thick and built from floor to ceiling. Characters R1-R9 refer to machinery and equipment commonly located in these rooms.

5.2.1 Fire Source

According to [58], plastic tanks of wet benches (see figure 16) are likely to catch fire when safety interlocks of immersion heaters fail. Recordings between 1985 and 1999 show 52 losses in which tanks of this kind were involved. Therefore a wet bench fire was assumed to be the initial fire source in all FDS models. Data arises from a free-burn test carried out on a 280 kg, 1.0 m x 1.8 m x 1.8 m Polypropylene wet bench [59]. Following test recordings, the fire grew within three minutes to it's maximum HRR of approximately 10 MW. Due to cell properties in the model and the approachable wet bench size of 4.5 m², the max. HRR had to be approximated to 9999 kW.

4.5 [m²] x 2222 [kW; HRRPUA] = 9999 [kW]

According to NFPA 72, fire HRR increase proportionally with the square of time as given in equation 5 and table 4 [60].

$$HRR = \alpha t^2 \qquad (5)$$ [61]

58 Brown, Alastair, 2002
59 Ferreira, Michael, 1999
60 SFPE, 2008
61 SFPE, 2008

HRR Increase	HRR [kW]
Slow	$\dot{Q}$=0.00239 t²
Medium	$\dot{Q}$=0.01172 t²
Fast	$\dot{Q}$=0.0469 t²
Ultrafast	$\dot{Q}$=0.1876 t²
customised	$\dot{Q}$=0.1111 t²

Table 4: T-Squared fire increase [62].

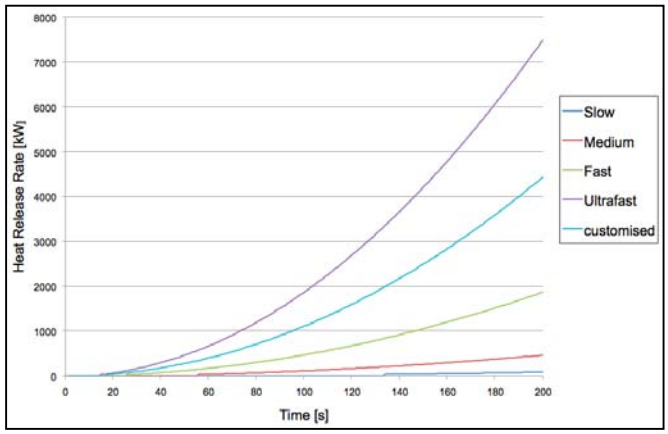

Figure 11: Graphs according to table 4.

In the described fire test, the wet bench was deliberately set on fire at nine different points and both chemical baths were ignited at the same time. In order to reproduce a more realistic alpha value (initially only one bath on fire), duration to the maximum HRR was extended from 180 s to 300 s. This assumption makes sense since the calculated alpha value in the real wet bench test would be 0.3086 (equation 5) and approx. 1.65 times faster than even an ultrafast fire. Using equation 5, the new alpha value based on t=300 s is 0,1111. This value can still be considered as an ultrafast t²-fire.

Assuming a wet bench fire follows the t²-curve, an appropriate way to represent this behaviour had to be found. Applying a HRRPUA ramp-up following the command *RAMP_Q* was not applicable. The ramp stays at the prescribed value after reaching its maximum. This would not allow a ramp-down (cooling phase) of the fire [63]. Instead user-defined ramps were chosen to represent an averaged t²-fire behaviour.

In the present case, the fire begins 200 s after the simulation starts and ramps up in 15 s-time-steps following the t²-curve, using equation 5 and the developed alpha value of 0.1111.

62 SFPE, 2008

63 McGrattan, Kevin, 2009

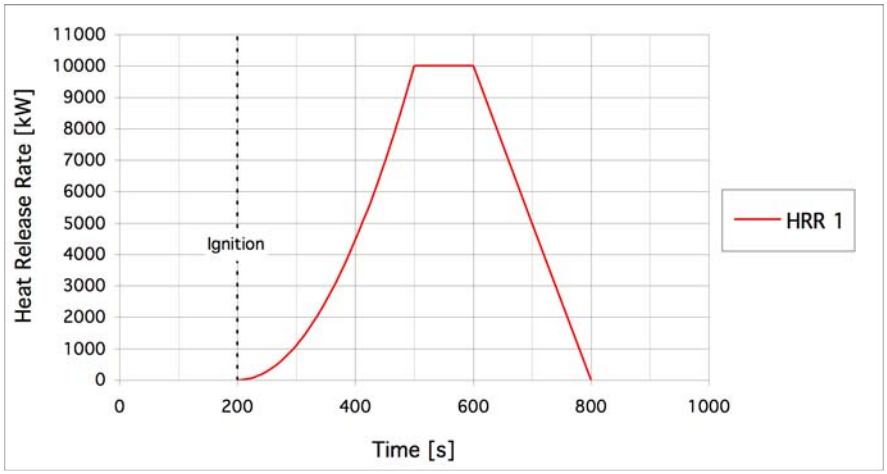

Figure 12: HRR applied in cases I to VI as function of time.

Figure 12 illustrates the actual fire growth used in different simulations. The ramp-up is followed by a steady HRR of approximately 10 MW over 100 s, and then ramps-down linearly for 200 s.

5.2.2 Airflow Characteristics

As mentioned before, airflow in cleanrooms features complex characteristics that are unique compared to common production facilities. In order to represent air velocities between 0.13 and 0.4 ms^{-1}, FFU's were set in different simulations to 0.3, 0.4, 0.5, 0.6 and 1.5 ms^{-1}. Theoretically this leads to average cleanroom velocities as shown in table 5.

FFU velocity [ms^{-1}]	Average c/r velocity [ms^{-1}]
0.3	0.12
0.4	0.16
0.5	0.20
0.6	0.24
1.5	0.60

Table 5: FFU and cleanroom velocities in various model setups.

The following states how the assumptions in table 5 were derived:

The total surface area of the cleanroom ceiling, as well as the perforated floor, is 5000 m^2 each. The FFU-equipped and the non-FFU-equipped parts in the ceiling are equally distributed and arranged in the shape of a grid, which means that 50 % of the

ceiling consists of FFU's. The aisle (100 x 5 m ; 10% of the total surface area) in the middle of the ceiling is solid and does not contain any FFU's. Hence, 40 % of the ceiling produces a certain airflow rate which escapes through the entire perforated floor. Therefore the initial air velocity is reduced by 60 % whilst travelling through the cleanroom (see table 5).

In the actual FDS models the average velocities differ slightly from theoretical calculations because of obstructions like compartment walls and equipment which have effects on the airflow.

5.3 Sensitivity Study of Mesh Properties

In order to validate the chosen mesh (0.25 m cubic cells), different sensitivity studies were carried out. A small scale cleanroom setup was developed that could be adopted to various suitable cubic cell sizes of 0.1 m, 0.25 m, 0.5 m and 1.0 m, matching the FFU properties of 1.0 x 0.5 m. Table 6 compares cell sizes to the total amount of cells. An even smaller cell size of 0.05 m could not be tested because of computational limitations.

Cell edge length	Total cell number
0.05 m (not tested)	7.040.000
0.1 m	880.000
0.25 m	56.320
0.5 m	7.040
1.0 m	880

Table 6: Comparison of cell size and cell number.

Figure 13 shows the actual room design that was chosen to run the sensitivity study. Basically it simulates a small cleanroom with dimensions of 5 x 10 x 5 m within an outer domain of 5 x 16 x 11 m which represents the surrounding cleanroom sections, similar to the ones described in figure 10.

For recording and plotting air velocities, metering devices were placed at 2.5 m height above the floor and along the middle axis within the cleanroom. The output data is shown in figure 14.

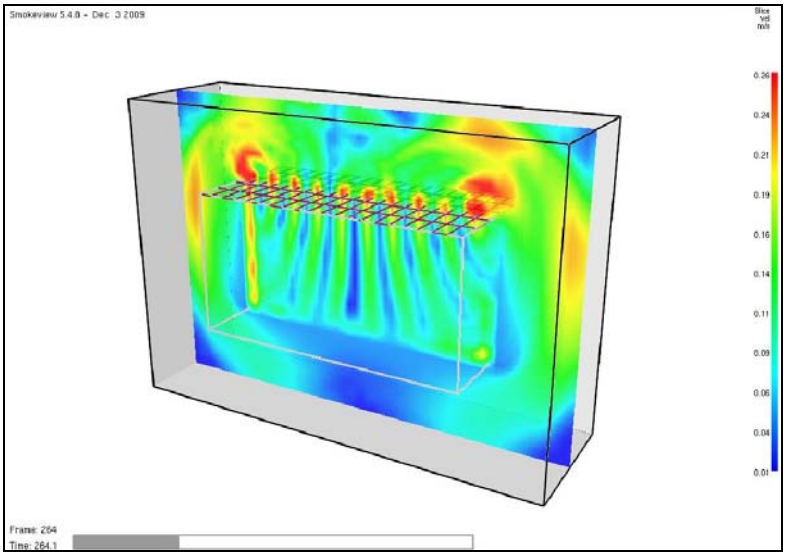

Figure 13: Sensitivity study setup.

Figure 14 shows that cell sizes of 0.5 and 1.0 m cannot be used in the CFD model.

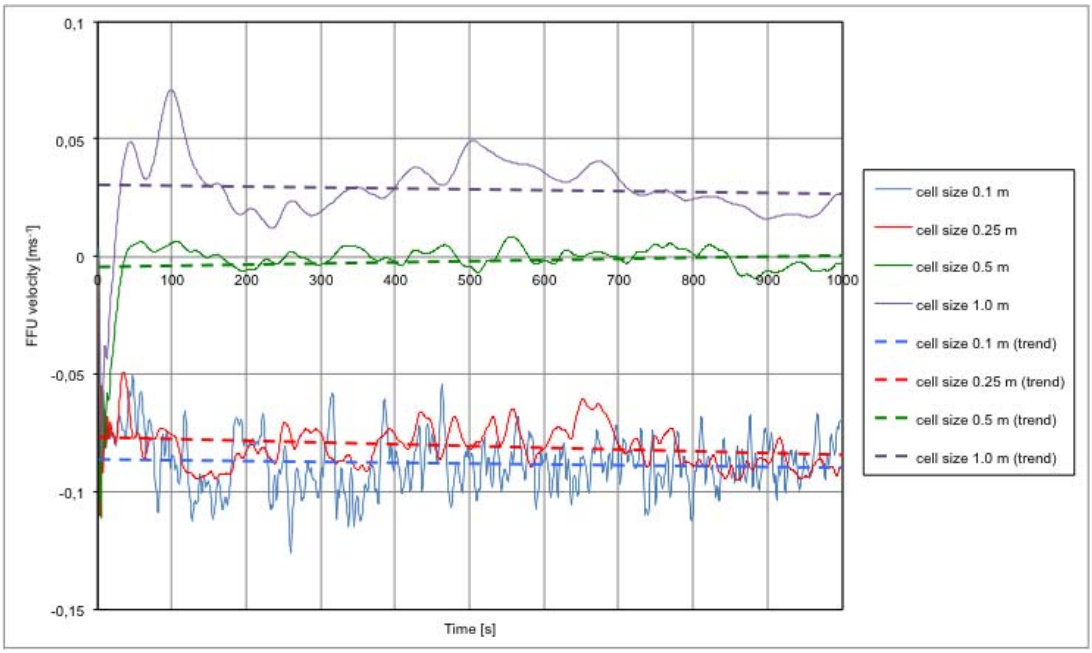

Figure 14: Sensitivity study of various cell sizes at 0.3 ms^{-1} velocity.

The corresponding velocities differ vastly from the ones with smaller, more accurate cell sizes of 0.10 m and 0.25 m. Moreover, they point towards the airflow's opposite direction.

Since no severe difference between air velocities of 0.1 m and 0.25 m cells can be observed (see trendlines in figure 14), latter size can be sufficiently applied to the cleanroom model.

5.4 Modelling Cases

Taking computing resources into account, all cases were developed to reality as close as possible. Flow pattern and room design in actual cleanrooms were immitaded as shown in figure 9 and 10. The main objective is to compare different FFU velocities and their effects on smoke spread as shown in chapter 5.1. Unlike FFU velocity and HRR curve (see table 7), model features remain constant throughout all cases.

Case	FFU velocity [ms^{-1}]	max. HRR [MW]
I	0.0	10
II	0.3	10
III	0.4	10
IV	0.5	10
V	0.6	10
VI	1.5	10
VII	0.6	0.675

Table 7: FFU velocity and max. HRR settings in different cases.

Due to computing limitations, Smokeview output could not be obtained in case I, VI and VII. The behavior of smoke could only be read out by using MATLAB [64].

In case VII the fire was controlled by a fire sprinkler. It was assumed that a water sprinkler (glass bulb breaks at 68°C), covering a surface area of 15 m^2, is installed in r = 2.18 m (derived by equation 6).

$$r = \sqrt{\left(\frac{A}{\pi}\right)} \tag{6}$$

At radial distances greater than r/h = 0.18, the max. temperature in the ceiling jet depends on the distance to the plume centerline at ceiling hight (see equation 8).

$$\frac{r}{H} > 0.18 \tag{7}$$ [65]

$$\frac{r}{H} = \frac{2.18[m]}{4[m]} = 0.55$$

[64] numerical computing environment

[65] NFPA, 2003

The temperature in 2.18 m distance from the impingement point reaches 68.98°C when the total HRR of the fire equals 675 kW.

$$T_{m(jet)} = 5.38\frac{\left(\frac{\dot{Q}_c}{r}\right)^{\frac{2}{3}}}{h} + T_\infty \qquad (8)\ ^{66}$$

$$T_{m(jet)} = 5.38\frac{\left(\frac{472.5[kW]}{2.18[m]}\right)^{\frac{2}{3}}}{4[m]} + 20[°C]$$

$$T_{m(jet)} = 68.98°C$$

The relevant FDS input file was therefore adjusted as follows:

Using equation 5, a HRR of 675 kW and the appropriate alpha value of 0.111, the time until the sprinkler goes off (after fire starts) is 78 s.

$$t = \sqrt{\frac{675kW}{0.111}} = 77.98s$$

Since the fire starts after T = 200 s, the input value changes to T = 278 s.

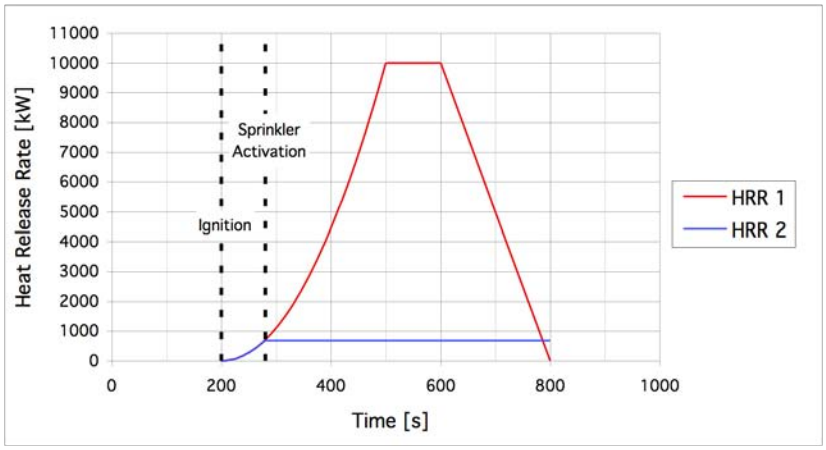

Figure 15: HRR of case VII over time.

The fire still follows the derived t^2-fire curve (see figure 15), but it is assumed that the sprinkler system keeps the fire controlled on a steady level of 675 kW until the 800th

66 NFPA, 2003

second. This is also expected to happen in a real fire szenario since wet benches are partly covered by hoods (see figure 16).

Figure 16: Wet bench [67].

Some burning machinery parts cannot be reached and extinguished by water spray from a fire sprinkler mounted to the ceiling.

5.5 Physical Discussion of CFD Results

This chapter aims at the physical description of results obtained by CFD modelling. A comparison of different simulations is to explain the influence of down flow air velocity on smoke spread. In table 8 timestep plots at 300, 400 and 500 s of cases II and V are listed. Smokeview output of cases I, VI and VII could not be displayed due to computing limitations. These results are discussed later on the basis of sensor data in MATLAB (see table 9). Table 8 compares smoke behaviour at an average clean air velocity of 0.3 ms^{-1} to a velocity twice as high.

Timestep 300 (100 s after burn starts) shows one of the major findings achieved in the course of this thesis. A duplication, or generally an increase in FFU velocity involves the decrease of radial smoke spread. An example for this theory is case V where the aisle is not contaminated by smoke unlike case II where smoke enters through the room's opening. Furthermore, it can be noticed that a larger amount of smoke enters the nearby return air path, coming from the subfab (as per smoke sensity). Due to higher clean air fluxes entering the cleanroom from the ceiling, larger volumes of smoke are drained away through the perforated floor. Hence, radial smoke spread is reduced (see also chapter 5.1).

[67] UOC, 2010

Time [s]	Case II (0.3 ms^{-1})	Case V (0.6 ms^{-1})
300	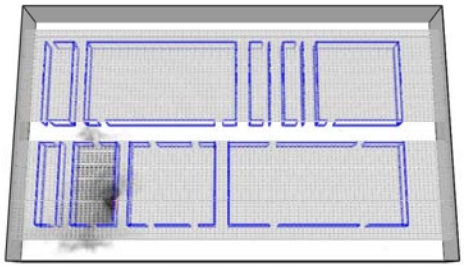	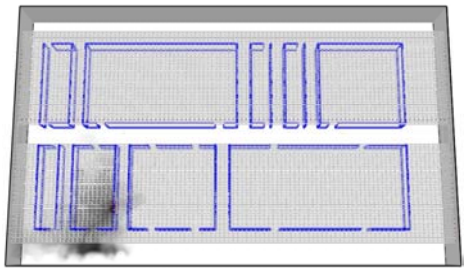
400	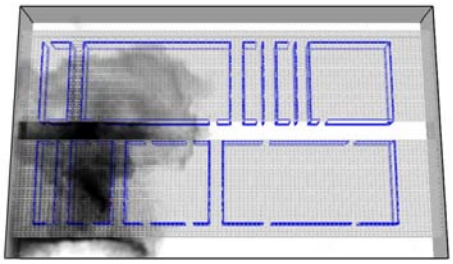	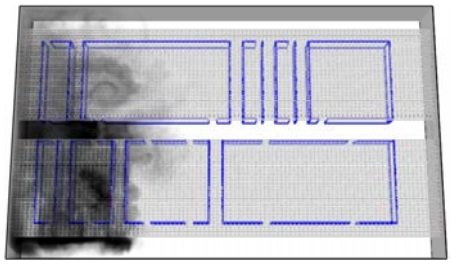
500	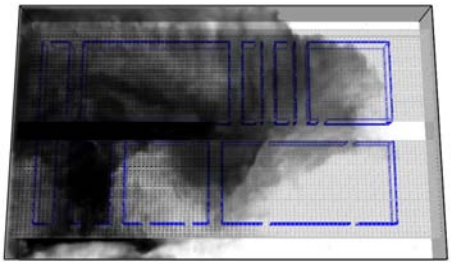	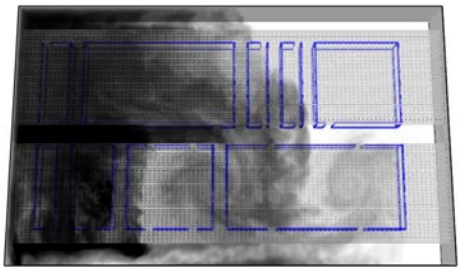

Table 8: Smoke spread in case I & V.

The theory developed in this thesis is referred to as *buoyancy control* and explained in detail in chapter 7.

Timestep 400 underlines the observations made at 300 s. Less smoke fills and contaminates the aisle but larger volumes can now be found in the nearby return air path starting to enter the plenum.

In timestep 500 dilution of smoke is the reason for a decrease of smoke density in the plenum (case V). Before entering the plenum, smoke should have been removed already, either in the subfab or in the return air paths. The still working FFU's would reinject plenum smoke into other sections of the cleanroom, yet maybe uncontaminated.

In order to compare even greater varieties in clean air velocities, which also include case I (FFU's shut off), table 9 was implemented. An overlay of sensors and obstructions in the actual CFD model caused a sensor unequipped area in the bottom right corner of the MATLAB plots. This does not affect the overall results.

However, the assumptions made in table 8 by using Smokeview can be confirmed when compared to the recorded data in table 9. A further increase in velocity to 1.5 ms^{-1} leads to an intensified reduction of smoke spread (note changed colour mapping in case VI). Moreover, it is now visible that denser mixture fractions are restricted to a smaller area within the vicinity of the fire source. This bases on the fact that larger volumes of smoke are drained away quicker and in a smaller area by higher FFU velocities.

Case I features no clean air velocity and can only be applied partly to real cleanroom conditions. Due to FDS 5 modelling possibilities smoke is able to leave the cleanroom via the virtual FFU's into the plenum (see appendix 24). This could theoretically happen also in reality, but not before HEPA filters burned through. Then smoke directly enters the plenum. Despite this fact, it becomes obvious that smoke hits the cleanroom worst under these conditions. In timestep 400 nearly the whole cleanroom is contaminated by smoke.

In reality the damage value in the cleanroom would be much higher since smoke cannot leave, resp. is not forced to leave, the cleanroom. Appendix 21 hardly shows any smoke penetration into the subfab. Only when it comes to a sufficient loss in smoke buoyancy it sags through the perforated floor into this storey.

Generally it can be seen that increasing FFU velocities reduce smoke spread in the beginning stadium of the fire on cleanroom level. Therefore subfab, recirculation air paths and plenum are contaminated earlier (camparing appendices 7,10,13,16,19,22,2 & 9,12,15,18,21,24) when smoke is not removed before entering these sections by additional extraction systems.

Case [ms^{-1}]	Timestep 300	Timestep 400
Case II (0.3)	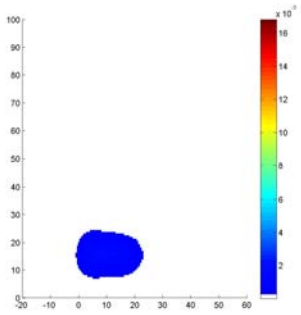	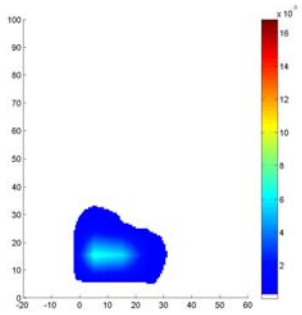
Case V (0.6)	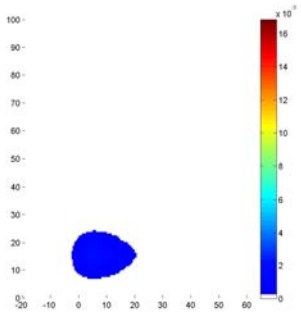	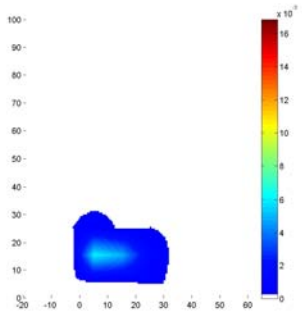
Case VI (1.5)	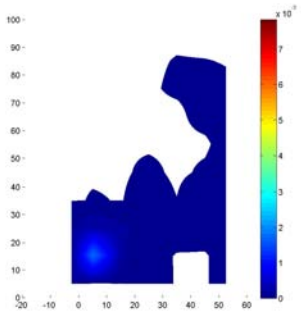	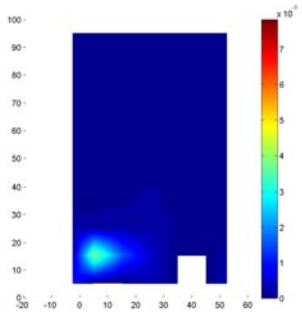
Case I (0.0)	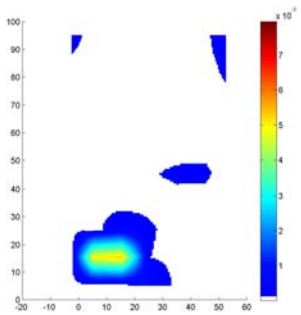	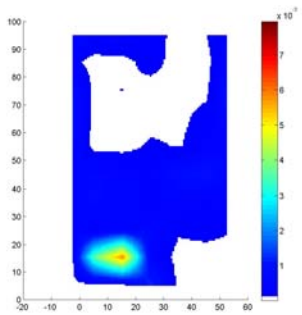

Table 9: Mixture Fractions plotted for several FFU-velocities at 300 s and 400 s.

6 Costs, Hazards and Losses

The semiconductor industry, with a total annual revenue of US$ 267.5 billion (figures from 2007 [68]), is the fastest growing industry in the world. Cleanrooms are of all industrial fabrication plants by far the most complex and expensive facilities, manufacturing silicon microchips is a high-value and high-risk process. Currently costs have risen up to US$ 1.5 billion per plant. With the advent of 300 mm waver fabs, costs are expected to be more than twice as high. This step-up from the older 200 mm wavers is seen by the Semiconductor Equipment and Materials International (SEMI) as the “largest industrial transition in history“ and is estimated to cost US$ 14 billion [69]. Typically, it takes two to three years to built a new cleanroom production facility.

The demand for mobile phones, computers and memory requiring software applications resulted in facilities, operating 24/7 to satisfy customer needs [70].

Figure 17: Small damage to machine, total loss likely to be over US$ 10 million [71].

Since the number of semiconductor fabs producing the latest types of microchips is approximately 250 worldwide, shut-downs of single factories have huge impact on the overall supply. Severe shortages consequently affecting many different branches of the electronic industry can occur. Even the smallest event may cause delays in production and losses of millions of US Dollars (see figure 17).

68 GSA, 2007
69 IMIA, 1999
70 Brown, Alastair, 1996
71 Brown, Alastair, 1996

The insurance industry and cleanroom risk management face unparalleled challenges through the combination of sophisticated and vulnerable production processes using high value equipment and some of the most aggressive chemicals. Hazards mostly arise from factors like [72]:

- highly flammable and explosive gases and liquids
- ducts and pipes made of combustible materials (PP,PVC)
- large fire sections (open plan design) containing high values
- gases and liquids (toxic and chemically aggressive)
- high temperature processes (up to 800°C)
- high voltage needed
- shock resistant equipment
- contamination and corrosion by chemical residues
- theft
- espionage

Risks increase when process equipment like wet benches (made of plastic) is used. These Polypropylene or PVC benches are up to 10 m long and replacement costs range from £ 15.000 to £ 1 million. Wet benches (also see chapter 5.4) are usually protected by fire sprinklers. Non-thermal damage caused by smoke can lead to the damage of other tools, work in progress and the cleanroom itself. Average clean-up opertion times are two to six weeks. Since delivery and installation of special equipment takes up to 12 months, restarting the production can accordingly take even longer. The largest foreseeable fire loss event is a burning group of wet benches connected to the same fume duct. Expected losses could run into hundreds of millions of US$ and stop fabrication for up to 12 months [73].

Table 10 shows loss data collected from FM Global's [74] semiconductor industry clients, covering the period between 1990 and July 2000. Total losses of US$ 383.3

72 IMIA, 1999

73 Brown, Alastair, 1996

74 Factory Mutual Insurance Company

million were reported in 232 incidents where fire was the second most frequent risk adding up to 17% of all incidents and 16 % of the total loss. The average loss per incident is estimated to US$ 1.61 million [75].

Peril	Incident number	% of total	Gross loss (US$ m)	% of total	$ per loss (US$ m)
Escaped liquids	44	19	97.6	25	2.22
Earth movement	4	2	68.1	18	17.03
Fire	39	17	62.6	16	1.61
Service interrupion	23	10	34.7	9	1.51
Electrical breakdown	37	16	24.1	6	0.65
Impact	3	1	14.3	4	4.77
Sprinkler leakage	13	6	7.0	2	0.54
Mech. breakdown	7	3	4.2	1	0.60
Water damage	7	3	4.0	1	0.57
Miscellaneous	28	12	60.3	16	2.15
All other	27	12	6.4	2	0.24
Total	232		383.3		1.65

Table 10: Loss data for the semiconductor industry (1990 – July 2000) [76].

According to [77], the average number of fire losses in cleanrooms per year is one in ten with an approximated size loss of US$ 8 million. For typical industrial plants, these average loss numbers are one out of 100 with an approximated size loss of US$ 250.000. Furthermore it is stated that a tool fire in a common cleanroom can cause property damages worth between US$ 20 million and US$ 100 million and two to eight weeks of production interruption.

Figures collected by [78] state that insurers tend to underestimate their financial exposure when insuring the semiconductor industry. This is because of a lack of adequate statistics and rapid changes in technology. The industries total losses are added up to US$ 60 million for the period from 1974 to 1986. The figure increased by 17 times to US$ 1 billion for the period between 1986 and 1998.

75 Barnes, Robert, 2002
76 Barnes, Robert, 2002
77 Peterkin, Heron, 2002
78 IMIA, 1999

6.1 Loss Estimation

This chapter approaches the development of a computer based method to revolutionise loss estimation for cleanrooms that is currently still inaccurate. This arises because spread of fire and smoke is difficult to predict not only because of the characteristic airflow that does not allow to compare fires in ordinary buildings to the ones in cleanrooms but also because their design and arrangement is subject to steady change.

Each FDS file contains 210 devices measuring MIXTURE FRACTION and TEMPERATURE within the cleanroom model. According to [79], the command MIXTURE FRACTION in FDS 5 gives the air/fuel ratio and is specified by the unit kg/kg. Generally speaking these devices meter temperatures and the amount of smoke per unit clean air and visualise the level of contamination at certain points. This allows to infer to the grade of damage that is done to:

- Buildung and Structure
- Machinery and Equipment
- Work in Progress

The collected sets of data are then transferred into MATLAB scripts which convert these into coloured 2-D plots representing the different levels of the cleanroom complex. It is now possible to check smoke spread and temperature profiles under certain conditions against each other. The main aim is to find out FFU velocity settings that have positive effects on these parameters. The results are later linked to a new way of loss estimation by adding different damage values for different cleanroom sections. The actual losses per square metre in cleanroom-, subfab- and the plenum- area are determined as shown in table 11. Damages caused by fire and smoke to B&S [80] are considered to have the same values in all areas since components and structures are generally the same throughout the whole complex. Higher losses are expected to emerge to M&E [81] particularly on cleanroom level containing the

[79] Gissi, Emanuele, 2009

[80] Building & Structure

[81] Machinery & Equipment

world's most expensive industrial fabrication equipment. The subfab level, usually open space containing less expensive machinery, shows a relatively low loss value.

	B&S ($/m²)	M&E ($/m²)	WIP ($/m²)
Cleanroom	50.000	100.000	50.000
Subfab	50.000	25.000	0
Plenum	50.000	50.000	0

Table 11: Loss/m² (B&S, M&E,WIP) in different areas of the cleanroom complex.

WIP [82] can only be found within the cleanroom and represents damage done to semi-finished products in the process of manufacture as well as to already packaged products. The data collected by each device represents a surface area of 100 m² on cleanroom level.

Mixture fraction	B&S % Damage	WIP % Damage	M&E % Damage
0.0	0.0	0.0	0.0
0.005	0.05	0.05	0.05
0.009	0.1	0.1	0.2
0.01	0.5	0.5	1.0
1.0	0.5	0.5	1.0

Table 12: Mixture fraction linked to % damages.

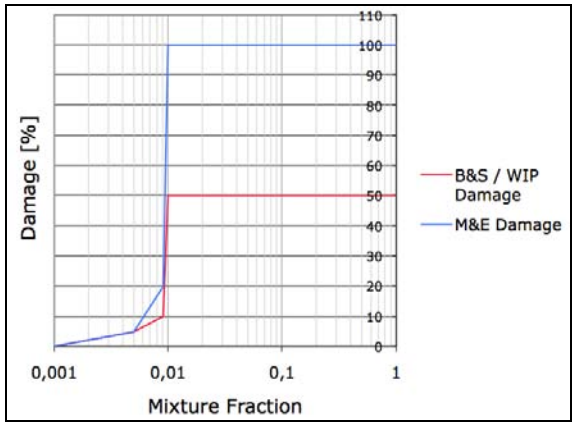

Figure 18: Data corresponding to table 12.

The applied MATLAB script interpolates each value between its adjacent values in the mixture fraction column as shown in table 12 and multiplies the appropriate percent damage value for B&S, WIP and M&E with it's according value in table 11.

[82] Work in Progress

7 Loss Estimation based Discussion of CFD Results

This chapter covers financial aspects of the outcomes observed by CFD modelling. The following conclusions were drawn basing on procedures given in chapter 6.1. and data listed in appendix 1-38 and figures 19-21. As stated before, MATLAB colour mapping was used to dedicate different loss values and consequently infer to the overall results.

7.1 Subfab area

According to appendix 24, 27, 30, 33 & 36 the maximum temperature reaches 33°C at a velocity of 0.5 ms^{-1} (in 1.5m room height). No temperature damage is to be expected in this storey. Figure 19 shows loss lestimation values for the subfab. It can be seen that there is relatively little damage caused when FFU's are completely shut off in the event of fire (US$ 206.780). The sprinklered case (velocity 0.6 ms^{-1}) causes an insignificantly higher damage (US$ 369.460) due to a lower HRR of 675 kW.

Figure 19 and table 13 show decreasing damage at 400 s (200 s after the fire starts) with decreasing FFU velocities and a peak value of about US$ 500.000 at the highest velocity of 1.5 ms^{-1}. In this case the higher the air velocity, the more plume buoyancy gets lost and the more smoke is pushed through the floor. Chapter 5.1 and 5.5 describe the effect of unidirectional airflow on smoke spread. This pattern can still be seen after 700 s, however, the highest velocity causes noticably less damage (US$ 2.4 million) than velocities of 0.6 / 0.5 / 0.4 / 0.3 ms^{-1} after this period of time. Further research has to be carried out to clarify this fact. The increasing dillution (decreasing mixture fraction) of smoke could be an explanation. The highest loss of US$ 5.239.100 million is caused by a velocity of 0.6 ms^{-1} after 800 s.

Generally it can be inferred that lower clean air velocities cause less damage on subfab level.

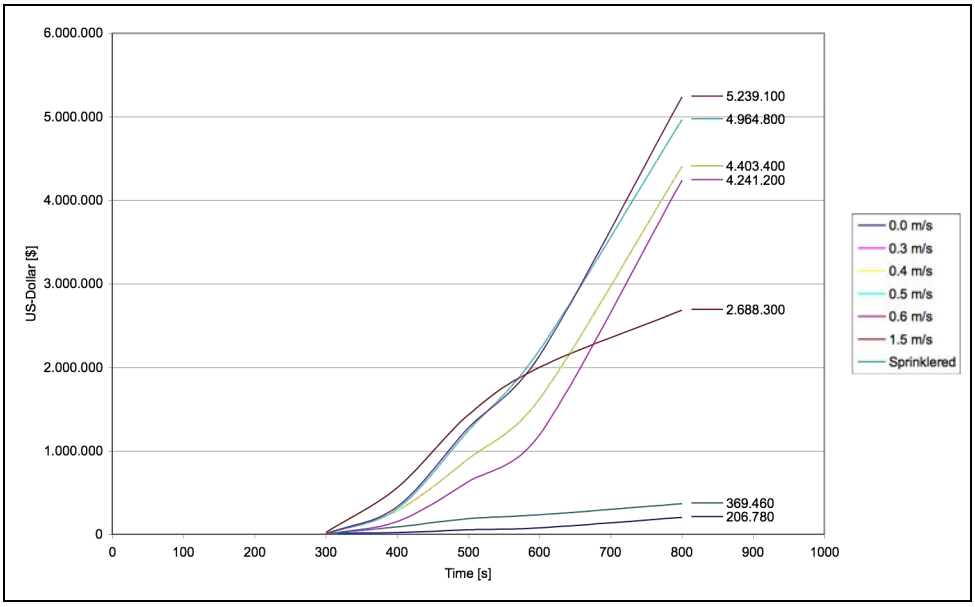

Figure 19: Subfab loss values in US$ at various FFU velocities over time.

Subfab	400 s	1.5	0.6	0.5	0.4	0.3	S [83]	0.0
	700 s	0.6	0.5	0.4	0.3	1.5	S	0.0

Table 13: FFU velocities [ms^{-1}] in damage descending order (fig. 19) .

7.2 Cleanroom area

At this level temperature damage is mostly limited to the room and the equipment contained. The sensors allocated in the vicinity around the room meter maximum temperatures of about 180°C at a FFU velocity of 0.5 ms^{-1} (2.5 m room height).

Higher and lower clean air velocities than 0.5 ms^{-1} caused decreasing max. temperatures which can be explained by a) dilution and b) smoke layer height above 2.5 m since the airflow could not overcome buoyancy effectively enough at these near by sensors (see appendix 25, 28, 31, 34, 37).

On cleanroom level the highest damage at timestep 400 (about US$ 6 million) occurs when there is no airflow working against smoke buoyancy. The loss value is more than halved (US$ 2.5 m) when 1.5 ms^{-1} are applied. In general it can be inferred that increasing velocities cause less damage in the initial stadium of the fire by reducing the smoke spread diameter around the fire source (see also chapter 5.1 and 5.5). This assumption stays true up to a certain point in time when, driven by the air

[83] Sprinklered

recirculation process within the cleanroom complex, contaminated air is reinjected from plenum to fab. Then higher velocities cause higher (o.5 ms^{-1} / US$ 28.244.000) damage due to larger volumes of smoke entering the cleanroom. This means that higher FFU velocities in combination with an early smoke management system in the subfab can decrease smoke damage in the cleanroom.

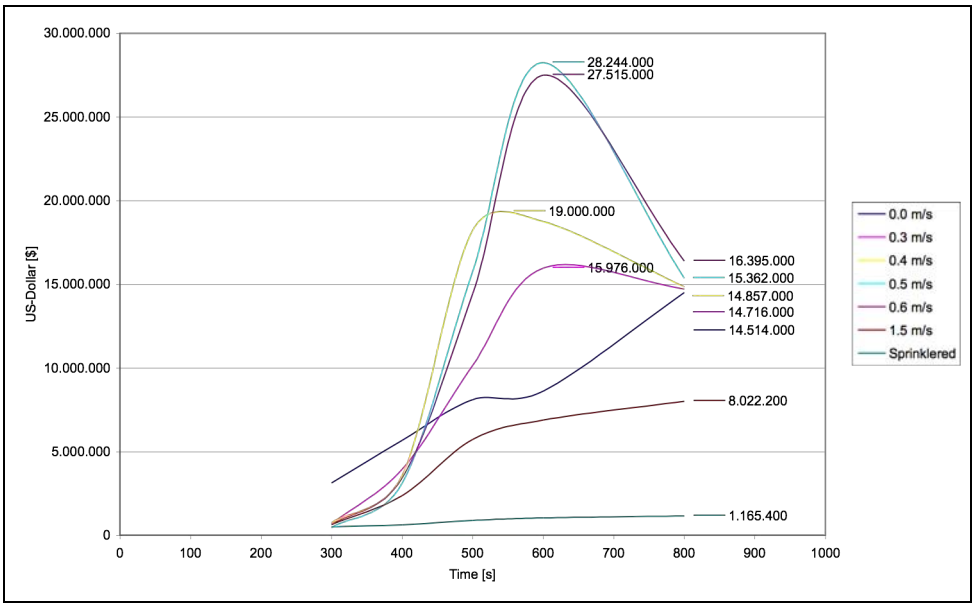

Figure 20: Cleanroom loss values in US$ at various FFU velocities over time.

Cleanroom	400 s	0.0	0.3	0.4	0.6	0.5	1.5	S
	700 s	0.6	0.5	0.4	0.3	0.0	1.5	S

Table 14: FFU velocities [ms^{-1}] in damage descending order (fig. 20).

The reason why the highest velocity shows the lowest damage (except for the sprinklered case) still has to be investigated. A possible explanation could again be smoke dilution. The measuring devices meter the clean air/smoke ratio which is much lower if well mixed by relatively high FFU velocities.

7.3 Plenum area

Plots as shown in appendix 26, 29, 32, 35 and 38 reveal that plenum temperatures are not high enough to cause severe damage. Loss and smoke behaviour estimated in figure 21 (case 0.0 ms^{-1}) is physically true but due to several limits within FDS not applicable (also see chapter 5.5). As stated in chapter 7.2 and obvious in figure 21

higher FFU velocities direct larger volumes of smoke into the plenum. A loss difference of US$ 1.242.800 gaps between 0.6 ms^{-1} (US$ 7.271.600) and 0.3 ms^{-1} (US$ 6.028.800) at timestep 800. If smoke is not removed before entering the plenum, higher losses are to be expected when higher velocities are applied.

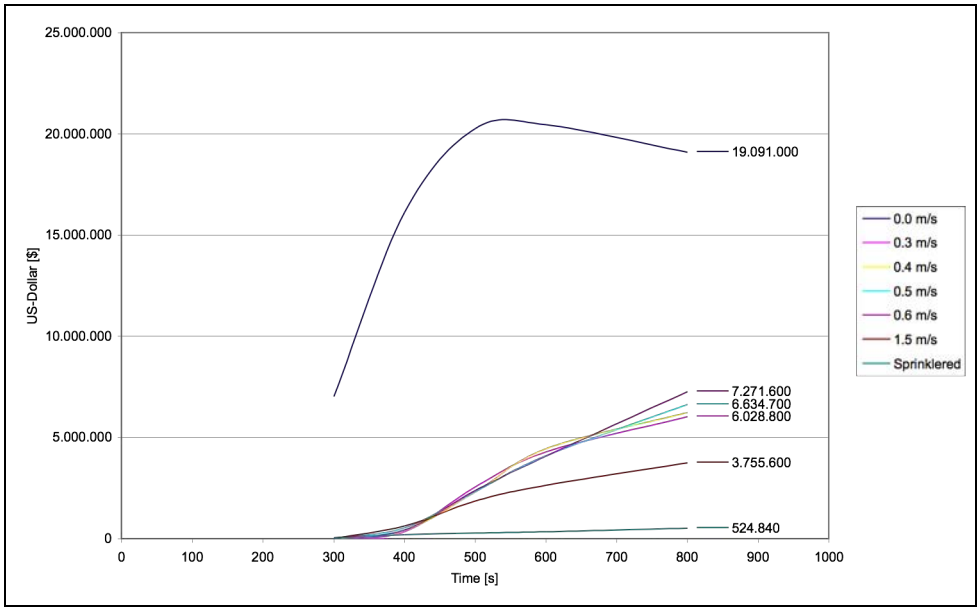

Figure 21: Plenum loss values in US$ at various FFU velocities over time.

Plenum	400 s	0.0	1.5	0.5	0.6	0.4	0.3	S
	700 s	0.0	0.6	0.5	0.4	0.3	1.5	S

Table 15: FFU velocities [ms^{-1}] in damage descending order (fig. 21).

7.4 Discussion

Chapter 7 proves that numerical modelling can be sufficiently linked to cleanroom loss estimation. The achieved outcomes help to improve accuracy and efficiency in this field by estimations basing on sensor data and facts observed in various simulations.

It becomes clear that there cannot be one single way, respectively velocity, to reduce cleanroom losses caused by fire and smoke. However, the combination of a generally increased clean air velocity and early stage smoke extraction is a way to successful smoke management.

An innovative concept called *buoyancy control* reveals a new way of cleanroom smoke treatment. Unlike methods applied to common buildings, this approach works in a reverse way. The purpose is to deliberately decrease smoke buoyancy by injecting cold clean air through FFU's mounted to the ceiling. This results in an earlier sagging smoke layer which then follows the recirculation airflow pattern of cleanrooms. A smaller area around the fire source is contaminated on cleanroom level since smoke is drained away faster passing the perforated floor. The aim is to transform this hot layer of smoke into a usual, even though highly concentrated, cloud of smoke featuring the same physical circumstances as the ambient cleanroom air.

Completely stopping the FFU's is not recommended since nearly the entire room gets contaminated when smoke travels unhindered along the ceiling.

8 Conclusions and Further Work

Numerical fire modelling in cleanrooms is an issue of growing interest with progress made in computing performance and facilitates a time and cost effective method to simulate and investigate airflow mechanisms in an event of fire. The results obtained by CFD are linked to cleanroom loss estimation to upgrade superseded methods used in this high-value industry.

Instead of validating the effectiveness of common fire safety strategies in smoke control or fire suppression, a so far not rated approach named *buoyancy control* was developed and tested. It demonstrates a seperate way of contamination control, additionally to the ones already existing. One advantage is that cleanrooms do not have to be modified in general, thus implementation costs compared to other strategies are relatively low and the introduction phase is shortened.

The conducted research shows that buoyancy control is a promising and innovative way to minimise damage and losses caused by smoke in cleanrooms. This strategy is activated when fire or smoke is detected and works by simply increasing FFU airflow velocity within the cleanroom. After buoyancy is eliminated, smoke sags through the floor and is finally removed in the subfab or return air paths. However, this method can only be applied at the cleanroom level itself, smoke in other parts of the complex has to be treated differently.

In terms of loss estimation for the semiconductor industry this thesis presents a novel practise to utilise CFD data for advanced a priori loss calculation. It is now possible to simulate fire incidents and their effects. An advanced prediction of total loss values prevents insurers of highly under-, respectively overestimating their financial exposure.

Especially in the field of smoke spread and buoyancy control in cleanrooms further work has to be done to improve this first attempt. Additional time is required to test the impact of higher FFU velocities and define physical processes precisely. Furthermore it is expected that extra cold air applied by FFU's is beneficial to the concept of buoyancy control.

In addition to this approach, smoke extraction has to be implemented in other areas of the building. Studies to locate the most effective arrangement and setup of these units have to be carried out. In case smoke enters the plenum area, smoke curtains

could be helpful to minimise the contaminated area. An advantage would be the relatively inexpensive subsequent installation of the system which could be activated in the event of fire.

Further improvements can also be made by validating loss estimation numbers more precisely.

REFERENCES

Van Zant, Peter, 1997 — Van Zant, Peter: *Microchip Fabrication – A Practical Guide to Semiconductor Processing, 3rd Edition.* McGraw-Hill, NY, 1997.

Sze, M.S., 2002 — Sze, M.S.: *Semiconductor Devices – Physics and Technology, 2nd Edition.* John Wiley & Sons, Inc., Hoboken, NJ, 2002.

Landers, Thomas, 1994 — Landers, Thomas L., et al.: *Electronics Manufacturing Processes.* Prentice-Hall Int., Inc., London, 1994.

Naughton, Phil, 2006 — Naughton, Phil, et al.: *High Efficiency Particulate Air (HEPA) Filter Velocity Reduction Study*. International SEMATECH Manufacturing Initiative, Austin, TX, 2006.

Cheng, M., 1998 — Cheng, M., et al.: *Approaches for improving airflow uniformity in unidirectional flow cleanrooms*. Building and Environment 34 (1999), 1998 Elsevier Science Ltd., 1998.

Tolliver, Donald, 1988 — Tolliver, Donald L.: *Handbook of contamination control in microelectronics*. Noyes Publications, Park Ridge, NJ, 1988.

Brown, Alastair, 2001 — Brown, Alastair: *Safe progress (S.25-27).* Fire Prevention, FPA Fire Protection Association, Issue 347, London, 2001.

ISO 14644, 1999 International Organization for Standardization: *International ISO Standard 14644-1, Cleanrooms and associated controlled environments — Part 1: Classification of air cleanliness.* International Organization for Standardization, Geneva, 1999.

Ramstorp, Matts, 2000 Ramstorp, Matts: *Introduction to Contamination Control and Cleanroom Technology*. Wiley-VCH Verlag GmbH, Weinheim, 2000.

Barnes, Robert, 2002 Barnes, Robert, et al.: *Recovery position (iii)*. Fire Prevention – Fire Engineers Journal, FPA Fire Protection Association, London, April 2002.

Ferreira, Michael, 1999 Ferreira, Michael, et al.: *Conference Proceedings Volume 1 interflamm '99, Emergency smoke control system design for semiconductor fabrication facilities: Is property protection achievable?*. Interscience Communications Limited 1999, London, 1999.

Heskestad, Gunnar, 2004 Heskestad, Gunnar: *Smoke distribution from fire plumes in uniform downdraft from a ceiling*. Fire Safety Journal 39 (2004) 358 – 374, Elsevier, 2004.

SFPE, 2008 Heskestad, Gunnar: *Fire Plumes, Flame Height, and Air Entrainment.* SFPE Handbook of Fire Protection Engineering, 4th Edition, National Fire Protection Association, Quincy, Massachusetts, 2008.

Brown, Alastair, 2002 Brown, Alastair: *Liquid measures (viii)*. Fire Prevention – Fire Engineers Journal, FPA Fire Protection Association, London, April 2002.

McGrattan, Kevin, 2009 McGrattan, Kevin, et al.: *NIST Special Publication 1019-5, Fire Dynamics Simulator (Version 5) User's Guide*. National Institute of Standards and Technology, Gaithersburg, MD, 2009.

Nam, Soonil, 2000 Nam, Soonil: *Numerical simulation of smoke movement in clean room environments*. Fire Safety Journal 34 (2000) 169 – 189, Elsevier, 2000.

I, Yet-Pole, 2009 I, Yet-Pole: *The simulation of air recirculation and fire/explosion phenomena within a semiconductor factory*. Journal of Hazardous Materials 163 (2009) 1040-1051, Elsevier, 2009.

NFPA, 2003 Budnick, Edward, et al.: *Simplified Fire Growth Calculations.* Fire Protection Handbook, 19th Edition, National Fire Protection Association, Inc., Quincy, Massachusetts, 2003.

UCT, 2010 Web page of Ultra Clean Tech: *http://www.uct-sh.com/en/UpFiles/UpLoadFile/20094714912232.jpg*,24.06.2010, Shanghai, China, 2010.

UOC, 2010 Web page of the University of Cincinnati, Nanoelectronics Laboratory: http://www.nanolab.uc.edu/equipment/Other/WetBench.jpg, Cincinatti, 2010.

Brown, Alastair, 1996 Brown, Alastair: *Computer chip clean rooms – a new fire protection challenge*. Fire Prevention, Issue 287, Fire Protection Association, Borehamwood, 1996.

Brown, Alastair, 2004 Brown, Alastair: *Keep it clean*. Fire Prevention – Fire Engineers Journal, Vol 64, Fire Protection Association, 2004.

Brown, Alastair, 2004 — Brown, Alastair: *Keep it clean*. Fire Prevention – Fire Engineers Journal, Vol 64, Fire Protection Association, 2004.

Peterkin, Heron, 2002 — Peterkin, Heron: *Supply and demand*. Fire Prevention – Fire Engineers Journal. Fire Protection Association, April 2002.

GSA, 2007 — GSA Global: http://www.gsaglobal.org/news/article.asp?Article=2008/0409, 13.05.2010, Dallas, Texas, 2007.

IMIA, 1999 — IMIA Meeting 1999: *Insurance for semiconductor plants during construction and operation – IMIA-WGP4(99)E*. Versailles, 1999.

Versteeg, 2007 — Versteeg, H. K., et al.: *An Introduction to Computational Fluid Dynamics – The Finite Volume Method.* Pearson Education Limited, Essex, 2007.

Gissi, Emanuele, 2009 — Gissi, Emanuele: *An introduction to Fire Simulation with FDS and Smokeview*. Genova, 2009.

Wang, Yi, 2009 — Wang, Yi, et al.: *Large Eddy Simulation of Thermal and Fire Plumes Based on OpenFOAM Toolbox.* Fourth OpenFOAM Workshop June 1-4 2009, Montreal, Canada, 2009.

CS&E, 2008 — Web page of Combustion Science & Engineering, Inc., http://www.firemodelsurvey.com/FieldModels.html, 11.08.2010, Columbia, Maryland, 2008.

LIST OF FIGURES

LIST OF TABLES

LIST OF APPENDICES

APPENDIX

Appendix 1: Case II (0.3 ms^{-1}).

t=300 s

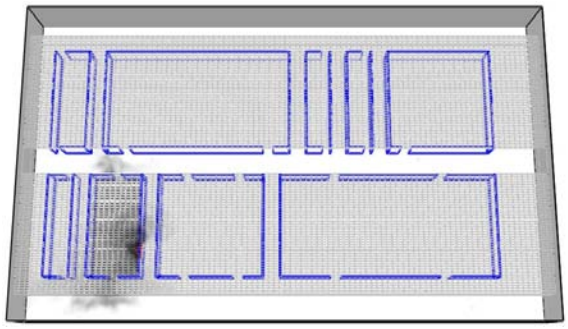

t=400 s

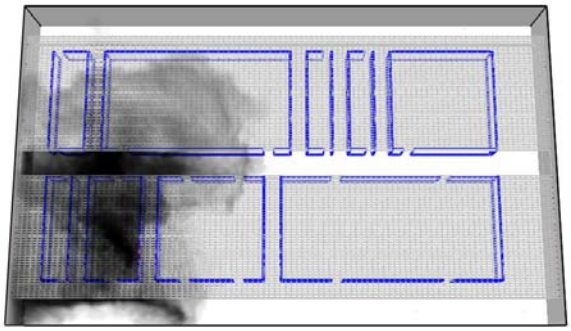

t=500 s

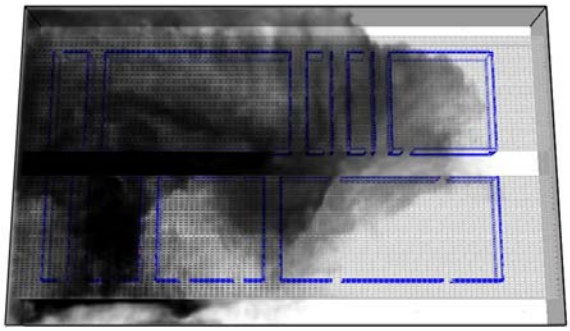

t=600 s

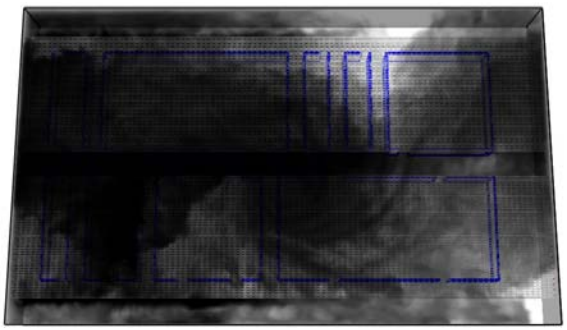

t=700 s

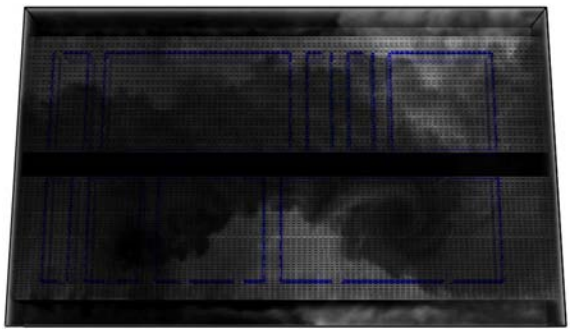

t=800 s

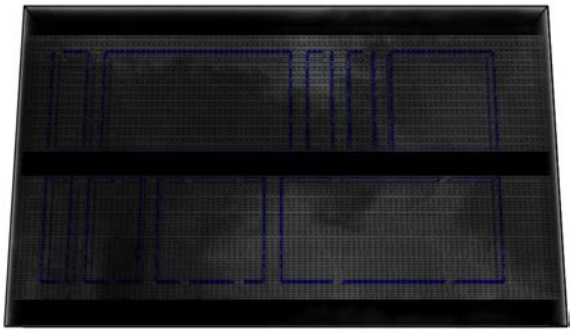

t=900 s

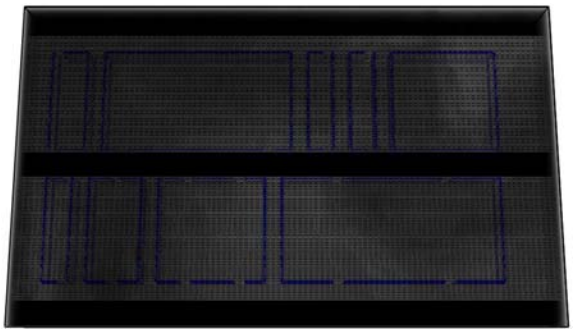

t=1000 s

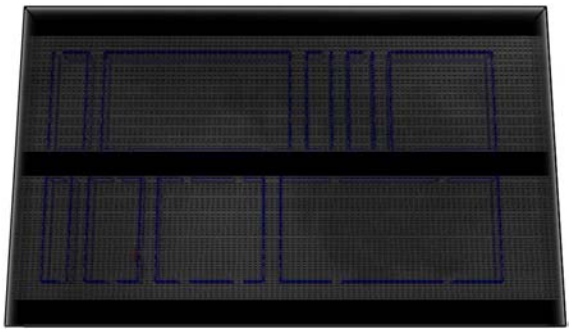

Appendix 2: Case III (0.4 ms^{-1}).

t=300 s

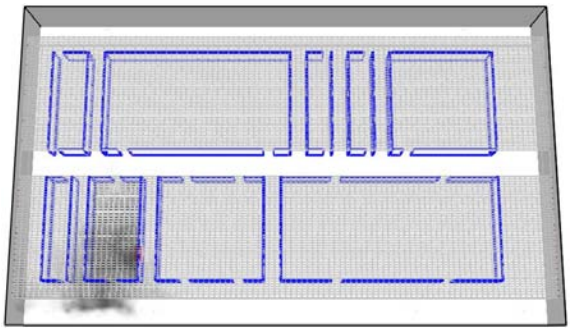

t=400 s

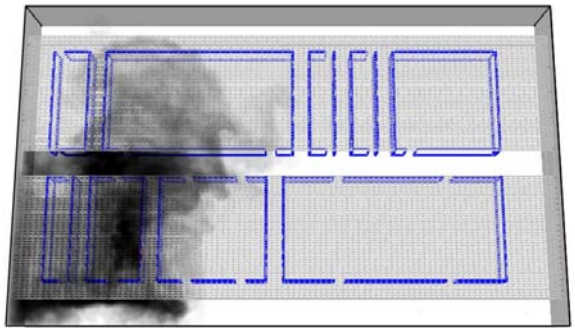

t=500 s

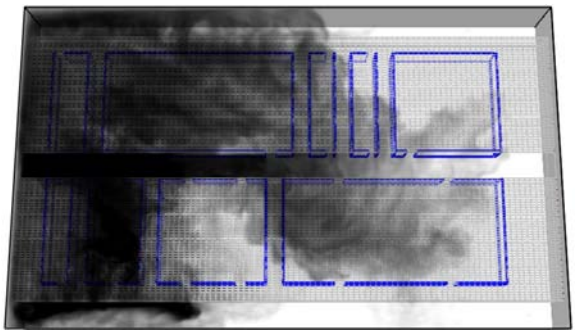

t=600 s

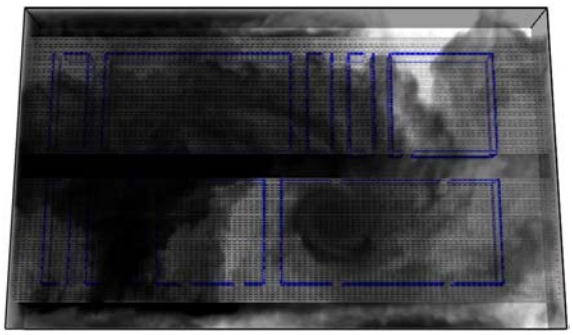

t=700 s

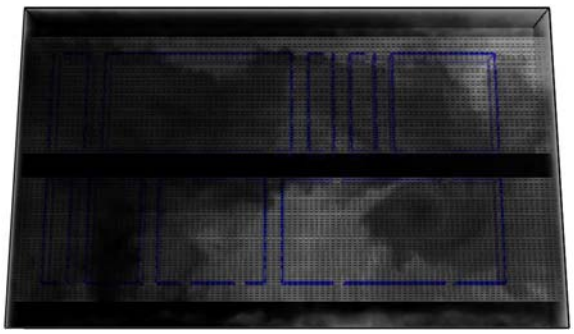

t=800 s

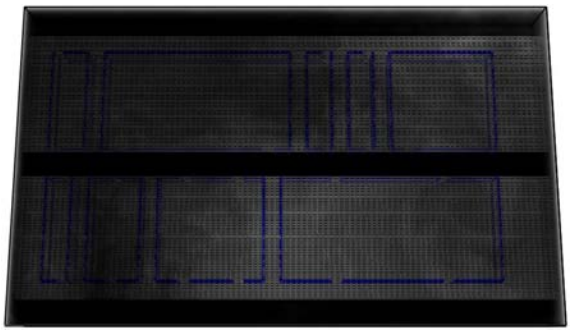

t=900 s

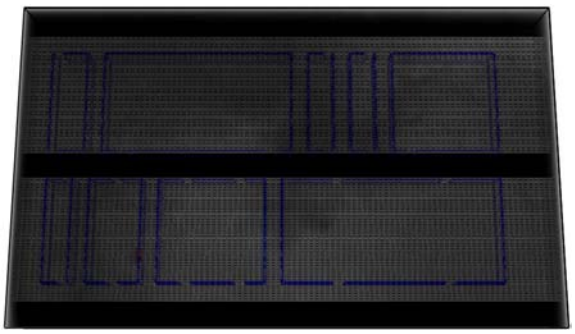

t=1000 s

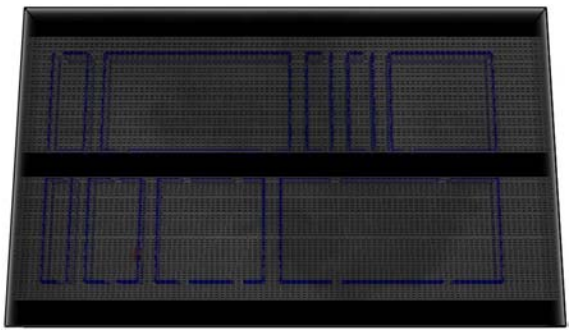

Appendix 3: Case IV (0.5 ms^{-1}).

t=300 s

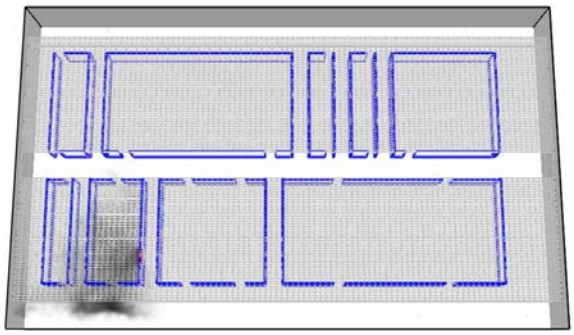

t=400 s

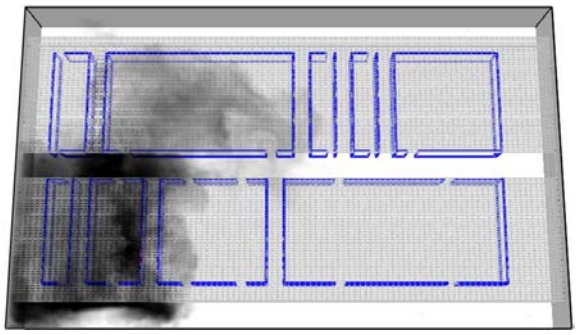

t=500 s

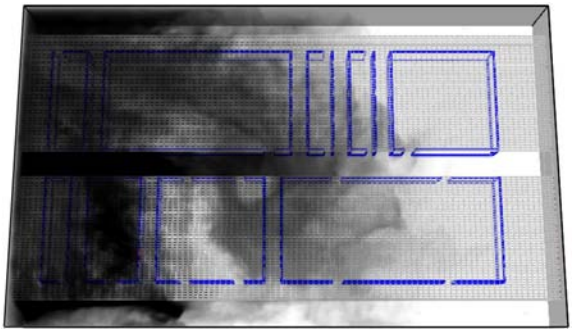

t=600 s

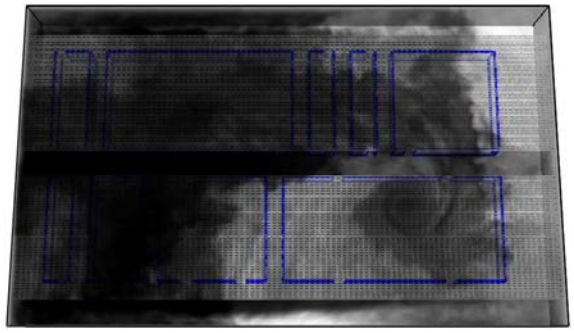

t=700 s

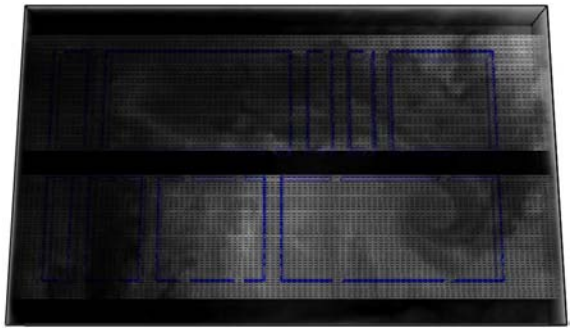

t=800 s

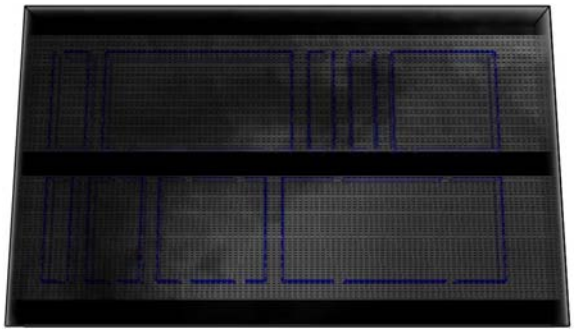

t=900 s

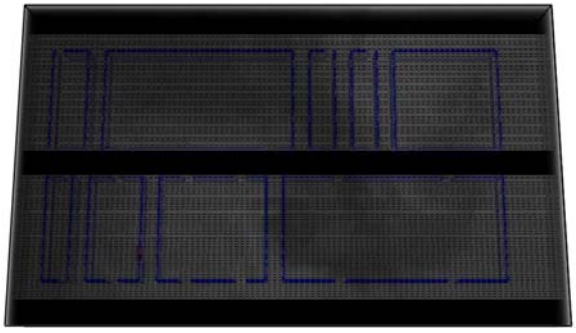

t=1000 s

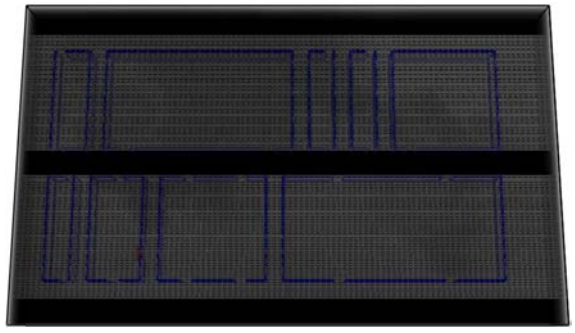

Appendix 4: Case V (0.6 ms^{-1}).

t=300 s

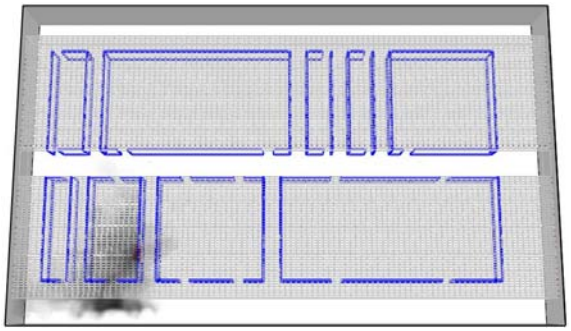

t=400 s

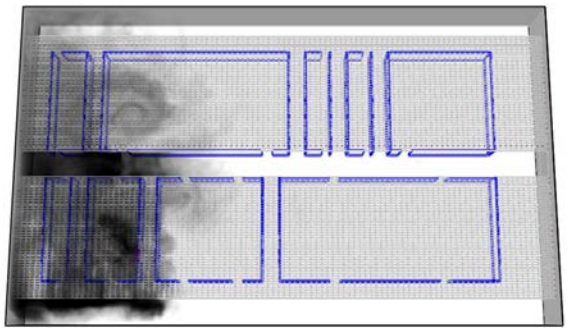

t=500 s

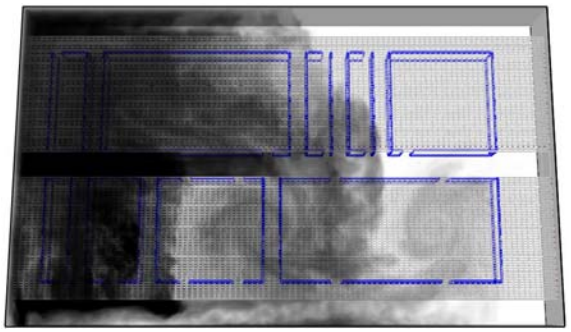

t=600 s

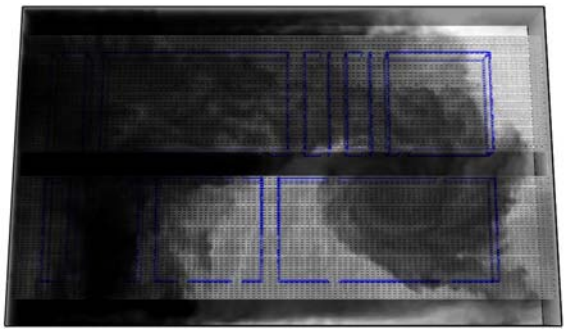

t=700 s

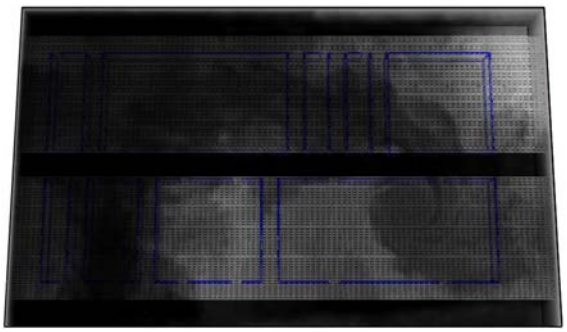

t=800 s

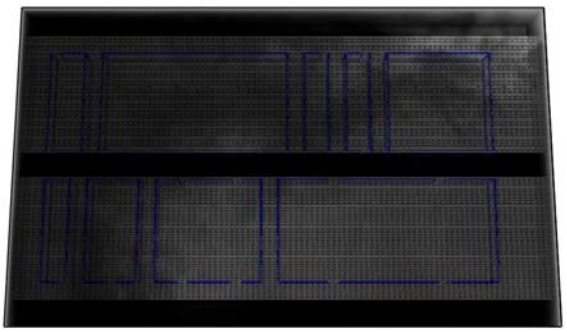

t=900 s

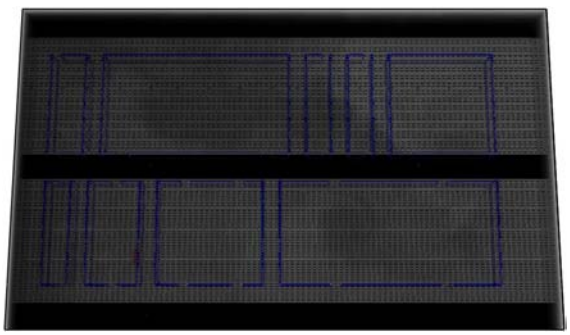

t=1000 s

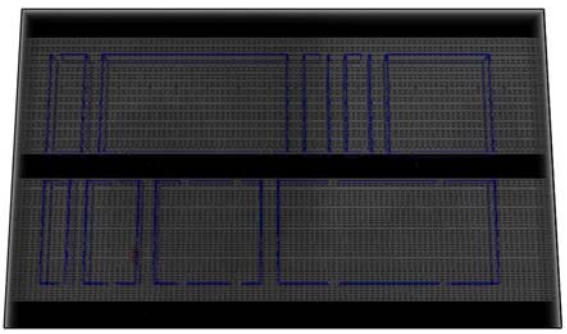

Appendix 5: Case VII (0.6 ms^{-1}; sprinklered)

t=300 s

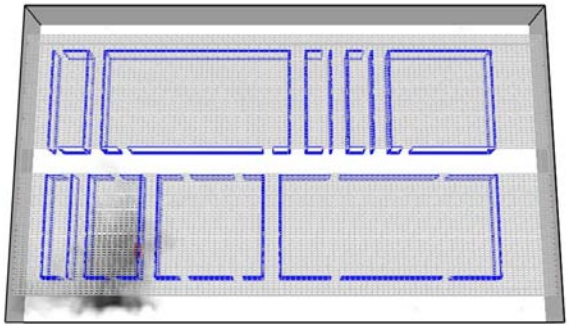

t=400 s

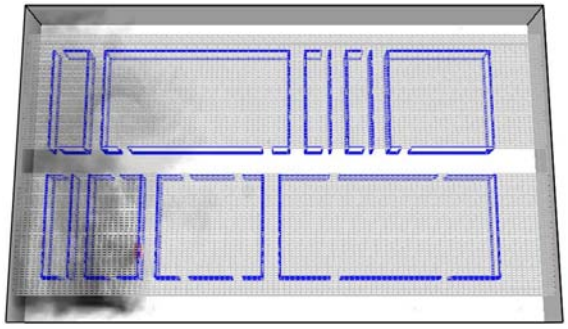

t=500 s

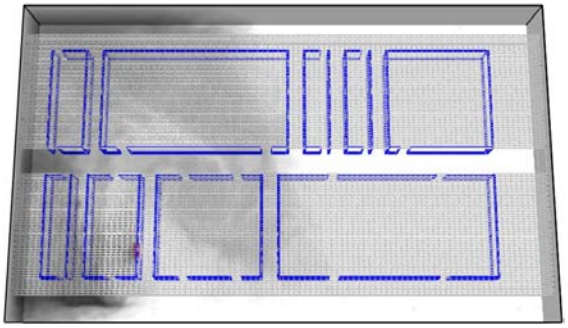

t=600 s

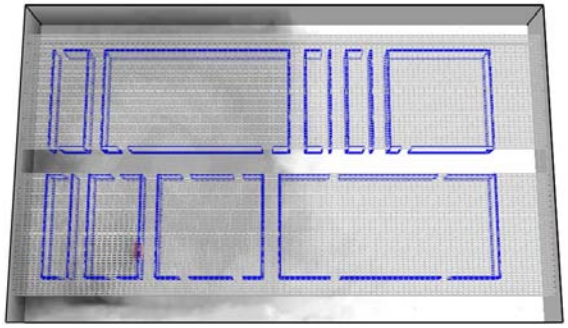

t=700 s

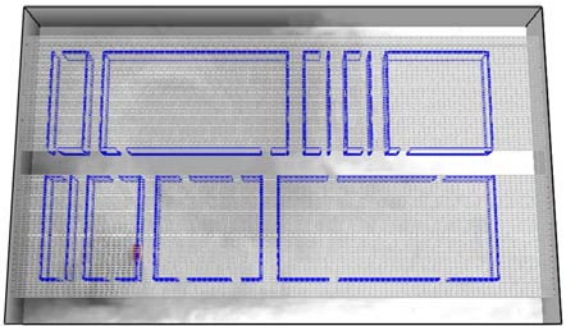

t=800 s

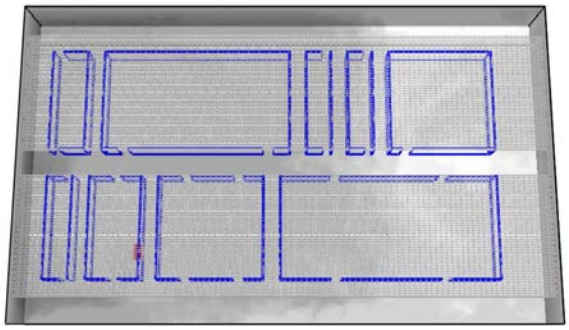

t=900 s

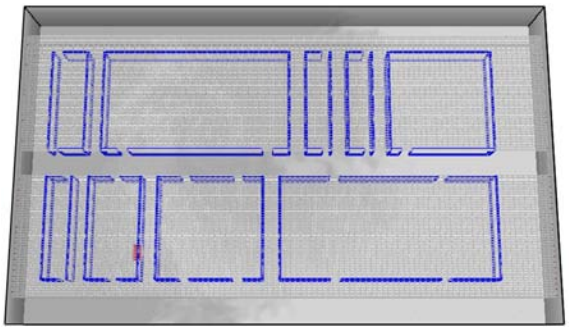

t=1000 s

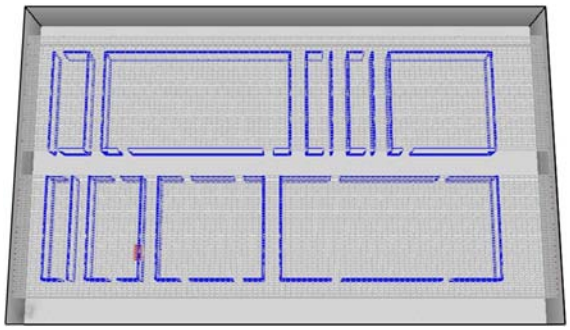

Appendix 6: Plots of mixture fraction sensor data in the subfab (0.3 ms^{-1}).

t=300 s

t=400 s

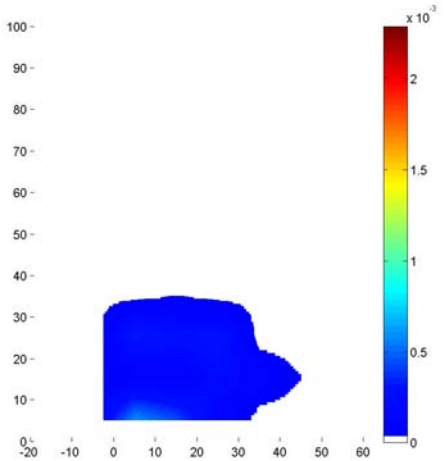

t=500 s

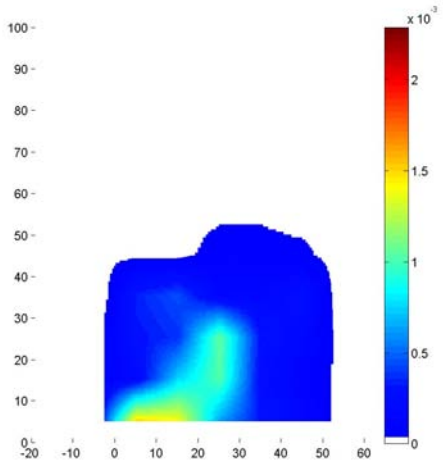

t=600 s

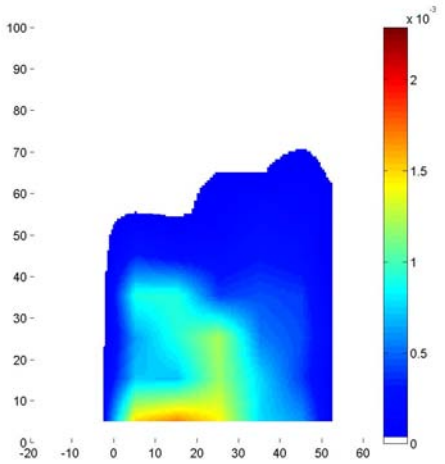

t=800 s

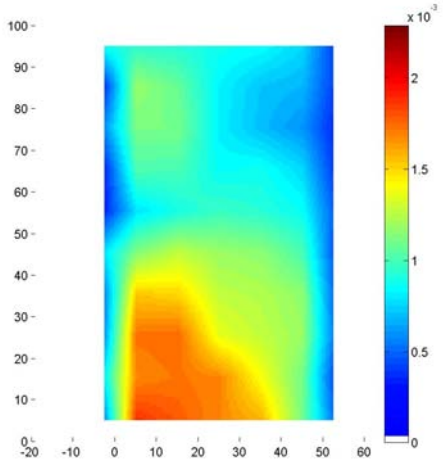

(high/average/low)

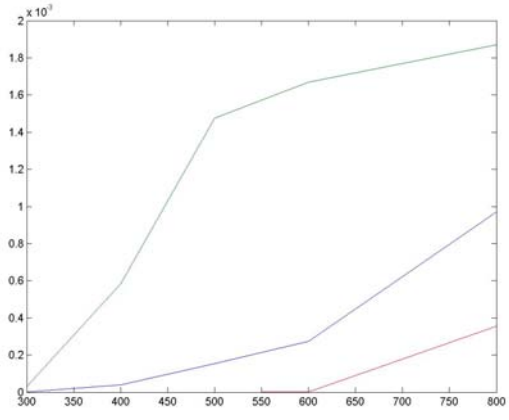

Appendix 7: Plots of mixture fraction sensor data in the fab (0.3 ms^{-1}).

t=300 s

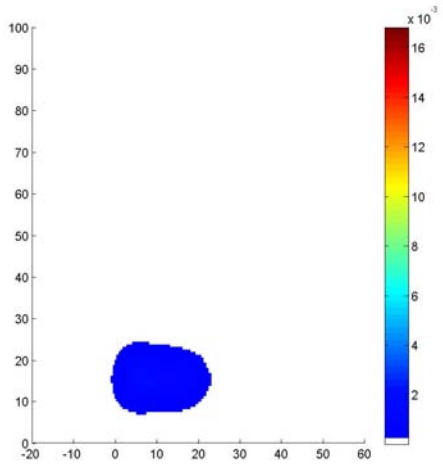

t=400 s

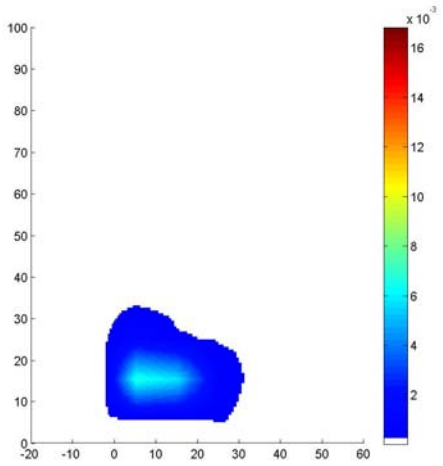

t=500 s

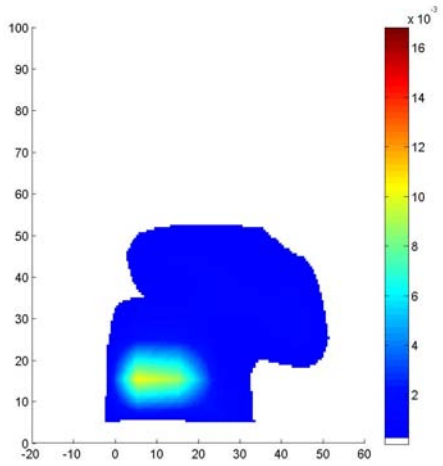

t=600 s

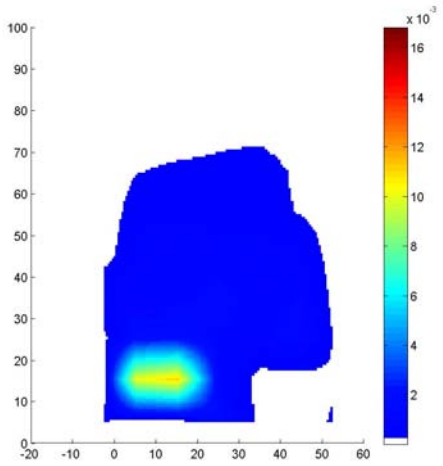

t=800 s

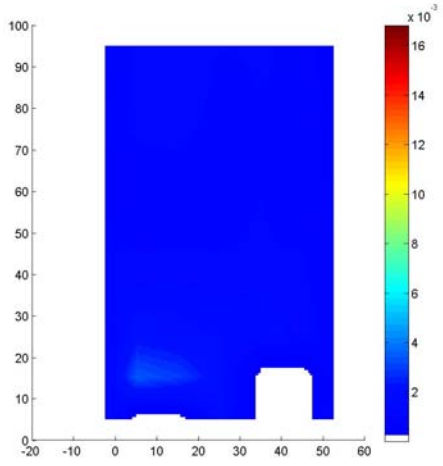

(high/average/low)

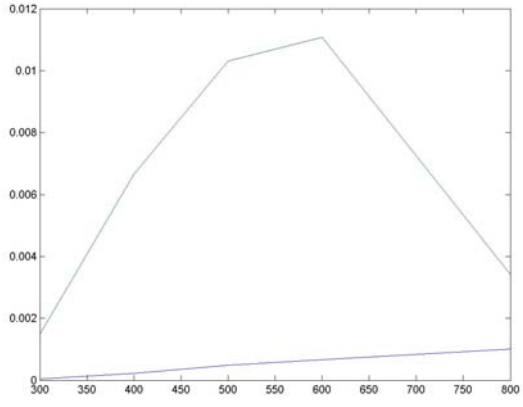

Appendix 8: Plots of mixture fraction sensor data in the plenum (0.3 ms^{-1}).

t=300 s

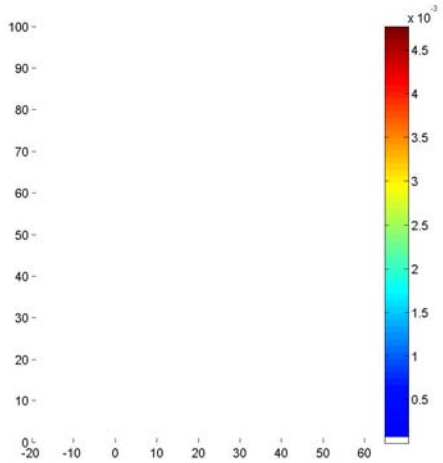

t=400 s

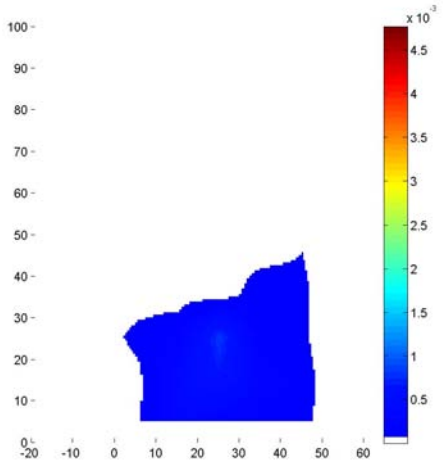

t=500 s

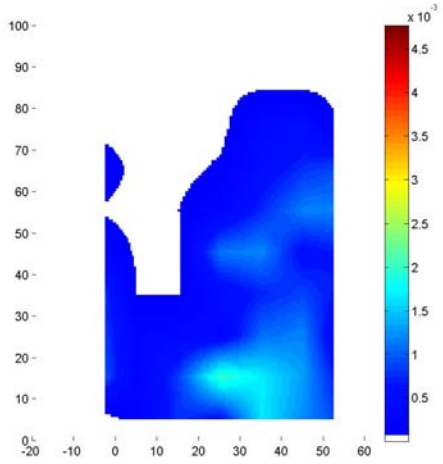

t=600 s

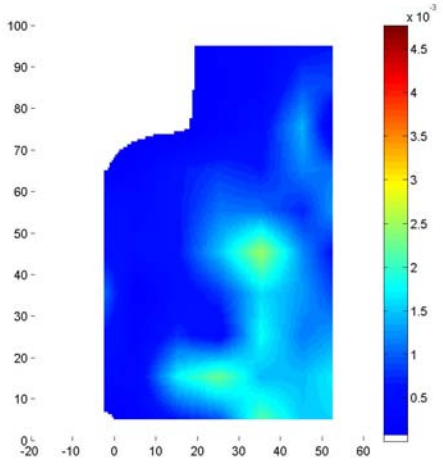

t=800 s

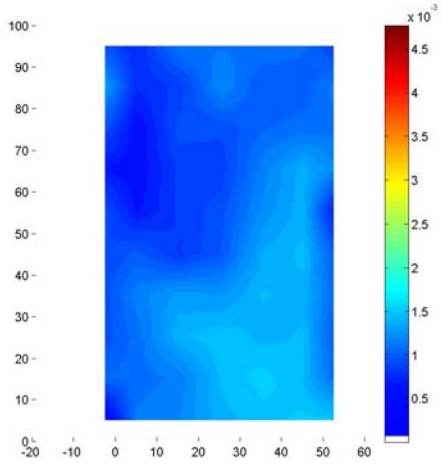

(high/average/low)

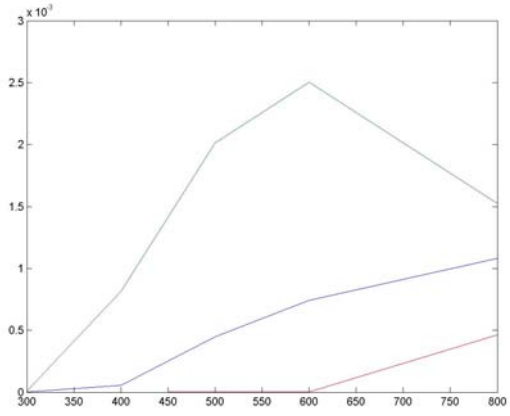

Appendix 9: Plots of mixture fraction sensor data in the subfab (0.4 ms^{-1}).

t=300 s

t=400 s

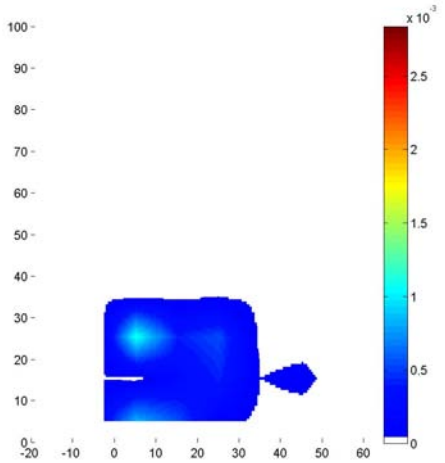

t=500 s

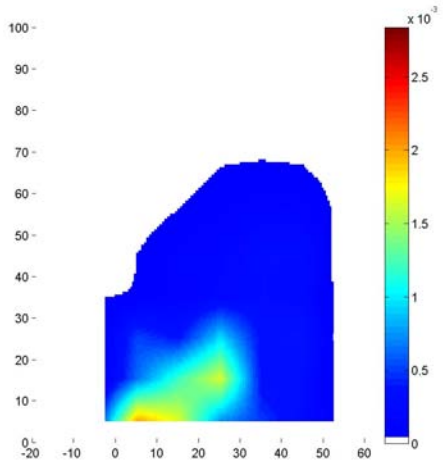

t=600 s

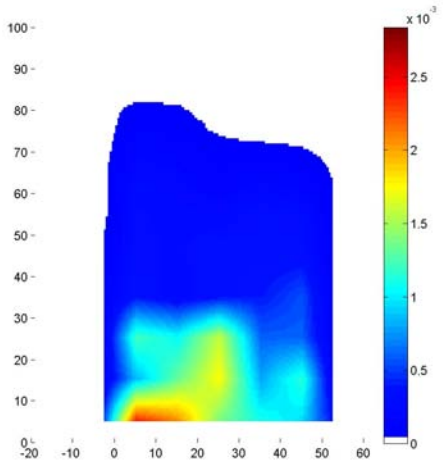

t=800 s

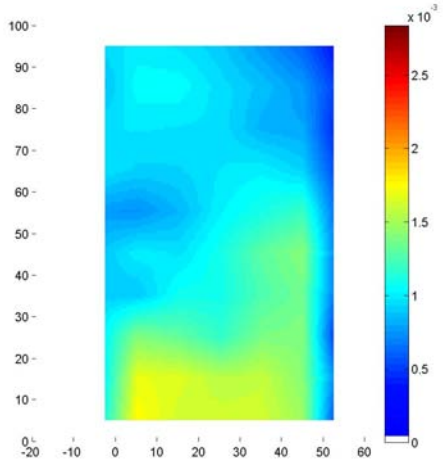

(high/average/low)

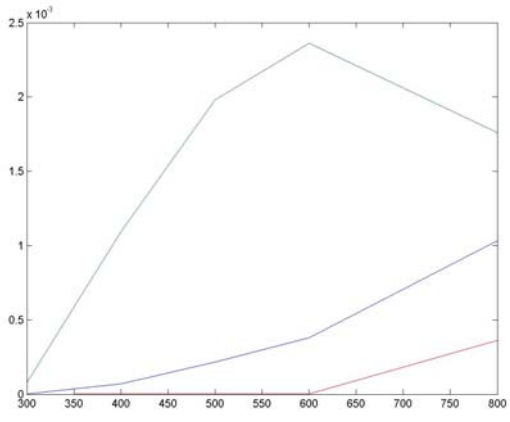

Appendix 10: Plots of mixture fraction sensor data in the fab (0.4 ms^{-1}).

t=300 s

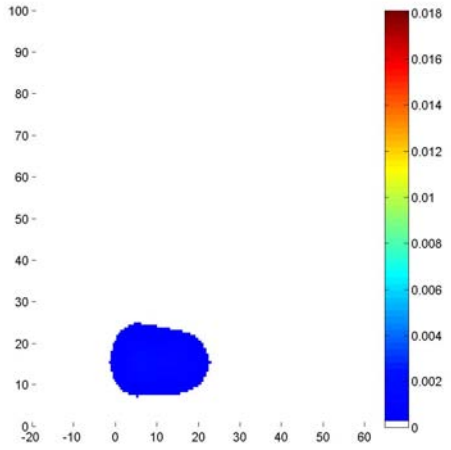

t=400 s

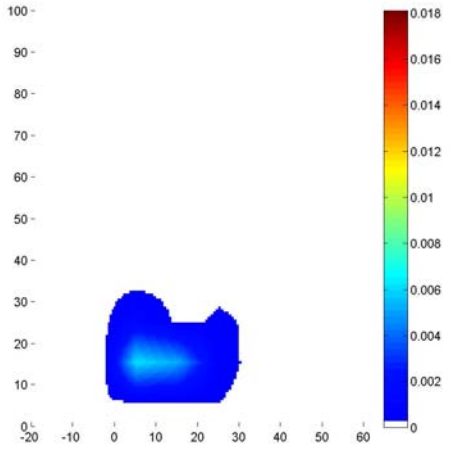

t=500 s

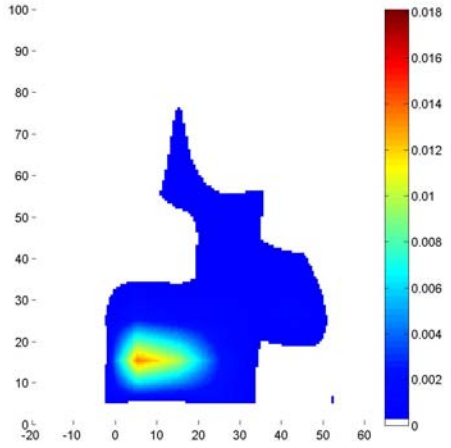

t=600 s

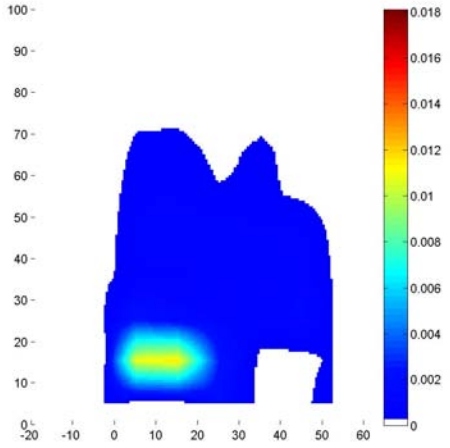

t=800 s

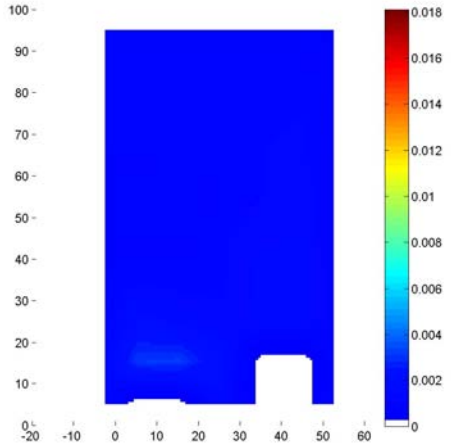

(high/average/low)

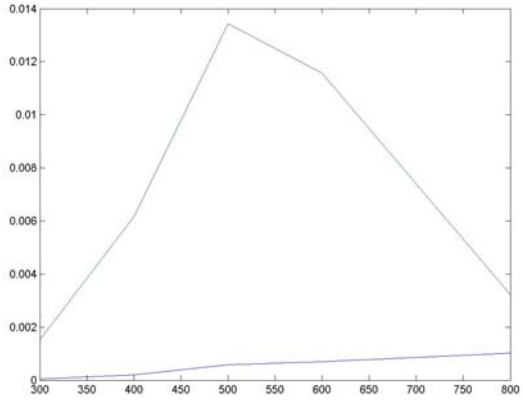

Appendix 11: Plots of mixture fraction sensor data in the plenum (0.4 ms^{-1}).

t=300 s

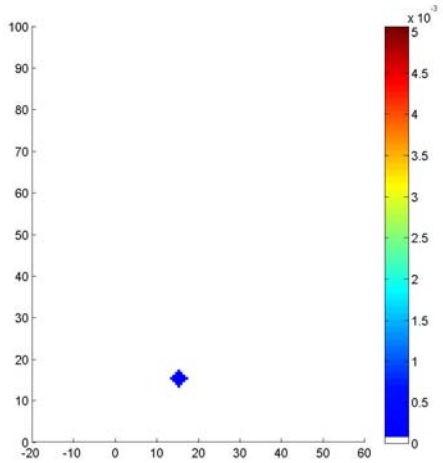

t=400 s

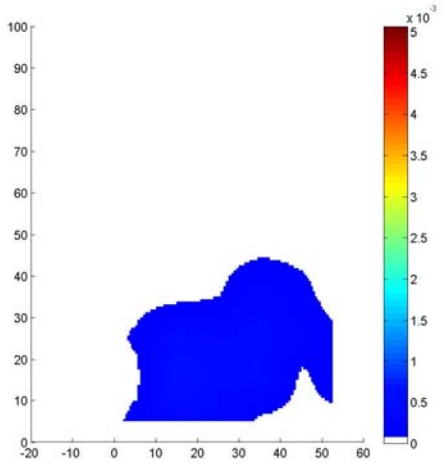

t=500 s

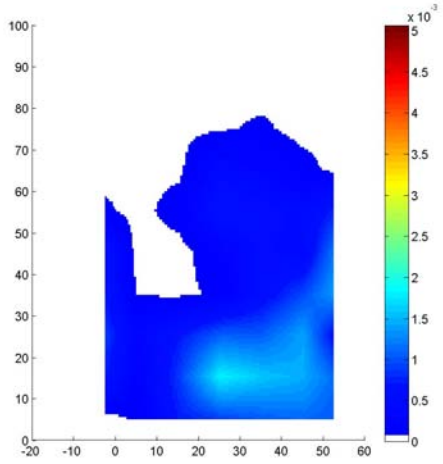

t=600 s

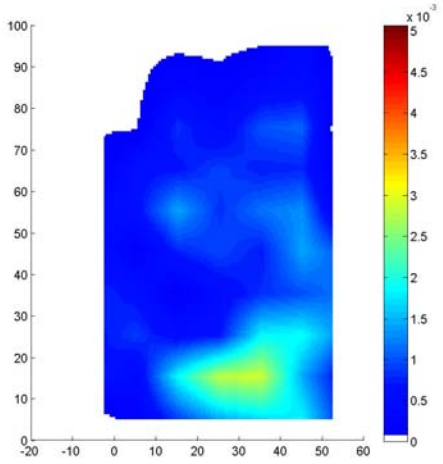

t=800 s

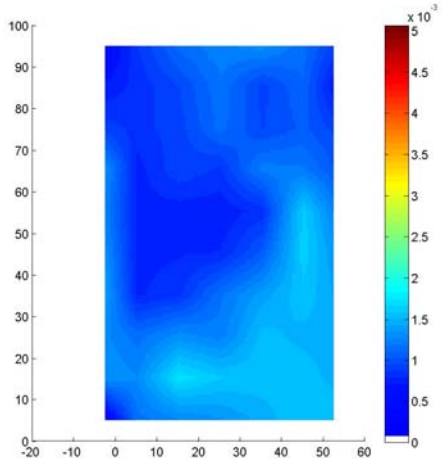

(high/average/low)

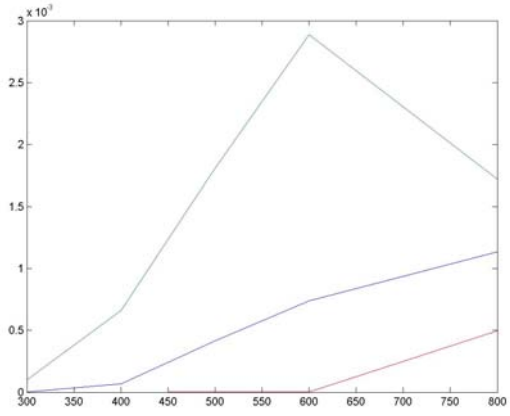

Appendix 12: Plots of mixture fraction sensor data in the subfab (0.5 ms^{-1}).

t=300 s

t=400 s

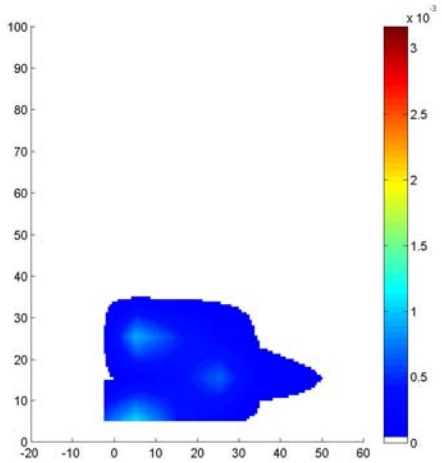

t=500 s

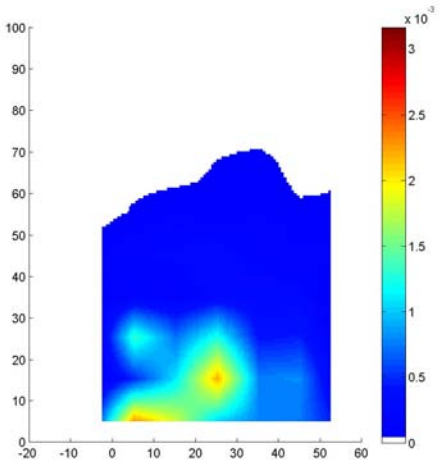

t=600 s

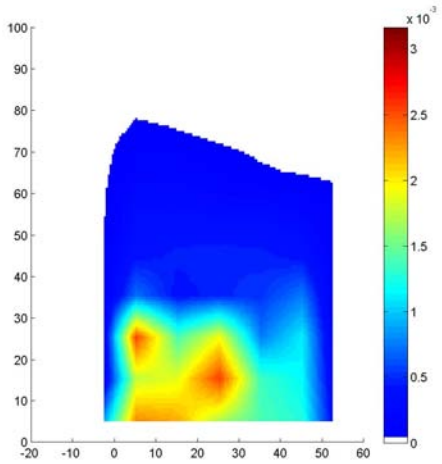

t=800 s

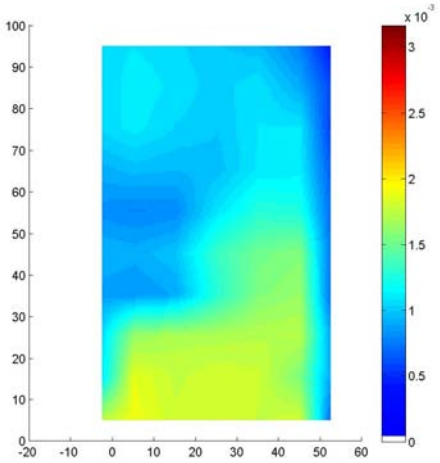

(high/average/low)

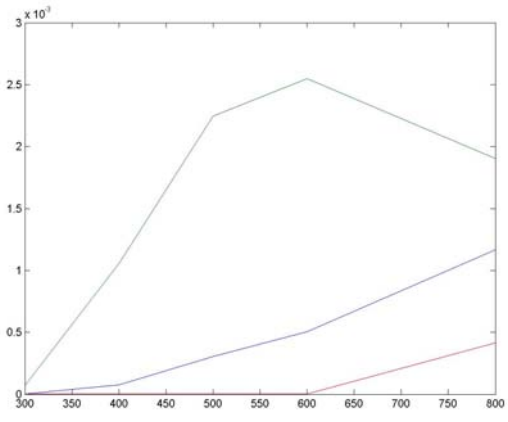

Appendix 13: Plots of mixture fraction sensor data in the fab (0.5 ms^{-1}).

t=300 s

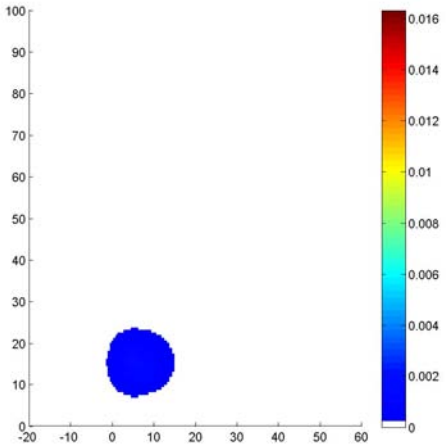

t=400 s

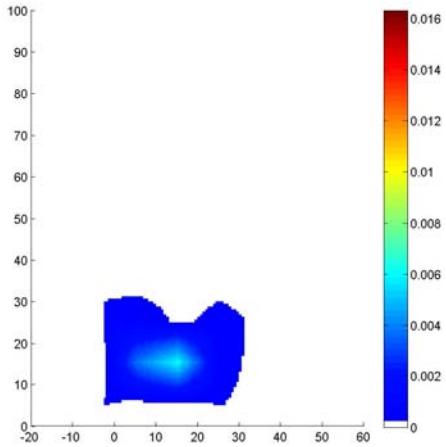

t=500 s

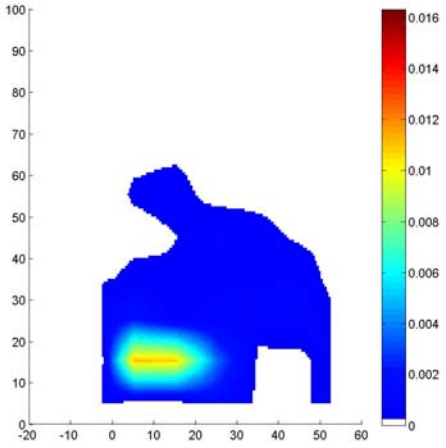

t=600 s

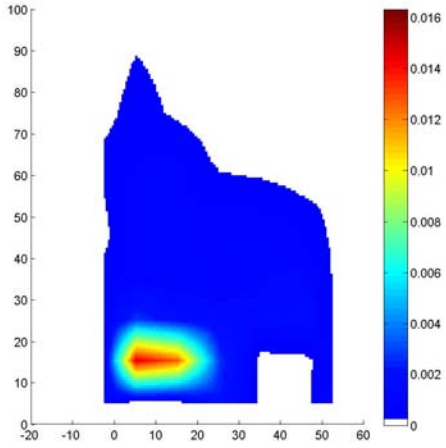

t=800 s

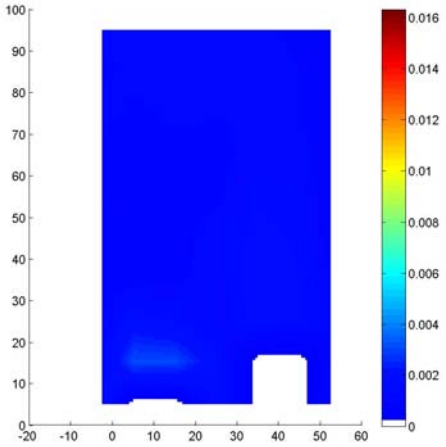

(high/average/low)

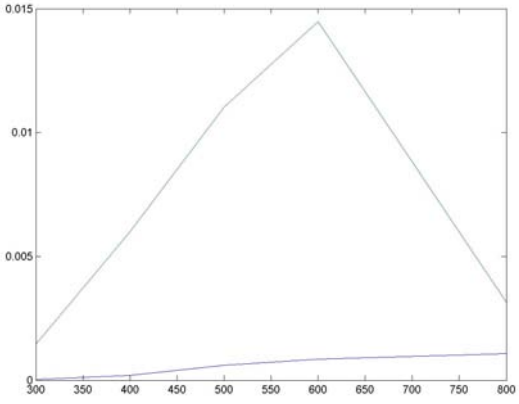

Appendix 14: Plots of mixture fraction sensor data in the plenum (0.5 ms^{-1}).

t=300 s

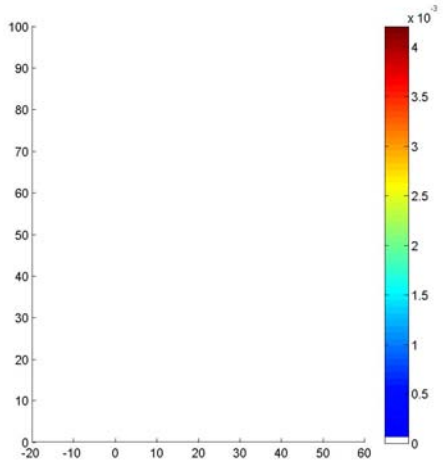

t=400 s

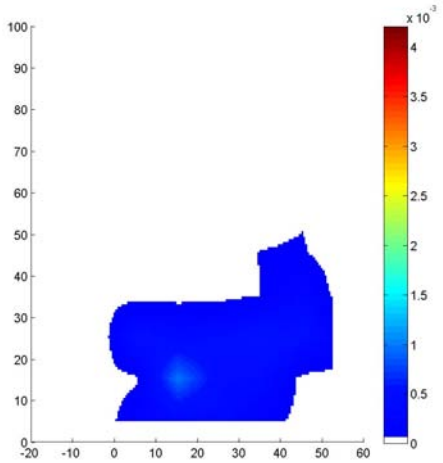

t=500 s

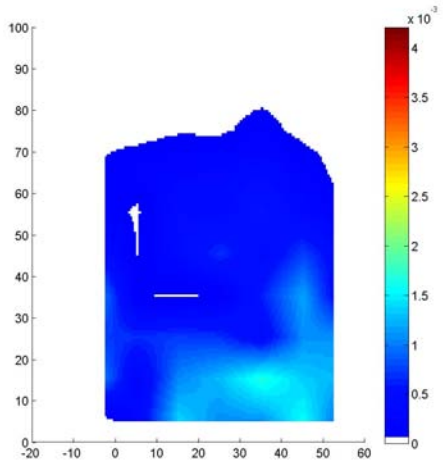

t=600 s

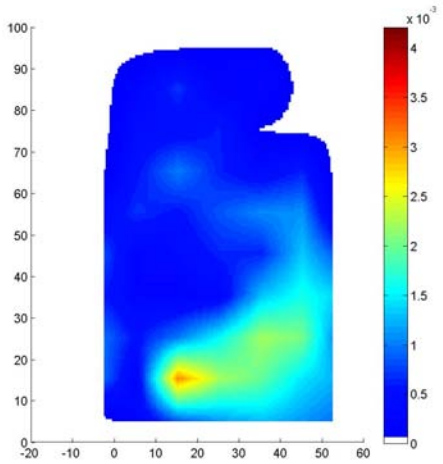

t=800 s

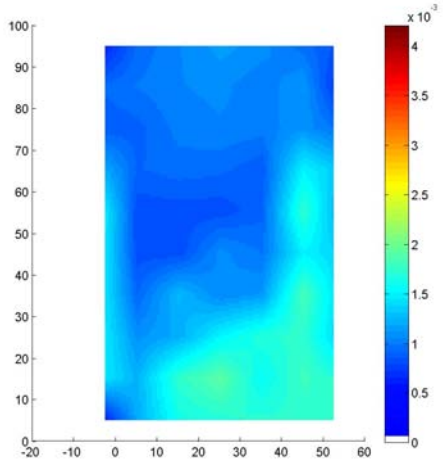

(high/average/low)

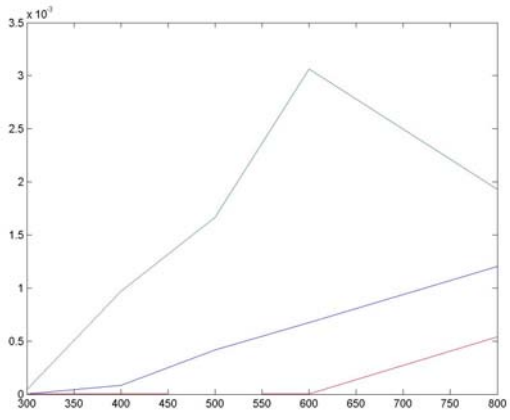

Appendix 15: Plots of mixture fraction sensor data in the subfab (0.6 ms^{-1}).

t=300 s

t=400 s

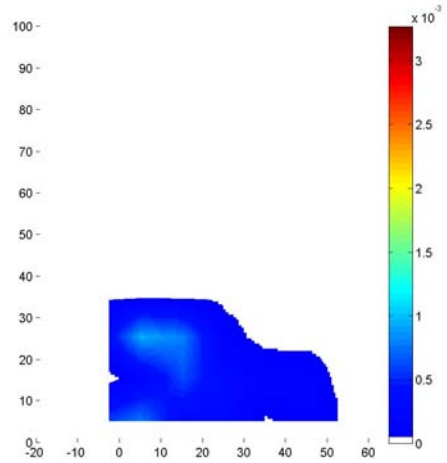

t=500 s

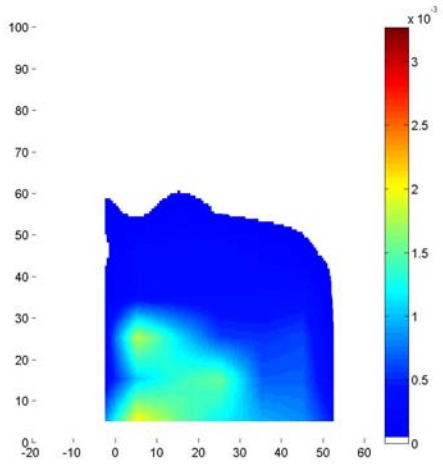

t=600 s

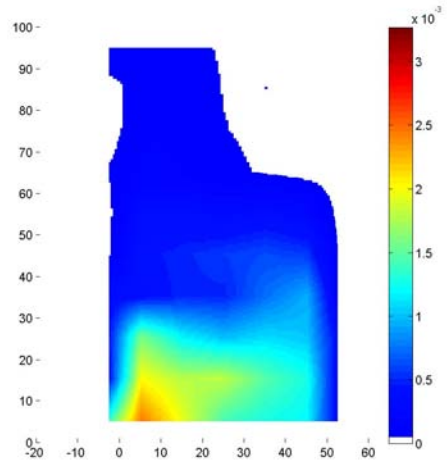

t=800 s

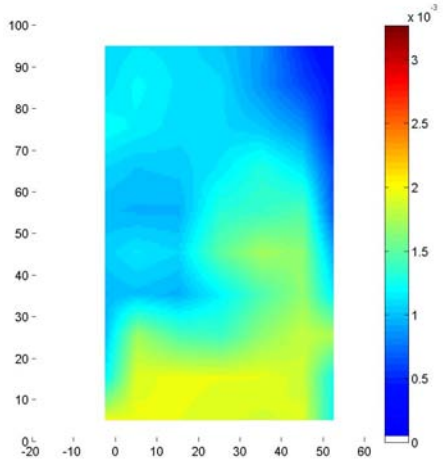

(high/average/low)

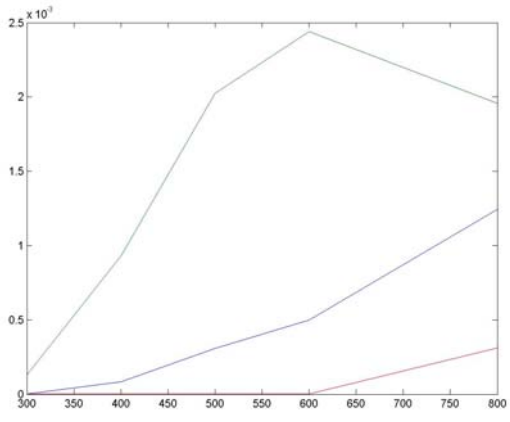

Appendix 16: Plots of mixture fraction sensor data in the fab (0.6 ms^{-1}).

t=300 s

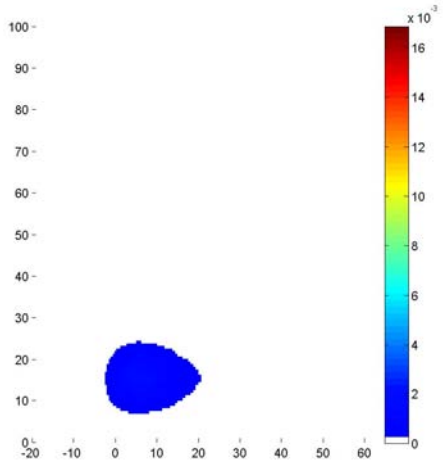

t=400 s

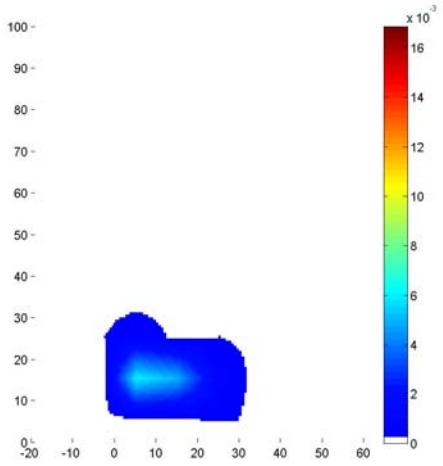

t=500 s

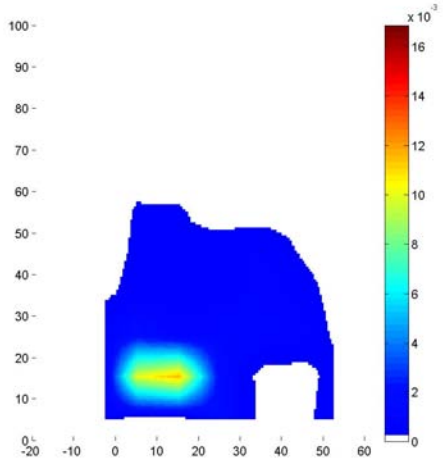

t=600 s

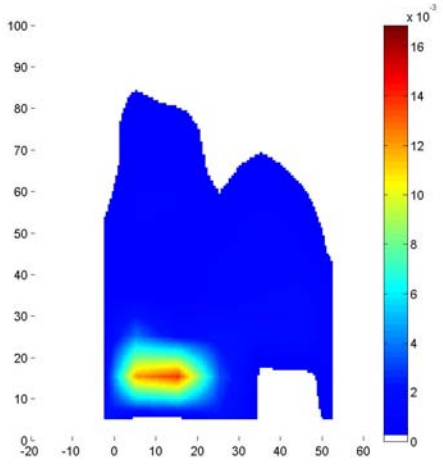

t=800 s

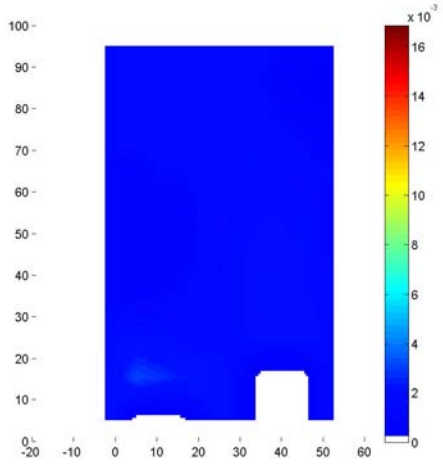

(high/average/low)

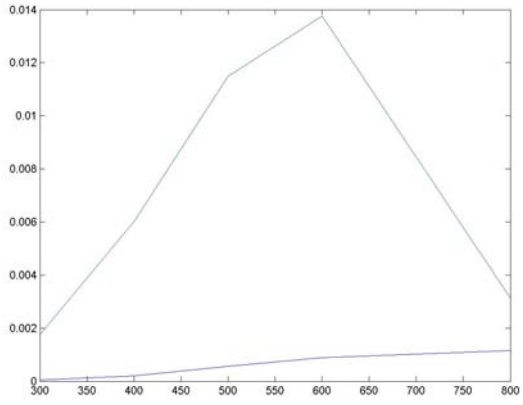

Appendix 17: Plots of mixture fraction sensor data in the plenum (0.6 ms^{-1}).

t=300 s

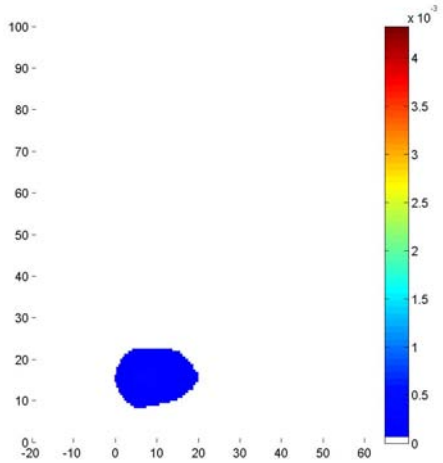

t=400 s

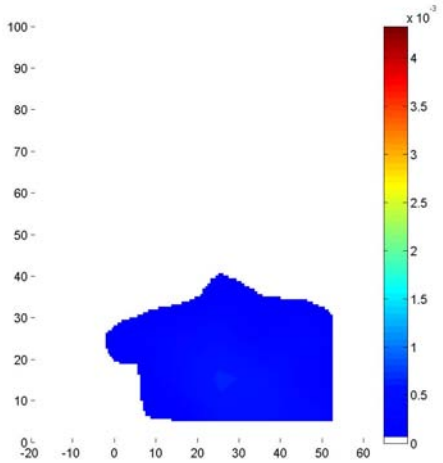

t=500 s

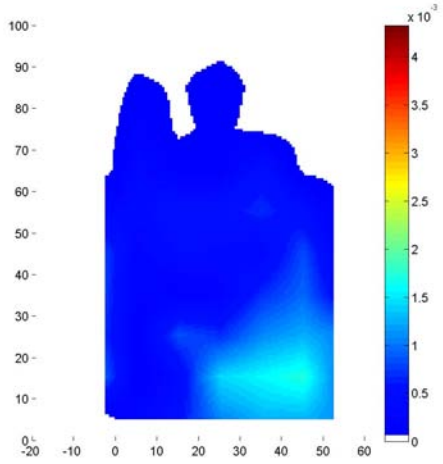

t=600 s

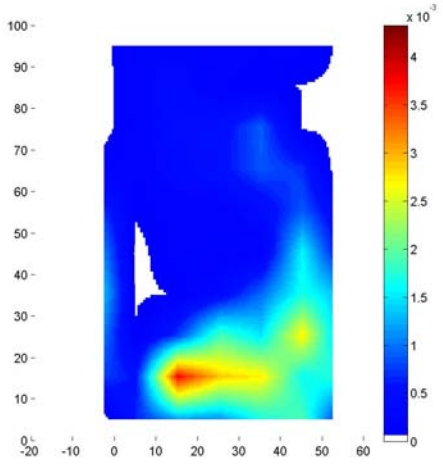

t=800 s

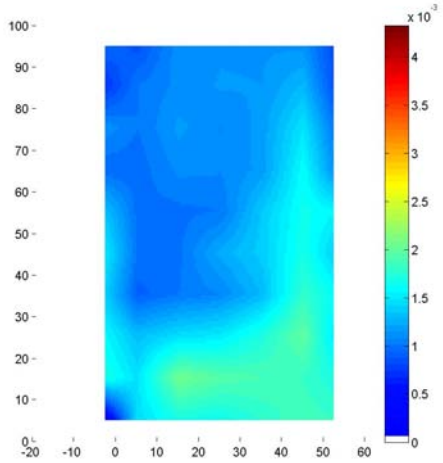

(high/average/low)

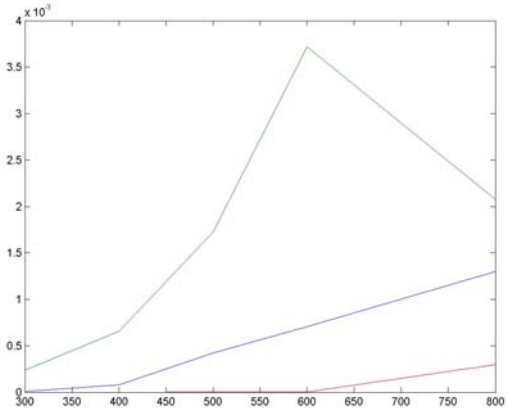

Appendix 18: Plots of mixture fraction sensor data in the subfab (1.5 ms^{-1}).

t=300 s

t=400 s

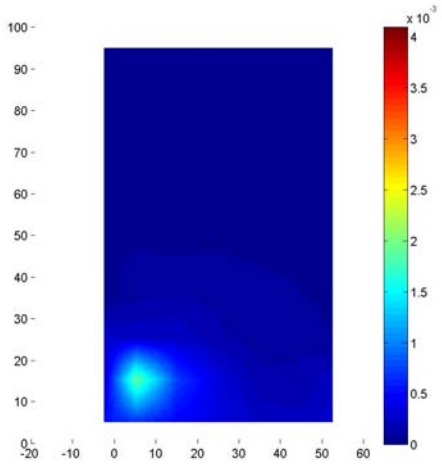

t=500 s

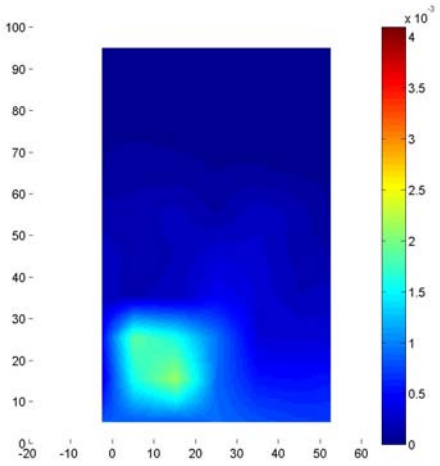

t=600 s

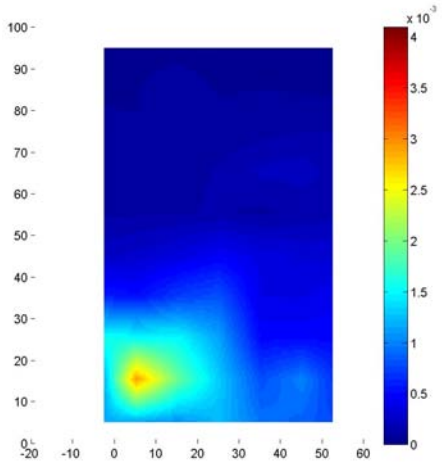

t=800 s

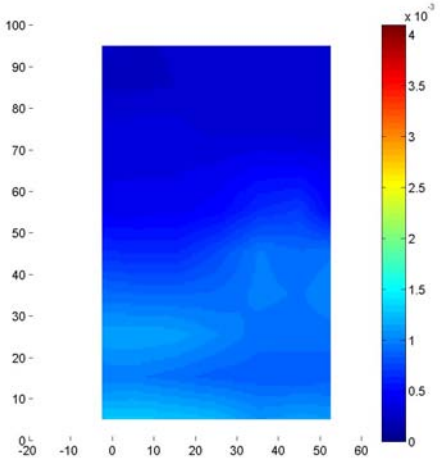

(high/average/low)

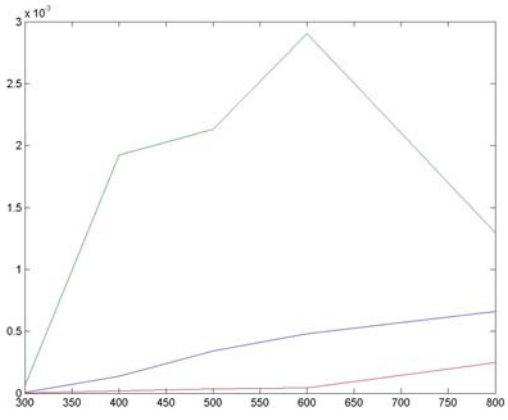

Appendix 19: Plots of mixture fraction sensor data in the fab (1.5 ms^{-1}).

t=300 s

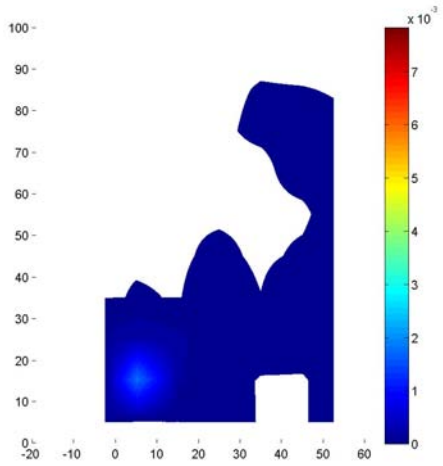

t=400 s

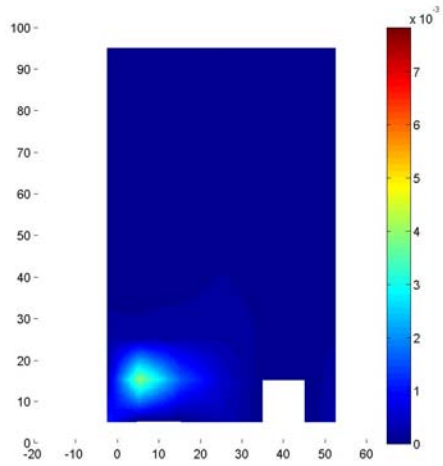

t=500 s

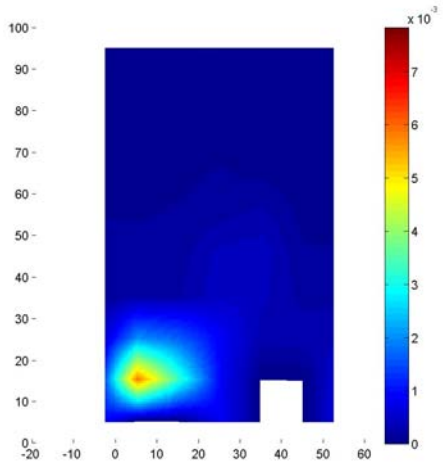

t=600 s

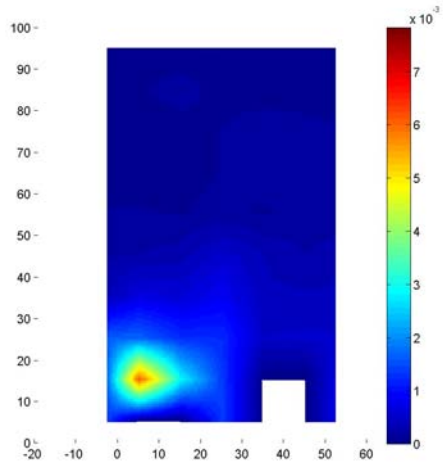

t=800 s

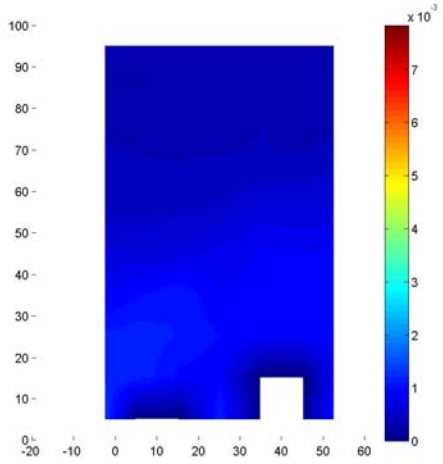

(high/average/low)

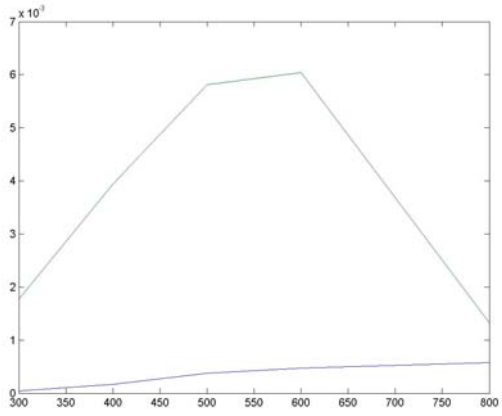

Appendix 20: Plots of mixture fraction sensor data in the plenum (1.5 ms^{-1}).

t=300 s

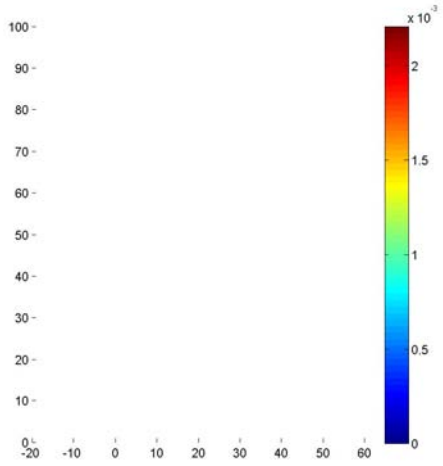

t=400 s

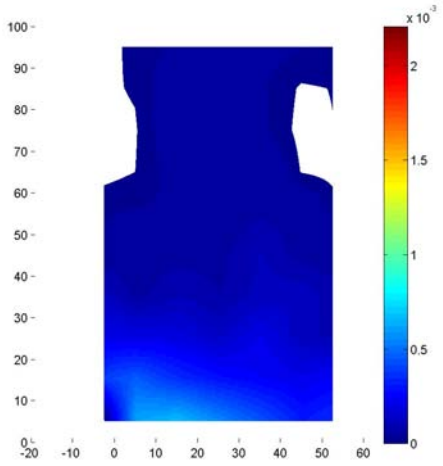

t=500 s

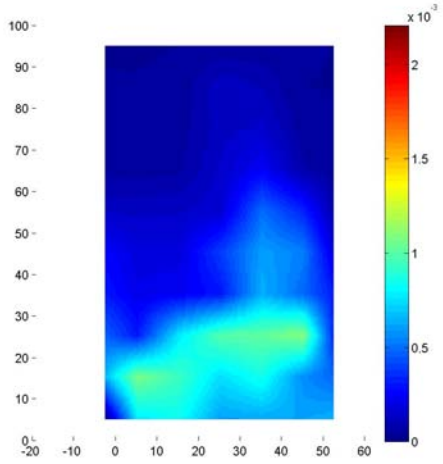

t=600 s

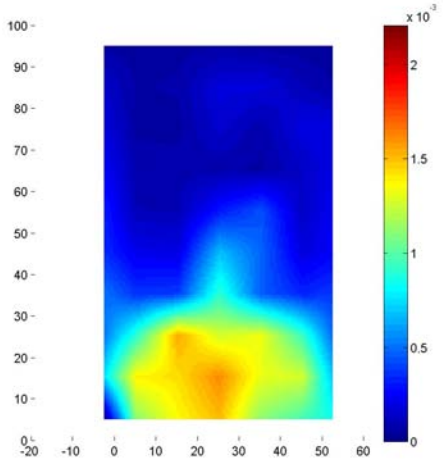

t=800 s

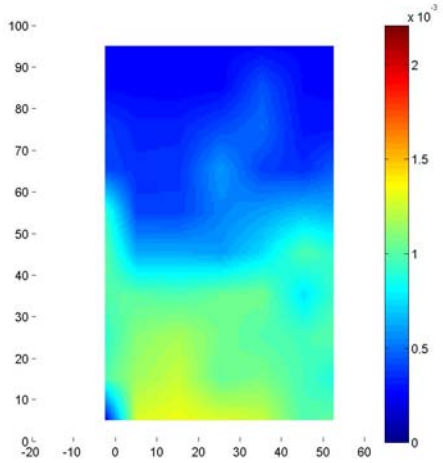

(high/average/low)

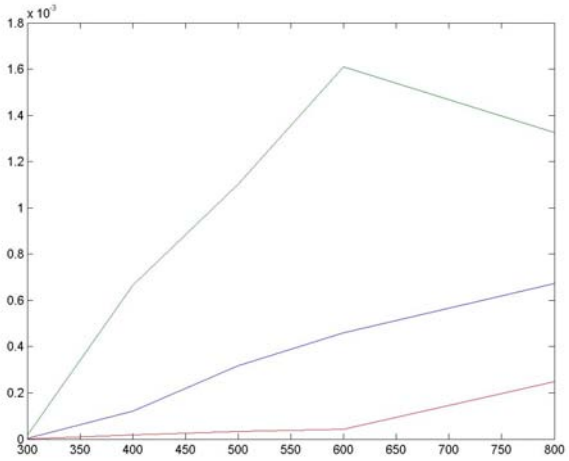

Appendix 21: Plots of mixture fraction sensor data in the subfab (0.0 ms^{-1}).

t=300 s

t=400 s

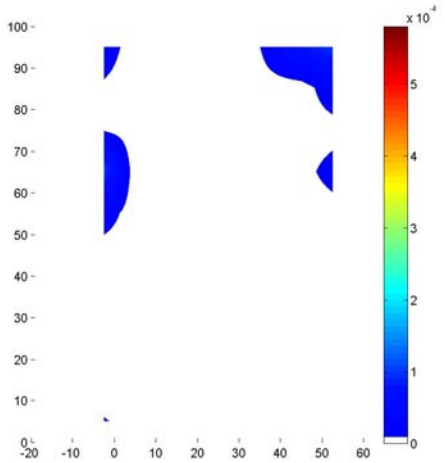

t=500 s

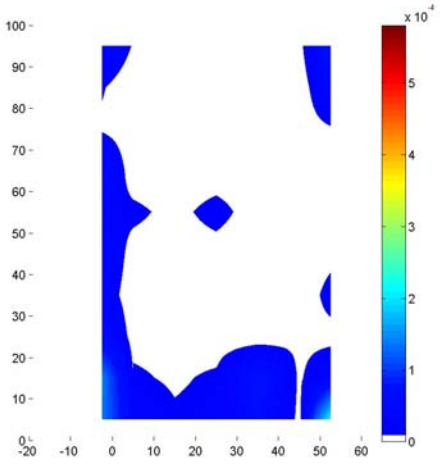

t=600 s

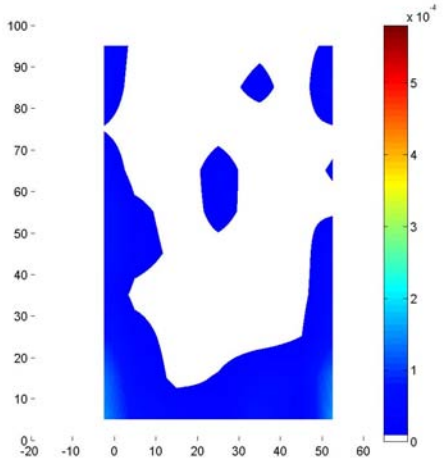

t=800 s

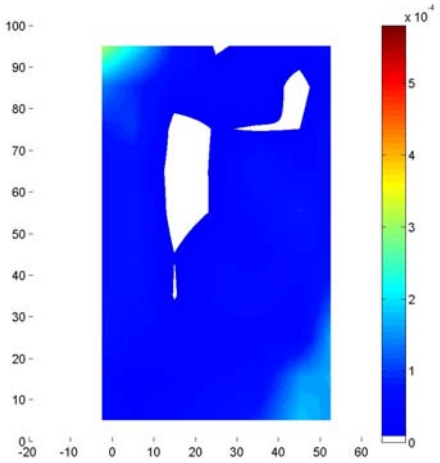

(high/average/low)

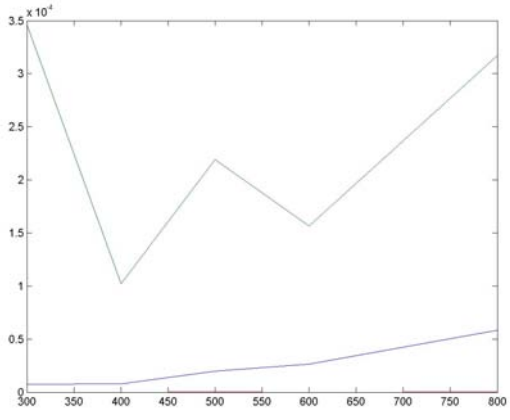

Appendix 22: Plots of mixture fraction sensor data in the fab (0.0 ms^{-1}).

t=300 s

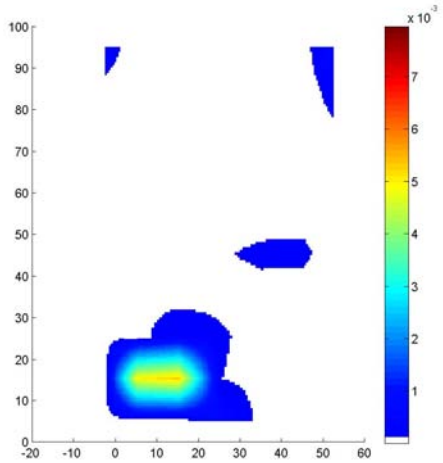

t=400 s

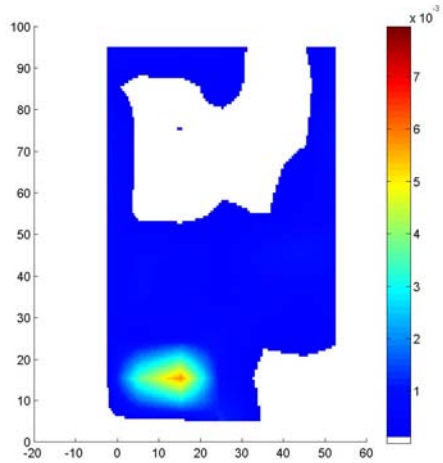

t=500 s

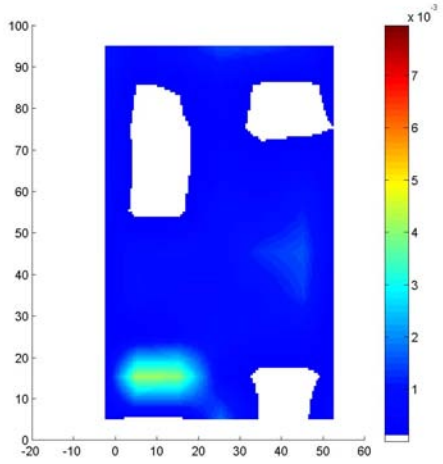

t=600 s

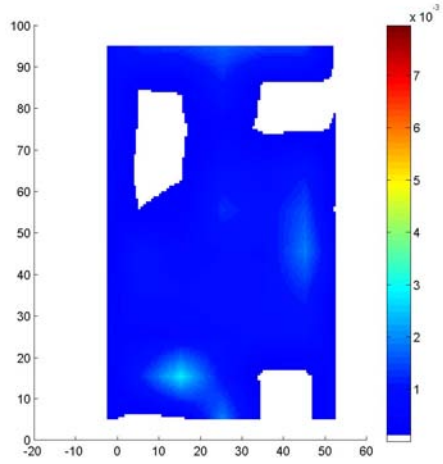

t=800 s

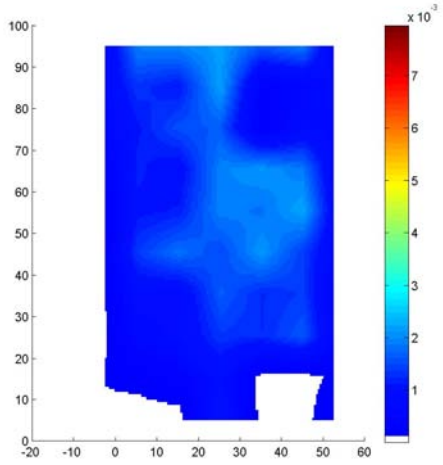

(high/average/low)

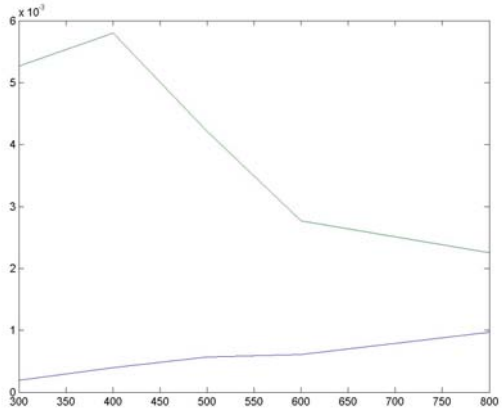

Appendix 23: Plots of mixture fraction sensor data in the plenum (0.0 ms^{-1}).

t=300 s

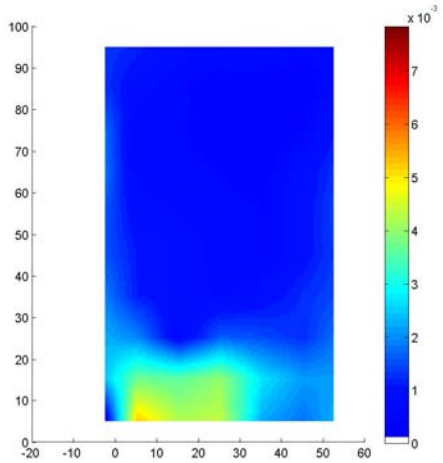

t=400 s

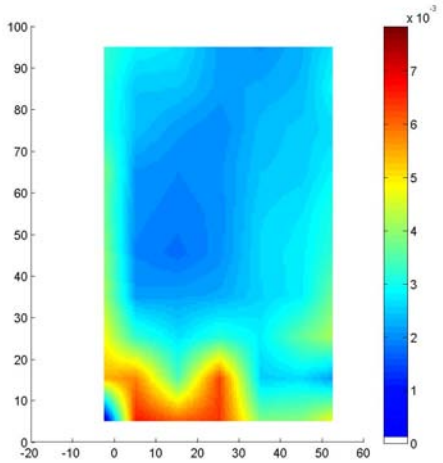

t=500 s

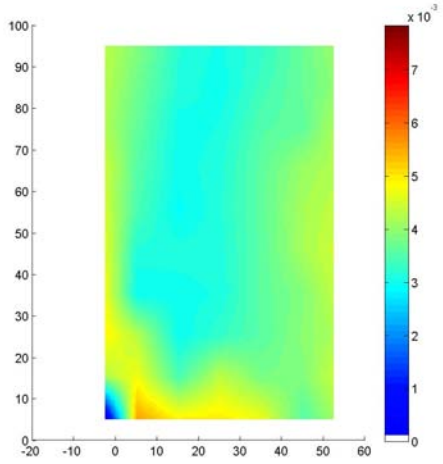

t=600 s

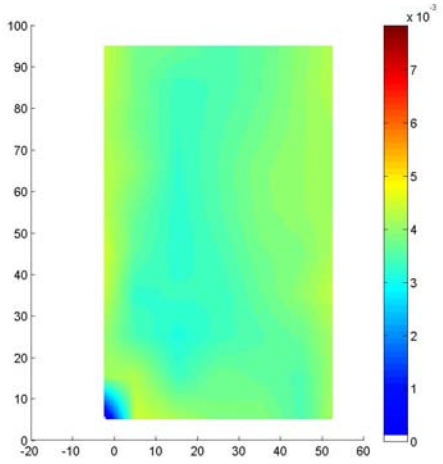

t=800 s

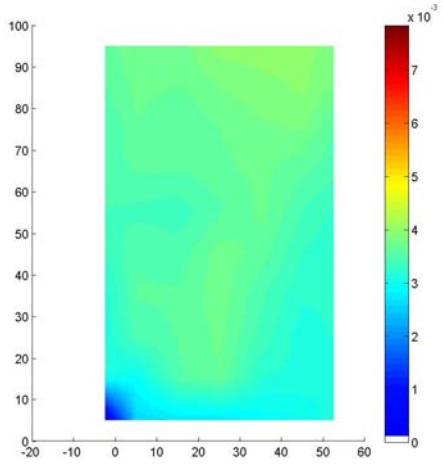

(high/average/low)

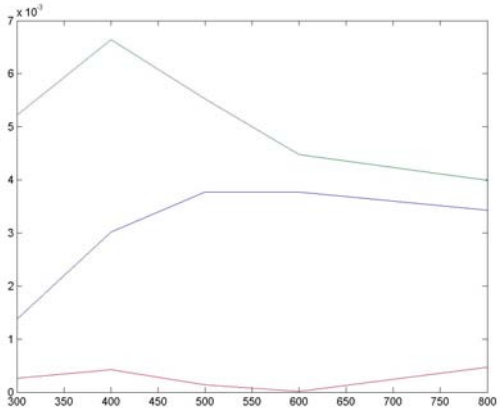

Appendix 24: Plots of temperature sensor data in the subfab (0.3 ms^{-1}).

t=300 s

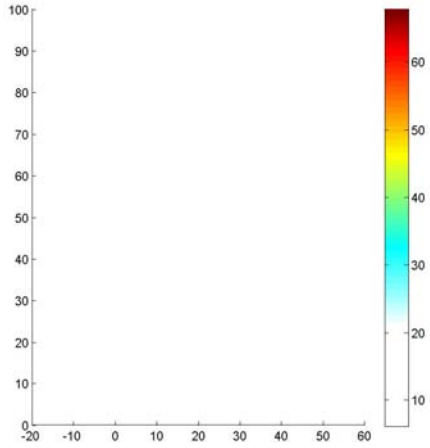

t=400 s

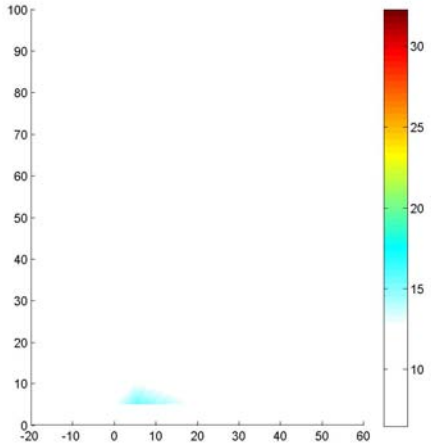

t=500 s

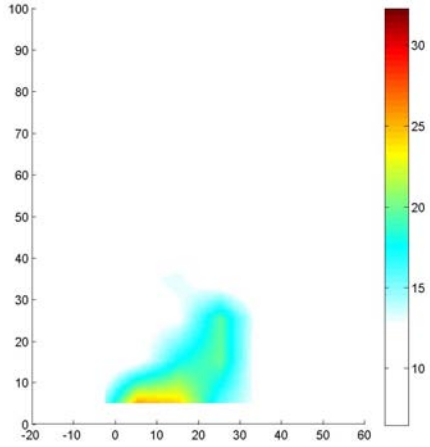

t=600 s

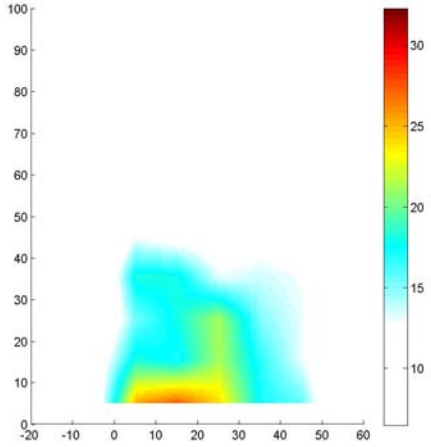

t=800 s

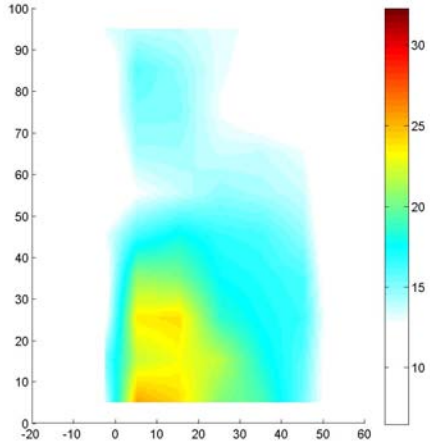

(high/average/low)

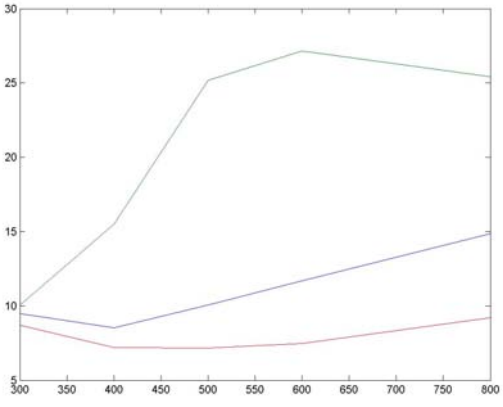

Appendix 25: Plots of temperature sensor data in the fab (0.3 ms^{-1}).

t=300 s

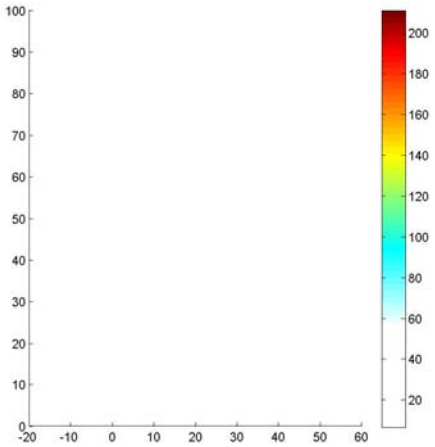

t=400 s

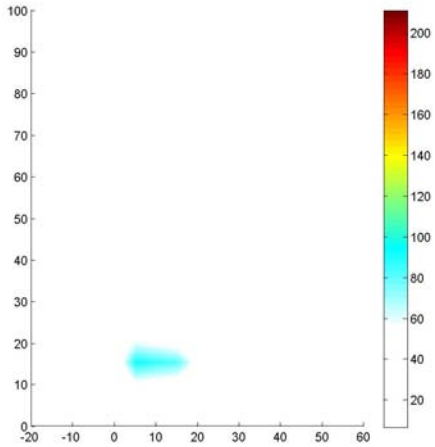

t=500 s

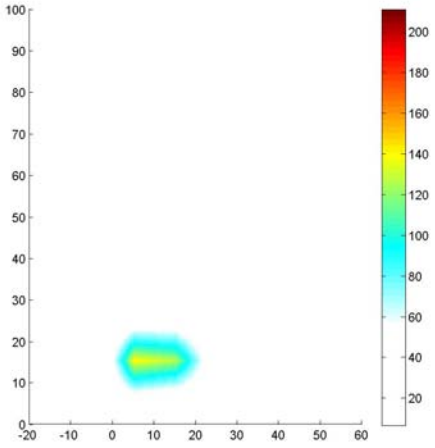

t=600 s

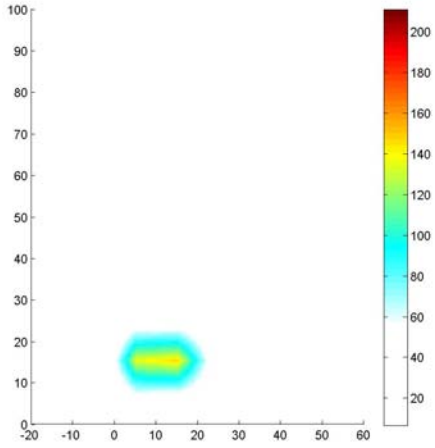

t=800 s

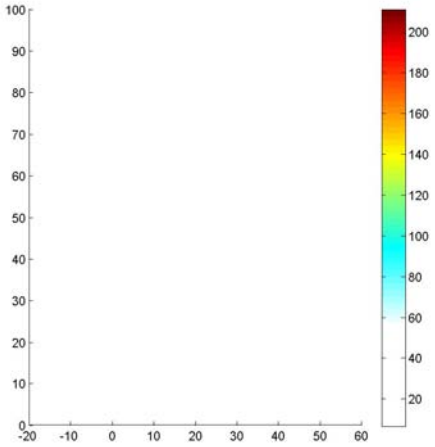

(high/average/low)

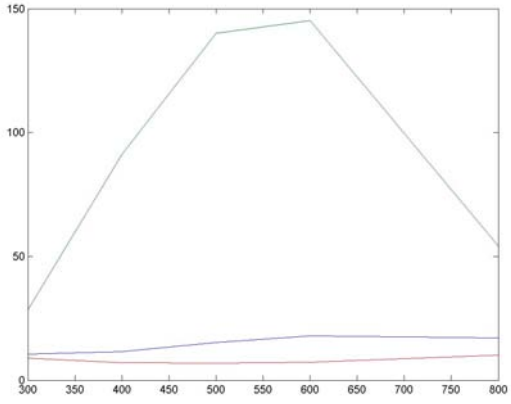

Appendix 26: Plots of temperature sensor data in the plenum (0.3 ms^{-1}).

t=300 s

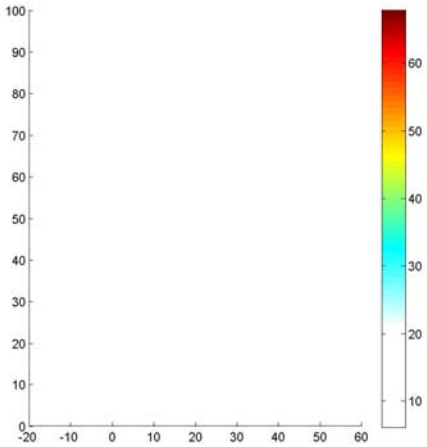

t=400 s

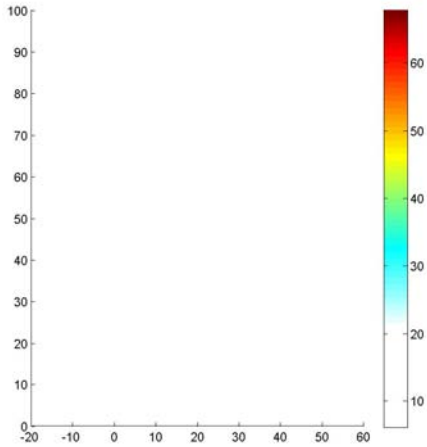

t=500 s

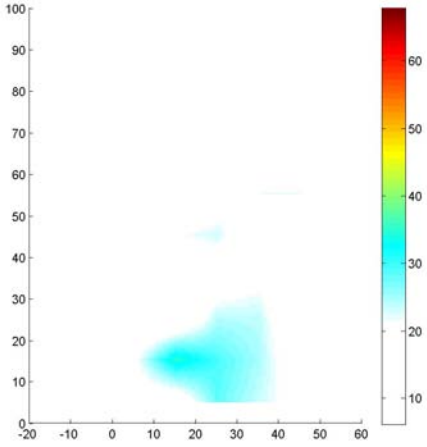

t=600 s

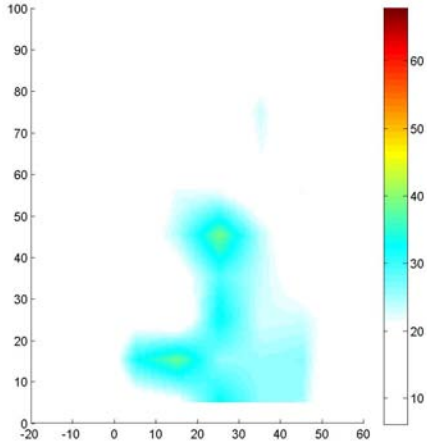

t=800 s

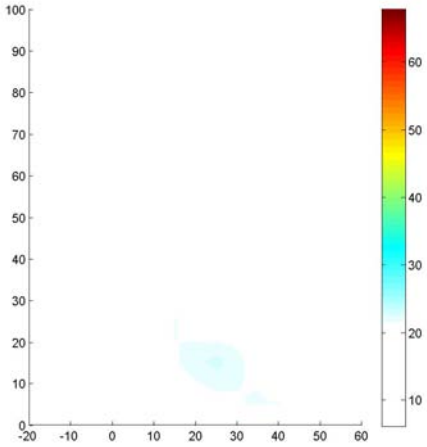

(high/average/low)

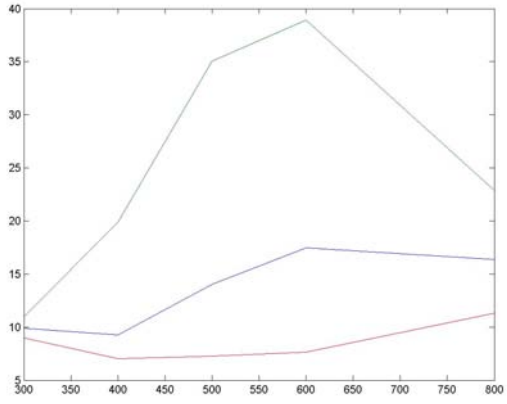

Appendix 27: Plots of temperature sensor data in the subfab (0.4 ms^{-1}).

t=300 s

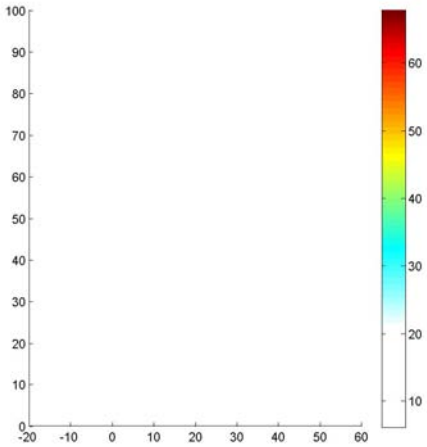

t=400 s

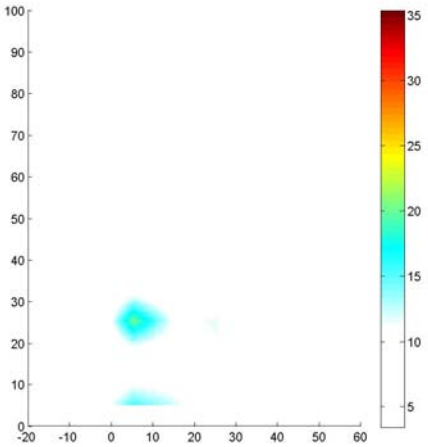

t=500 s

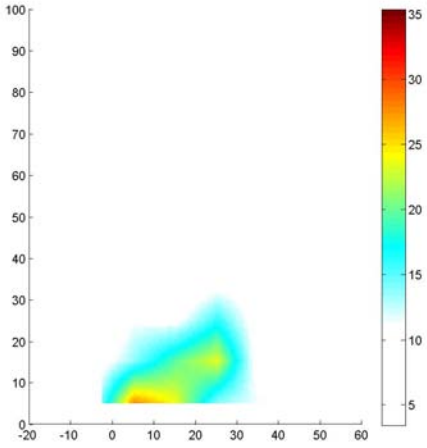

t=600 s

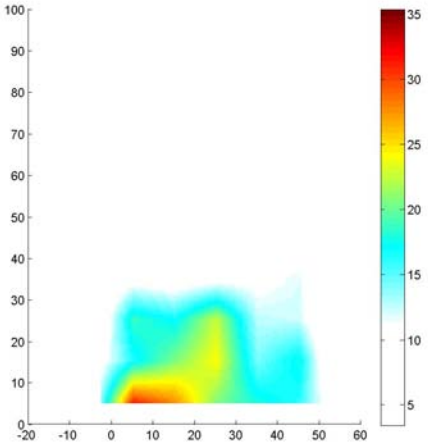

t=800 s

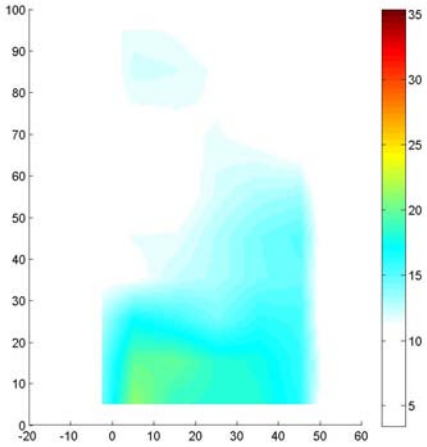

(high/average/low)

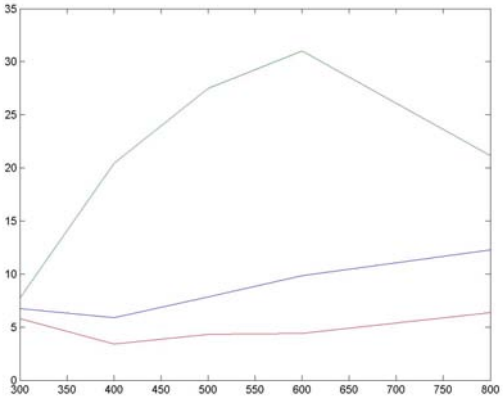

Appendix 28: Plots of temperature sensor data in the fab (0.4 ms^{-1}).

t=300 s

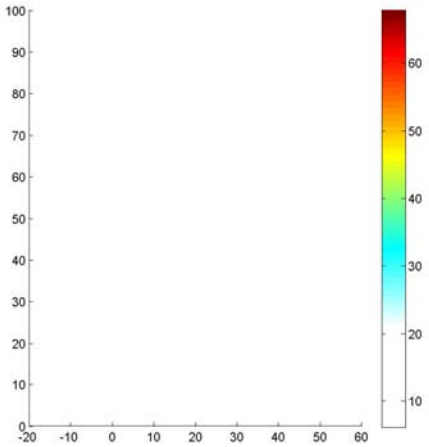

t=400 s

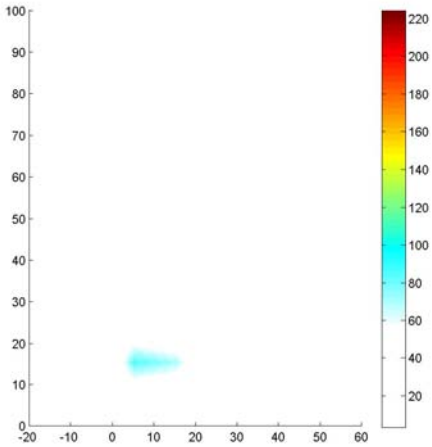

t=500 s

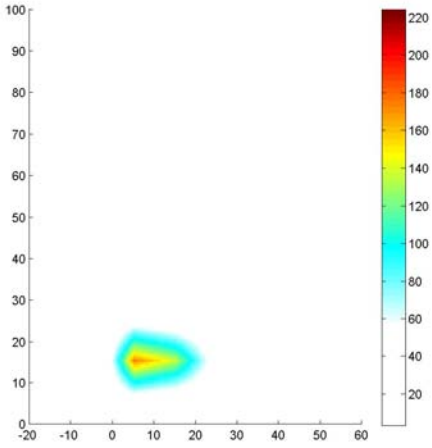

t=600 s

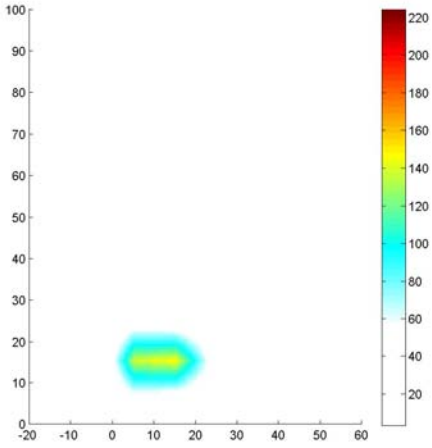

t=800 s

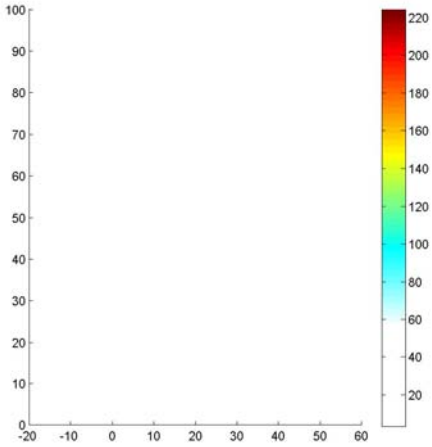

(high/average/low)

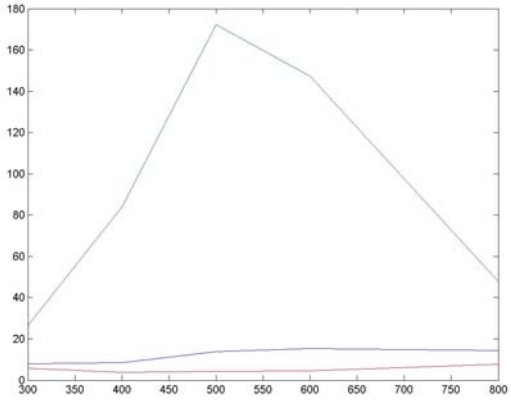

Appendix 29: Plots of temperature sensor data in the plenum (0.4 ms^{-1}).

t=300 s

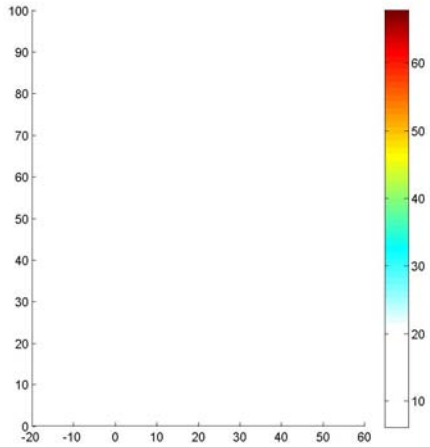

t=400 s

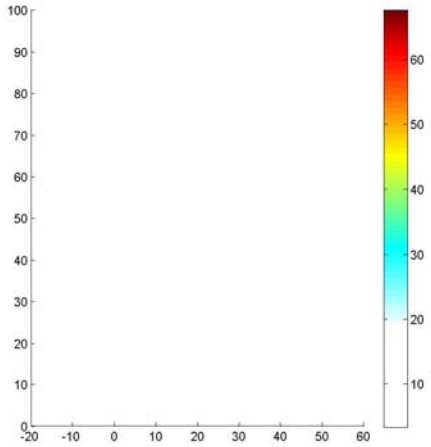

t=500 s

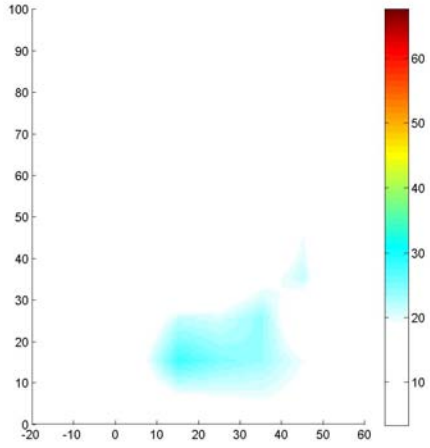

t=600 s

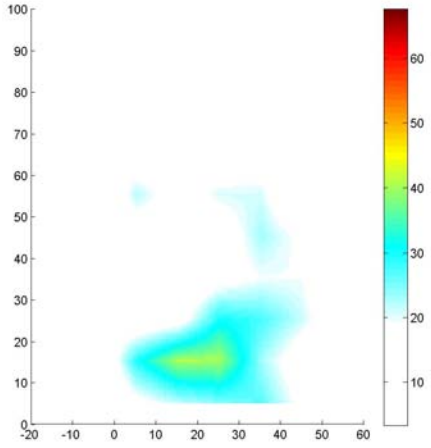

t=800 s

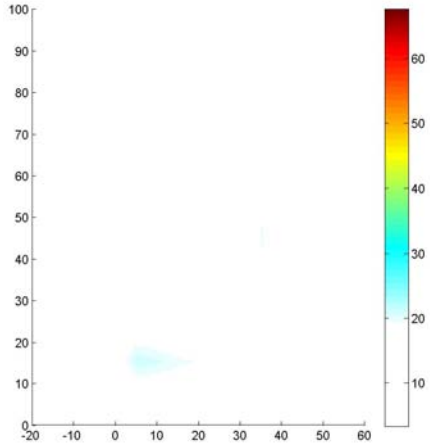

(high/average/low)

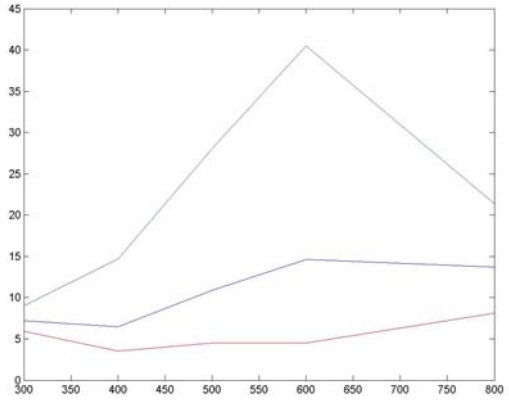

Appendix 30: Plots of temperature sensor data in the subfab (0.5 ms^{-1}).

t=300 s

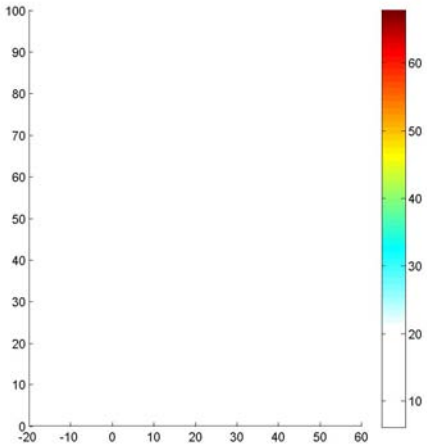

t=400 s

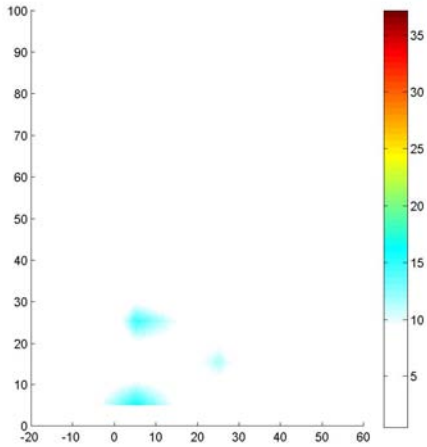

t=500 s

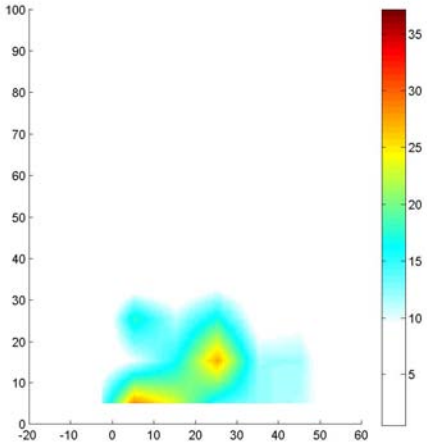

t=600 s

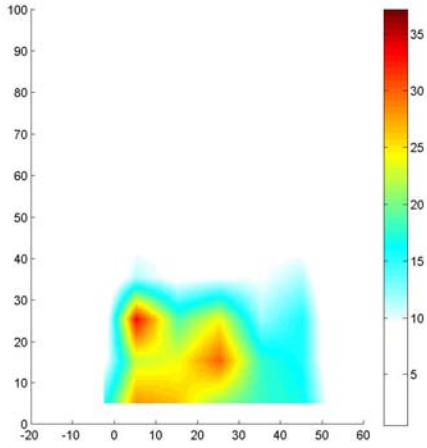

t=800 s

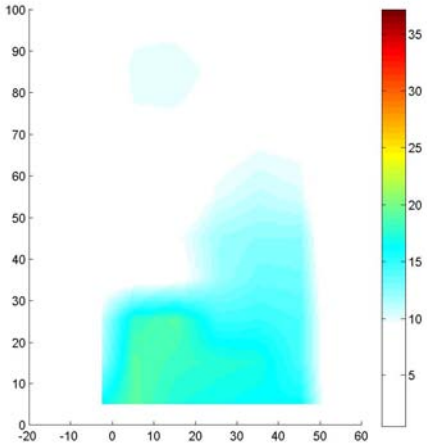

(high/average/low)

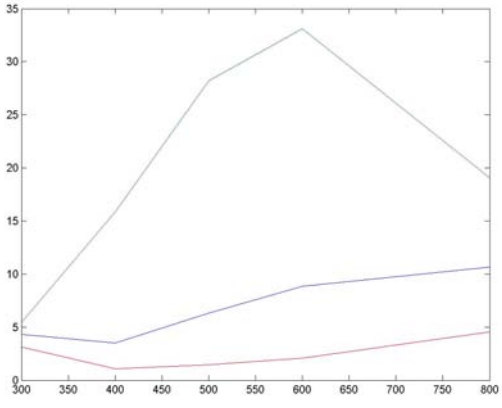

Appendix 31: Plots of temperature sensor data in the fab (0.5 ms^{-1}).

t=300 s

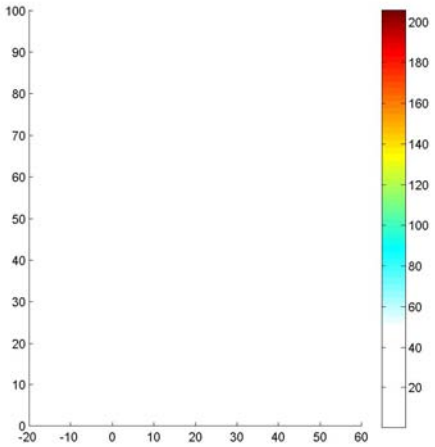

t=400 s

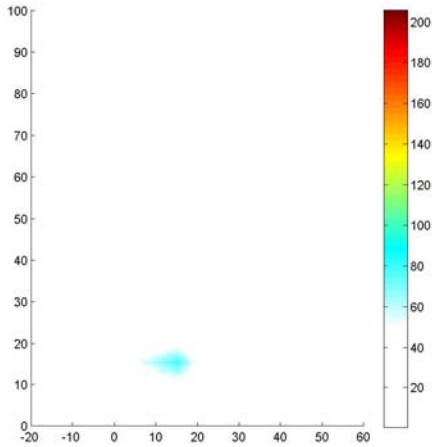

t=500 s

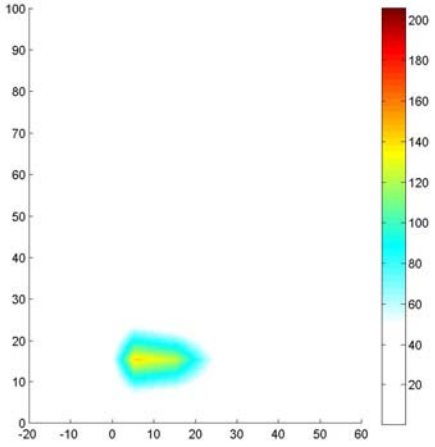

t=600 s

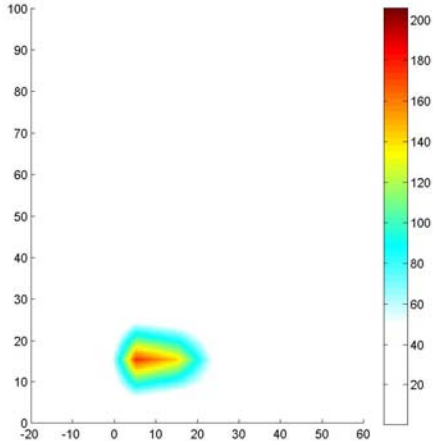

t=800 s

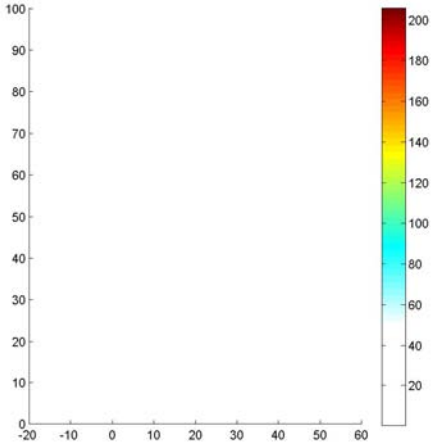

(high/average/low)

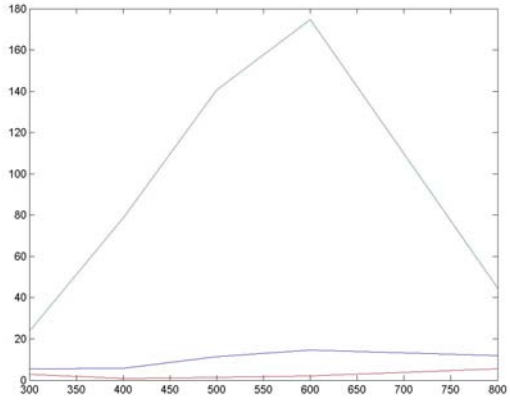

Appendix 32: Plots of temperature sensor data in the plenum (0.5 ms^{-1}).

t=300 s

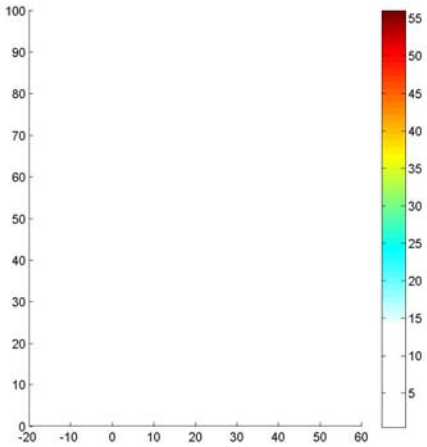

t=400 s

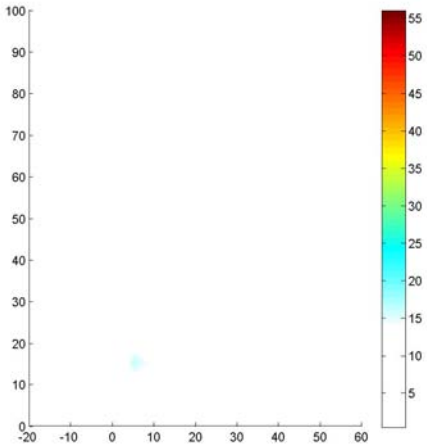

t=500 s

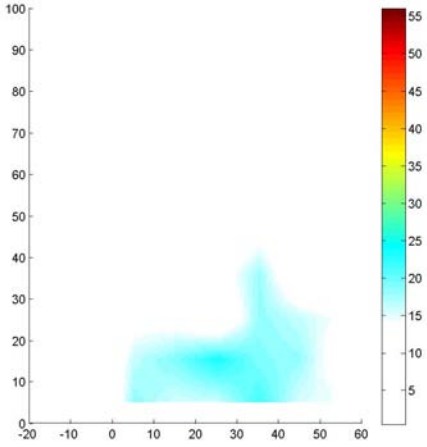

t=600 s

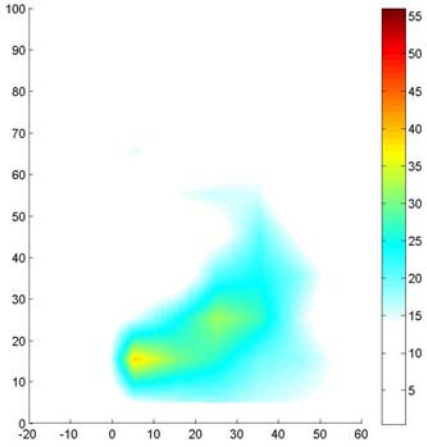

t=800 s

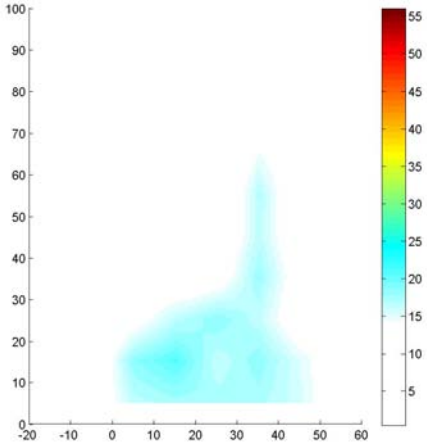

(high/average/low)

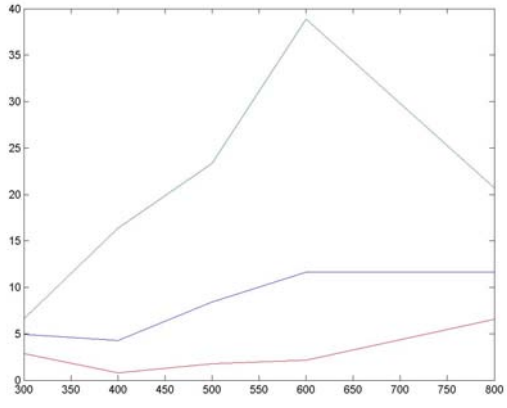

Appendix 33: Plots of temperature sensor data in the subfab (0.6 ms^{-1}).

t=300 s

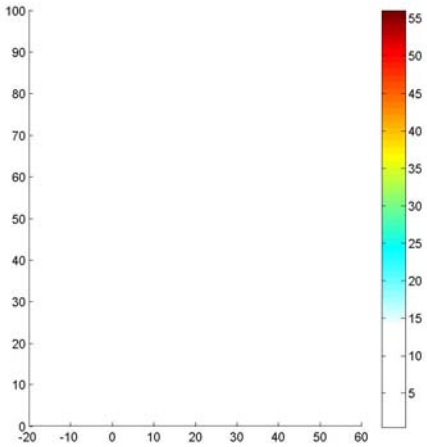

t=400 s

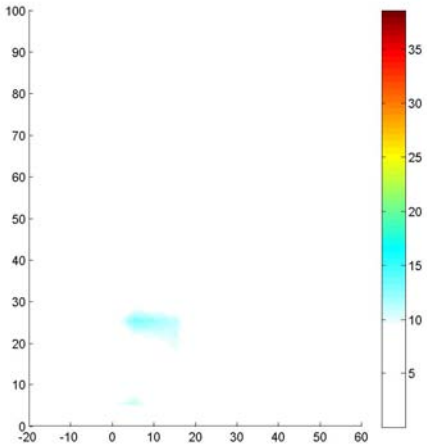

t=500 s

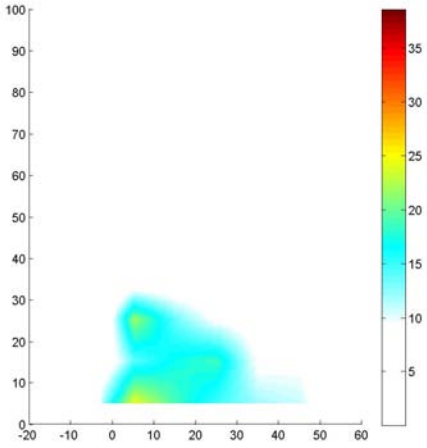

t=600 s

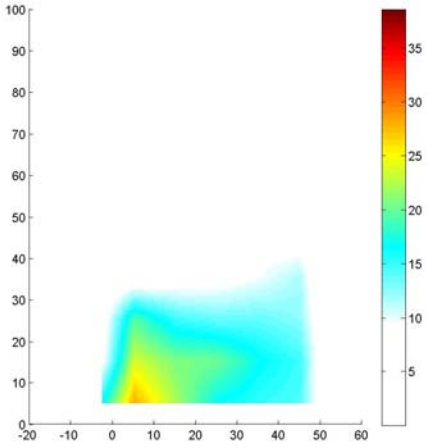

t=800 s

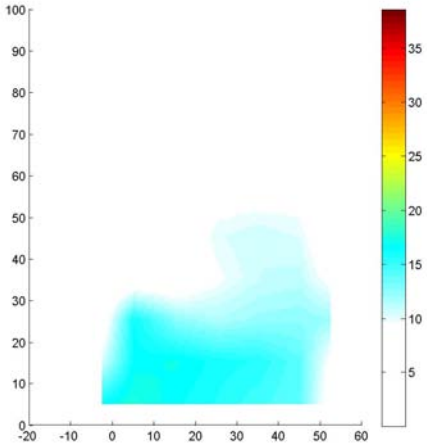

(high/average/low)

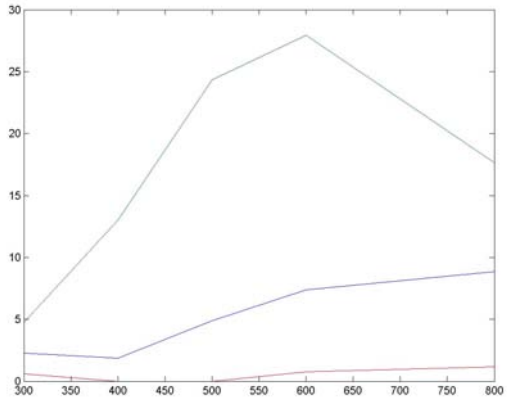

Appendix 34: Plots of temperature sensor data in the fab (0.6 ms^{-1}).

t=300 s

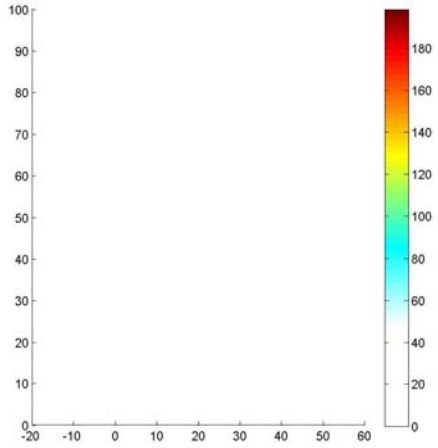

t=400 s

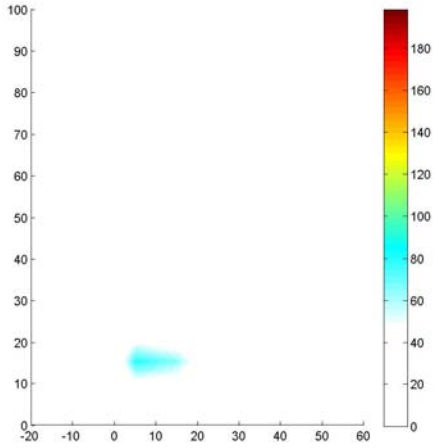

t=500 s

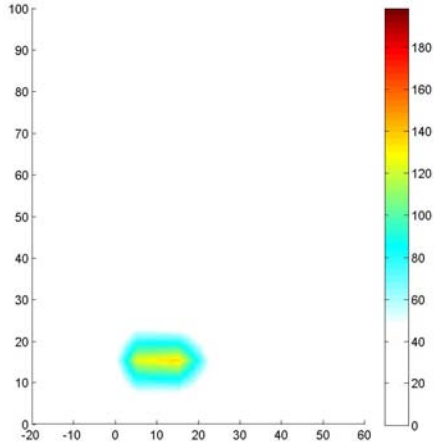

t=600 s

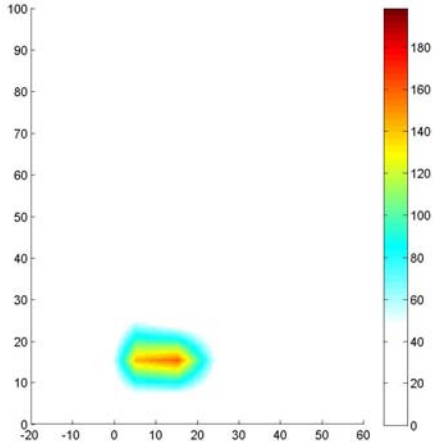

t=800 s

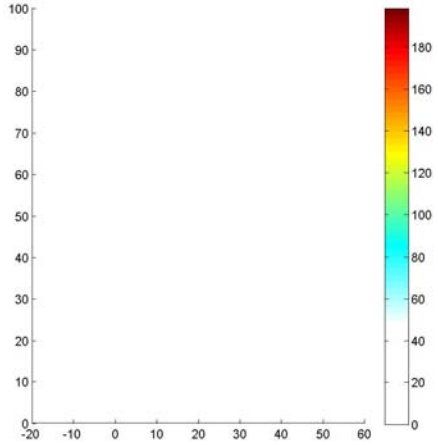

(high/average/low)

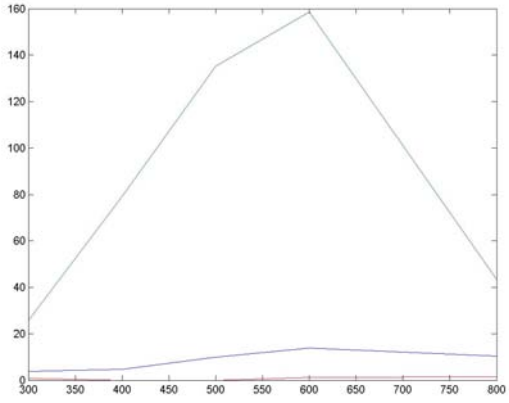

Appendix 35: Plots of temperature sensor data in the plenum (0.6 ms^{-1}).

t=300 s

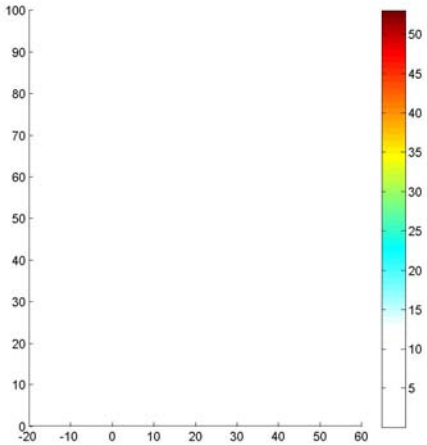

t=400 s

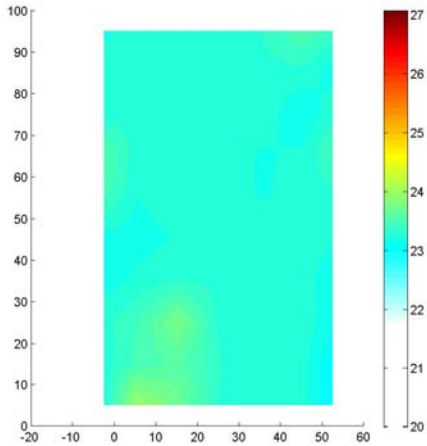

t=500 s

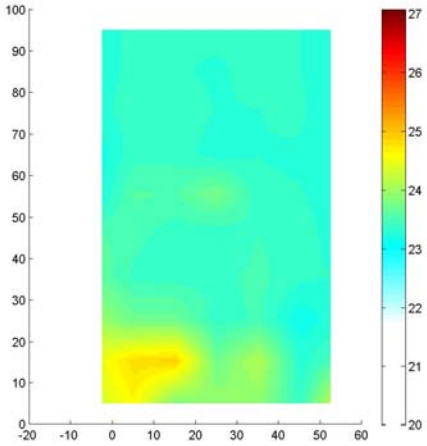

t=600 s

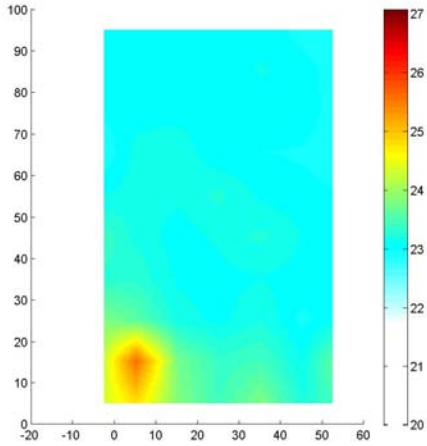

t=800 s

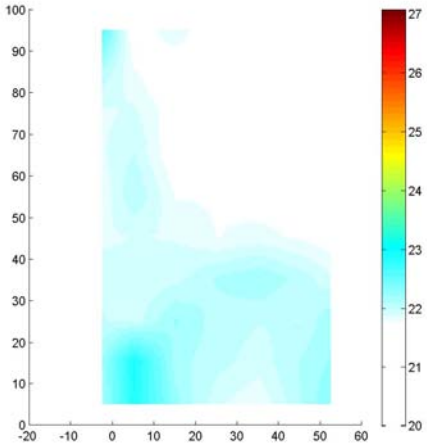

(high/average/low)

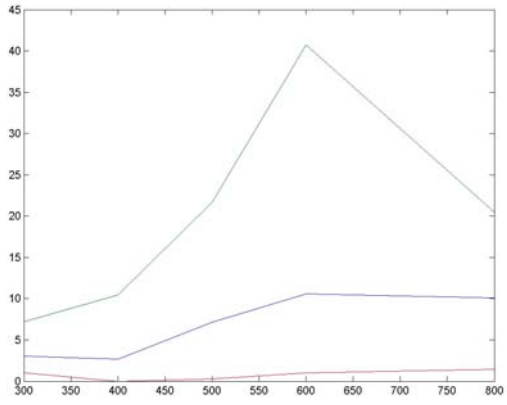

Appendix 36: Plots of temperature sensor data in the subfab (0.0 ms^{-1}).

t=300 s

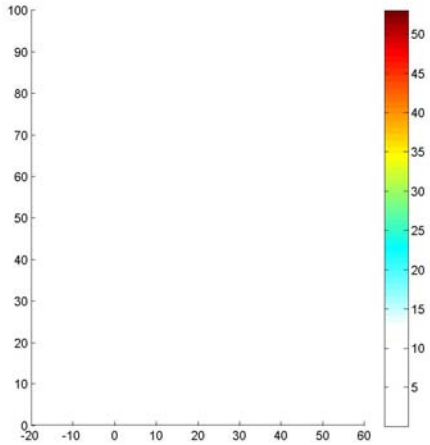

t=400 s

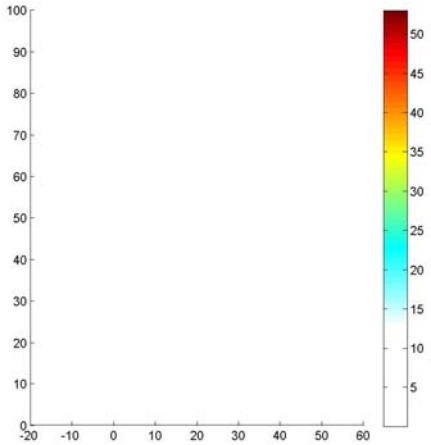

t=500 s

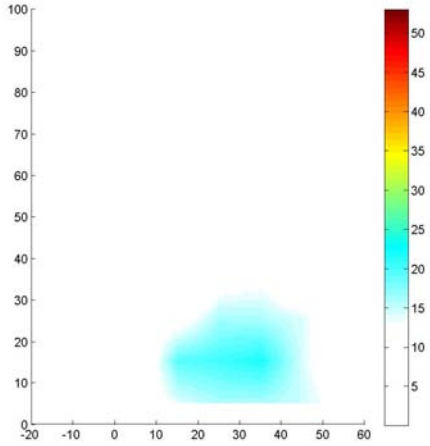

t=600 s

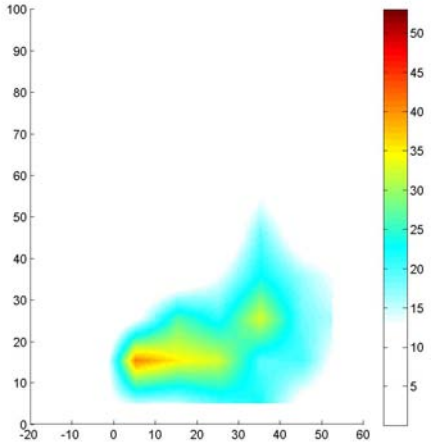

t=800 s

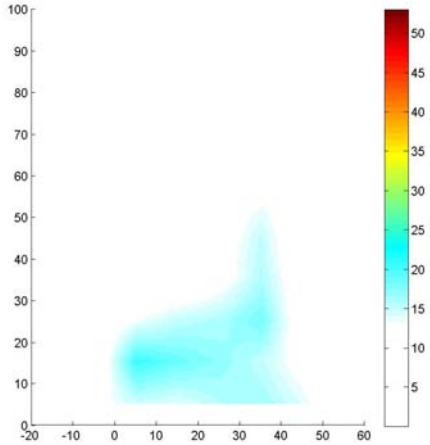

(high/average/low)

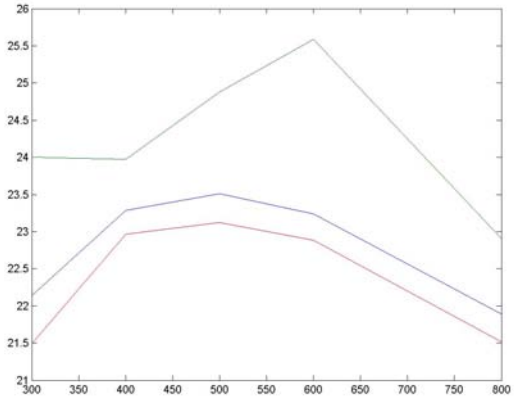

Appendix 37: Plots of temperature sensor data in the fab (0.0 ms^{-1}).

t=300 s

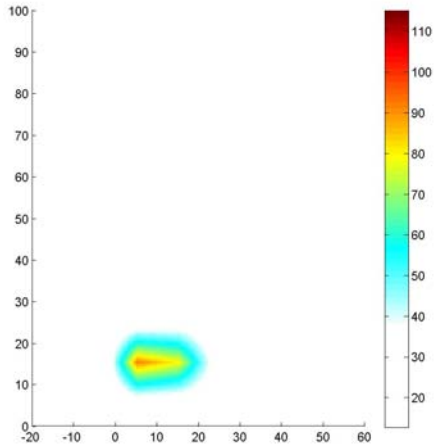

t=400 s

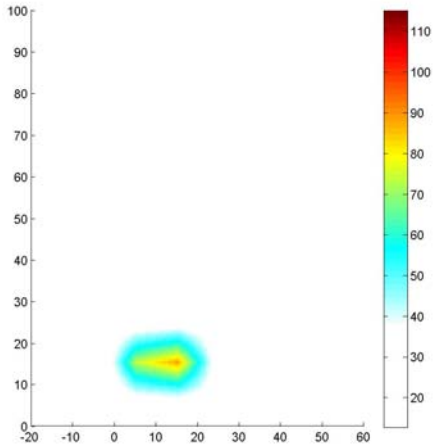

t=500 s

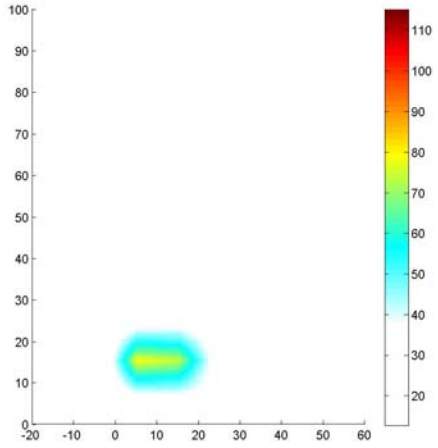

t=600 s

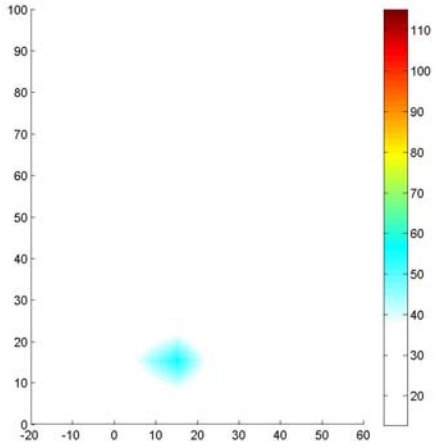

t=800 s

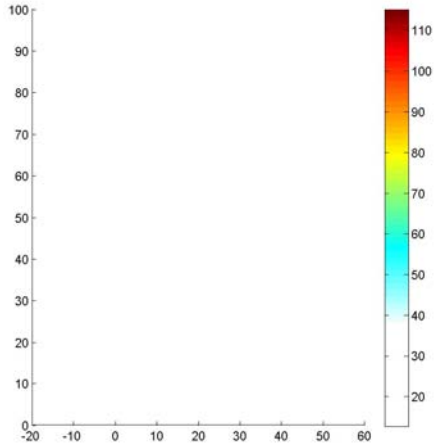

(high/average/low)

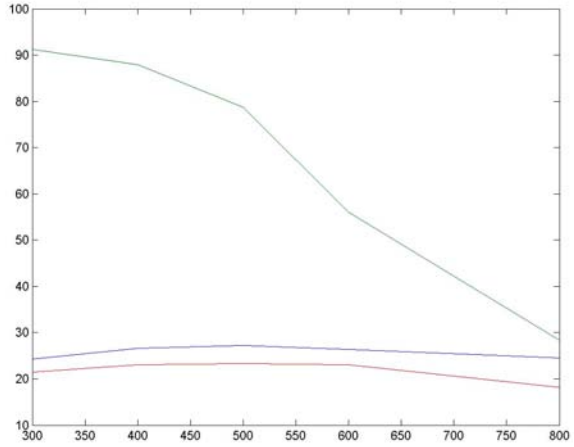

Appendix 38: Plots of temperature sensor data in the plenum (0.0 ms^{-1}).

t=300 s

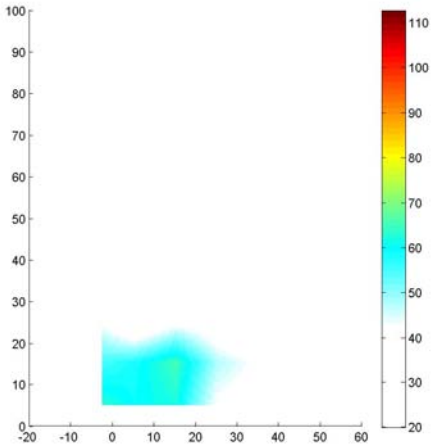

t=400 s

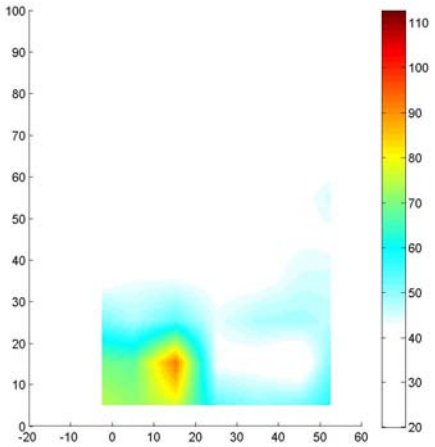

t=500 s

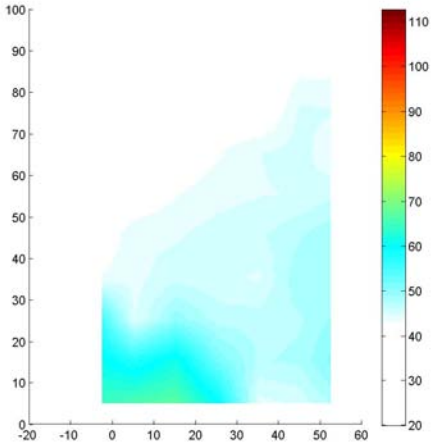

t=600 s

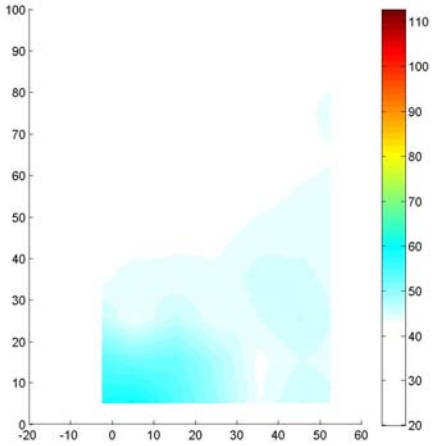

t=800 s

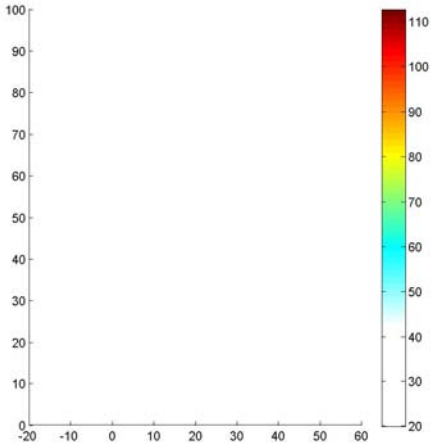

(high/average/low)

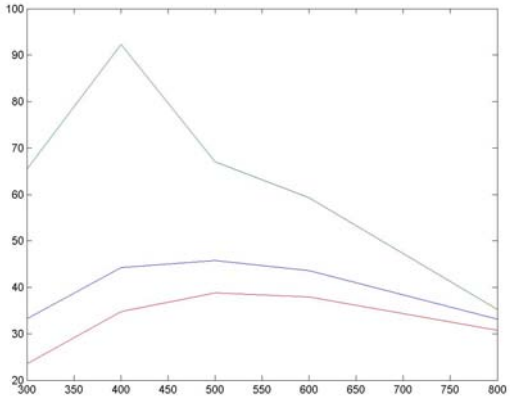

Appendix 39: FDS source code sample (case VI).

```
&HEAD CHID='FFU_velocity_0_6', TITLE='FFU_velocity_0.6'/

&MESH IJK=400,240,44,   XB= 0.0,100.0,-5.0,55,-3.0,8.0/

&MISC PRESSURE_CORRECTION=.TRUE./

&DUMP CHECK_VOLUME_FLOW=.TRUE./

&TIME T_END=1000/

&MISC SURF_DEFAULT='WALL'/

&REAC ID = 'POLYPROPYLENE'
    SOOT_YIELD = 0.06
    N = 1.0
    C = 6.3
    H = 7.1
    O = 2.1/

&SURF ID='BURNER',
    HRRPUA=2222,
    COLOR='RED',
    RAMP_Q='RAMP UP',/

&RAMP ID='RAMP UP',T=200,F=0.0/

&RAMP ID='RAMP UP',T=215,F=0.0025/

&RAMP ID='RAMP UP',T=230,F=0.01/

&RAMP ID='RAMP UP',T=245,F=0.0225/

&RAMP ID='RAMP UP',T=260,F=0.04/

&RAMP ID='RAMP UP',T=275,F=0.0625/
```

```
&RAMP ID='RAMP UP',T=278,F=0.0675/

&RAMP ID='RAMP UP',T=800,F=0.0/

&SURF ID='CEILING JET FAN',

    MATL_ID ='GYPSUM PLASTER'

    THICKNESS =0.012

    VEL=-1.5,

    POROUS=.TRUE.

    COLOR='RASPBERRY'/

&SURF ID='FLOOR'

    COLOR='SILVER'

    MATL_ID ='GYPSUM PLASTER'

    THICKNESS = 0.012

    POROUS=.TRUE./

&SURF ID ='WALL'

    COLOR='SILVER'

    MATL_ID ='GYPSUM PLASTER'

    THICKNESS = 0.012 /

&MATL ID ='GYPSUM PLASTER'

    CONDUCTIVITY = 0.48

    SPECIFIC_HEAT = 0.84

    DENSITY = 1440. /

&SURF ID ='COMPARTMENT WALL'

    COLOR='SKY BLUE'
```

MATL_ID ='GYPSUM PLASTER'

THICKNESS = 0.25/

&OBST XB= 0.0,100.0,0.0,0.0,0.0,5.0, SURF_ID = 'WALL'/ Wall, front

&OBST XB= 0.0,100.0,50.0,50.0,0.0,5.0, SURF_ID = 'WALL'/ Wall, back

&OBST XB= 0.0,0.0,0.0,50.0,0.0,5.0, SURF_ID = 'WALL'/ Wall 1

&OBST XB= 100.0,100.0,0.0,50.0,0.0,5.0, SURF_ID = 'WALL'/ Wall 2

&OBST XB= 0.0,100.0,0.0,50.0,0.0,0.0, SURF_ID = 'WALL'/

&OBST XB= 21.25,22.75,7.0,10.0,0.0,1.0 SURF_ID = 'WALL'/ Fuel

&VENT XB= 21.25,22.75,7.0,10.0,1.0,1.0 SURF_ID = 'BURNER'/ Burner

&OBST XB= 0.0,100.0,0.0,50.0,0.0,0.0, SURF_ID = 'FLOOR'/ Floor

&OBST XB= 0.0,100.0,22.5,27.5,5.0,5.0, SURF_ID='WALL'/

&OBST XB = 5.0,5.25,3.0,22.5,0.0,5.0, SURF_ID ='COMPARTMENT WALL', COLOR='BLUE', TRANSPARENCY =0.1/ R1 y1

&OBST XB = 9.75,10.0,3.0,22.5,0.0,5.0, SURF_ID ='COMPARTMENT WALL', COLOR='BLUE', TRANSPARENCY =0.1/ R1 y2

&OBST XB = 5.25,8.0,3.0,3.25,0.0,5.0, SURF_ID ='COMPARTMENT WALL', COLOR='BLUE', TRANSPARENCY =0.1/ R1 x1

&OBST XB = 5.25,8.0,22.25,22.5,0.0,5.0, SURF_ID ='COMPARTMENT WALL', COLOR='BLUE', TRANSPARENCY =0.1/ R1 x2

&OBST XB = 13.0,13.25,3.0,22.5,0.0,5.0, SURF_ID ='COMPARTMENT WALL', COLOR='BLUE', TRANSPARENCY =0.1/ R2 y1

&OBST XB = 22.75,23.0,3.0,22.5,0.0,5.0, SURF_ID ='COMPARTMENT WALL', COLOR='BLUE', TRANSPARENCY =0.1/ R2 y2

&OBST XB = 13.25,17.0,3.0,3.25,0.0,5.0, SURF_ID ='COMPARTMENT WALL', COLOR='BLUE', TRANSPARENCY =0.1/ R2 x1

&OBST XB = 19.0,22.75,3.0,3.25,0.0,5.0, SURF_ID ='COMPARTMENT WALL', COLOR='BLUE', TRANSPARENCY =0.1/ R2 x1

&OBST XB = 13.25,17.0,22.25,22.5,0.0,5.0, SURF_ID ='COMPARTMENT WALL', COLOR='BLUE', TRANSPARENCY =0.1/ R2 x2

&OBST XB = 19.0,22.75,22.25,22.5,0.0,5.0, SURF_ID ='COMPARTMENT WALL', COLOR='BLUE', TRANSPARENCY =0.1/ R2 x2

&OBST XB = 26.0,26.25,3.0,22.5,0.0,5.0, SURF_ID ='COMPARTMENT WALL', COLOR='BLUE', TRANSPARENCY =0.1/ R3 y1

&OBST XB = 45.75,46.0,3.0,22.5,0.0,5.0, SURF_ID ='COMPARTMENT WALL', COLOR='BLUE', TRANSPARENCY =0.1/ R3 y2

&OBST XB = 26.25,30.25,3.0,3.25,0.0,5.0, SURF_ID ='COMPARTMENT WALL', COLOR='BLUE', TRANSPARENCY =0.1/ R3 x1

&OBST XB = 32.25,40.25,3.0,3.25,0.0,5.0, SURF_ID ='COMPARTMENT WALL', COLOR='BLUE', TRANSPARENCY =0.1/ R3 x1

&OBST XB = 42.25,45.75,3.0,3.25,0.0,5.0, SURF_ID ='COMPARTMENT WALL', COLOR='BLUE', TRANSPARENCY =0.1/ R3 x1

&OBST XB = 26.25,30.25,22.25,22.5,0.0,5.0, SURF_ID ='COMPARTMENT WALL', COLOR='BLUE', TRANSPARENCY =0.1/ R3 x2

&OBST XB = 32.25,40.25,22.25,22.5,0.0,5.0, SURF_ID ='COMPARTMENT WALL', COLOR='BLUE', TRANSPARENCY =0.1/ R3 x2

&OBST XB = 42.25,45.75,22.25,22.5,0.0,5.0, SURF_ID ='COMPARTMENT WALL', COLOR='BLUE', TRANSPARENCY =0.1/ R3 x2

&OBST XB = 49.0,49.25,3.0,22.5,0.0,5.0, SURF_ID ='COMPARTMENT WALL', COLOR='BLUE', TRANSPARENCY =0.1/ R4 y1

&OBST XB = 89.75,90.0,3.0,22.5,0.0,5.0, SURF_ID ='COMPARTMENT WALL', COLOR='BLUE', TRANSPARENCY =0.1/ R4 y2

&OBST XB = 49.25,58.5,3.0,3.25,0.0,5.0, SURF_ID ='COMPARTMENT WALL', COLOR='BLUE', TRANSPARENCY =0.1/ R4 x1

&OBST XB = 60.5,79.0,3.0,3.25,0.0,5.0, SURF_ID ='COMPARTMENT WALL', COLOR='BLUE', TRANSPARENCY =0.1/ R4 x1

&OBST XB = 81.0,89.75,3.0,3.25,0.0,5.0, SURF_ID ='COMPARTMENT WALL', COLOR='BLUE', TRANSPARENCY =0.1/ R4 x1

&OBST XB = 49.25,58.5,22.25,22.5,0.0,5.0, SURF_ID ='COMPARTMENT WALL', COLOR='BLUE', TRANSPARENCY =0.1/ R4 x2

&OBST XB = 60.5,79.0,22.25,22.5,0.0,5.0, SURF_ID ='COMPARTMENT WALL', COLOR='BLUE', TRANSPARENCY =0.1/ R4 x2

&OBST XB = 81.0,89.75,22.25,22.5,0.0,5.0, SURF_ID ='COMPARTMENT WALL', COLOR='BLUE', TRANSPARENCY =0.1/ R4 x2

&OBST XB = 5.0,5.25,27.5,47.0,0.0,5.0, SURF_ID ='COMPARTMENT WALL', COLOR='BLUE', TRANSPARENCY =0.1/ R9 y1

&OBST XB = 11.75,12.0,27.5,47.0,0.0,5.0, SURF_ID ='COMPARTMENT WALL', COLOR='BLUE', TRANSPARENCY =0.1/ R9 y2

&OBST XB = 7.0,11.75,27.5,27.75,0.0,5.0, SURF_ID ='COMPARTMENT WALL', COLOR='BLUE', TRANSPARENCY =0.1/ R9 x1

&OBST XB = 7.0,11.75,46.75,47.0,0.0,5.0, SURF_ID ='COMPARTMENT WALL', COLOR='BLUE', TRANSPARENCY =0.1/ R9 x2

&OBST XB = 15.0,15.25,27.5,47.0,0.0,5.0, SURF_ID ='COMPARTMENT WALL', COLOR='BLUE', TRANSPARENCY =0.1/ R8 y1

&OBST XB = 50.75,51.0,27.5,47.0,0.0,5.0, SURF_ID ='COMPARTMENT WALL', COLOR='BLUE', TRANSPARENCY =0.1/ R8 y2

&OBST XB = 15.25,18.25,27.5,27.75,0.0,5.0, SURF_ID ='COMPARTMENT WALL', COLOR='BLUE', TRANSPARENCY =0.1/ R8 x1

&OBST XB = 20.25,45.75,27.5,27.75,0.0,5.0, SURF_ID ='COMPARTMENT WALL', COLOR='BLUE', TRANSPARENCY =0.1/ R8 x2

&OBST XB = 47.75,50.75,27.5,27.75,0.0,5.0, SURF_ID ='COMPARTMENT WALL', COLOR='BLUE', TRANSPARENCY =0.1/ R8 x3

&OBST XB = 15.25,50.75,46.75,47.0,0.0,5.0, SURF_ID ='COMPARTMENT WALL', COLOR='BLUE', TRANSPARENCY =0.1/ R8 x4

&OBST XB = 54.0,54.25,27.5,47.0,0.0,5.0, SURF_ID ='COMPARTMENT WALL', COLOR='BLUE', TRANSPARENCY =0.1/ R7 y1

&OBST XB = 58.75,59.0,27.5,47.0,0.0,5.0, SURF_ID ='COMPARTMENT WALL', COLOR='BLUE', TRANSPARENCY =0.1/ R7 y2

&OBST XB = 54.25,57.25,27.5,27.75,0.0,5.0, SURF_ID ='COMPARTMENT WALL', COLOR='BLUE', TRANSPARENCY =0.1/ R7 x1

&OBST XB = 54.25,57.25,46.75,47.0,0.0,5.0, SURF_ID ='COMPARTMENT WALL', COLOR='BLUE', TRANSPARENCY =0.1/ R7 x2

&OBST XB = 62.0,62.25,27.5,47.0,0.0,5.0, SURF_ID ='COMPARTMENT WALL', COLOR='BLUE', TRANSPARENCY =0.1/ R6 y1

&OBST XB = 66.75,67.0,27.5,47.0,0.0,5.0, SURF_ID ='COMPARTMENT WALL', COLOR='BLUE', TRANSPARENCY =0.1/ R6 y2

&OBST XB = 62.25,65.25,27.5,27.75,0.0,5.0, SURF_ID ='COMPARTMENT WALL', COLOR='BLUE', TRANSPARENCY =0.1/ R6 x1

&OBST XB = 62.25,65.25,46.75,47.0,0.0,5.0, SURF_ID ='COMPARTMENT WALL', COLOR='BLUE', TRANSPARENCY =0.1/ R6 x2

&OBST XB = 70.0,70.25,27.5,47.0,0.0,5.0, SURF_ID ='COMPARTMENT WALL', COLOR='BLUE', TRANSPARENCY =0.1/ R5 y1

&OBST XB = 89.75,90.0,27.5,47.0,0.0,5.0, SURF_ID ='COMPARTMENT WALL', COLOR='BLUE', TRANSPARENCY =0.1/ R5 y2

&OBST XB = 70.25,72.25,27.5,27.75,0.0,5.0, SURF_ID ='COMPARTMENT WALL', COLOR='BLUE', TRANSPARENCY =0.1/ R5 x1

&OBST XB = 74.25,89.75,27.5,27.75,0.0,5.0, SURF_ID ='COMPARTMENT WALL', COLOR='BLUE', TRANSPARENCY =0.1/ R5 x2

&OBST XB = 70.25,89.75,46.75,47.0,0.0,5.0, SURF_ID ='COMPARTMENT WALL', COLOR='BLUE', TRANSPARENCY =0.1/ R5 x2

Note: The following 8965 command lines represent FFU's (left out deliberately).
The corresponding pattern is as shown below.

&OBST XB=0.0,1.0,0.0,0.5,5.0,5.0,SURF_ID ='WALL'/

&OBST XB=1.0,2.0,0.0,0.5,5.0,5.0,SURF_ID ='CEILING JET FAN'/

Note: The following 210 command lines represent metering devices to measure W-VELOCITY, TEMPERATURE and MIXTURE FRACTION (left out deliberately). The corresponding pattern is as shown below.

&DEVC ID='VC-1',XYZ=5.0,-2.5,-1.5,QUANTITY='W-VELOCITY'/

```
&DEVC XYZ=5.0,-2.5,-1.5,QUANTITY='TEMPERATURE', ID='T-1'/

&DEVC XYZ=5.0,-2.5,-1.5,QUANTITY='MIXTURE FRACTION', ID='T-1'/
```

```
&SLCF PBX=22,  QUANTITY='VELOCITY', VECTOR=.TRUE./

&SLCF PBY=25,  QUANTITY='VELOCITY', VECTOR=.TRUE./

&SLCF PBY=8,  QUANTITY='VELOCITY', VECTOR=.TRUE./

&SLCF PBX=22,  QUANTITY='TEMPERATURE'/

&SLCF PBY=25,  QUANTITY='TEMPERATURE'/

&SLCF PBY=8,  QUANTITY='TEMPERATURE'/

&SLCF PBX=22,  QUANTITY='MIXTURE FRACTION'/

&SLCF PBY=25,  QUANTITY='MIXTURE FRACTION'/

&SLCF PBY=8,  QUANTITY='MIXTURE FRACTION'/

&TAIL/
```